DEVELOPMENT OF A REFINED THERMAL RADIATION MODEL FOR GAS AND LIQUID FUELS

By

MICHAEL CHONG VUI SAN

Thesis Submitted to the School of Graduate Studies, Universiti Putra Malaysia, in Fulfilment of the Requirements for the Degree of Doctor of Philosophy

July 2024

Abstract of thesis presented to the Senate of Universiti Putra Malaysia in fulfilment of the requirement for the degree of Doctor of Philosophy

DEVELOPMENT OF A REFINED THERMAL RADIATION MODEL FOR GAS AND LIQUID FUELS

By

MICHAEL CHONG VUI SAN

July 2024

Chairman : Mohd Zahirasri bin Mohd Tohir, PhD
Faculty : Engineering

This study evaluates the performance of thermal radiation models in fire safety engineering to enhance their applicability in various fire scenarios, with the goal of developing a refined thermal radiation model for gas and liquid fuels. The research is structured in three parts. The first part assesses the effectiveness of existing thermal radiation models for propane gas fires, using secondary experimental data from previous studies. The findings highlight the necessity of validation with different fuel phases to improve model reliability, noting that only liquid fuels were tested in this study. In the second part, the evaluation extends to liquid pool fires fueled by ethanol and isopropyl alcohol. Through a series of targeted experiments, the accuracy of thermal radiation models is assessed, providing insights into capturing the complexities associated with thermal radiation in liquid fuel fires. The findings of the research's first and second parts provide an ideal foundation for the development of newmodels that can better capture the complex phenomena of thermal radiation from the flame.

Consequently, the third part of the research focuses on the development of a novel thermal radiation model through semi-a priori modelling. By considering the thermal behaviour of both gas and liquid fires, this model aims to improve fuel by utilising fitting data from propane gas fire experiments, as well as ethanol and isopropyl alcohol pool fire tests. The major findings of the study indicate that the single point source model exhibits the best performance for gas and liquid fire scenarios. In addition, the assessment of the new model demonstrates its potential to capture the intricate nature of thermal radiation phenomena. Validation of the new model employs untested experimental and simulation data, comparing it with the single point source model to evaluate accuracy and effectiveness. This research provides valuable insights into thermal radiation modelling, offering tools for researchers and practitioners in selecting appropriate thermal radiation models for fire protection systems. By enhancing the accuracy and reliability of thermal radiation modelling, this study aims to foster the development of safer and more effective fire protection measures.

Keywords: Single Point Source Model, Radiative Heat Flux, Thermal Radiation Model, Heat Transfer, Semi-A Priori Modelling

SDG: GOAL 9: Industry, Innovation and Infrastructure

Abstrak tesis yang dikemukakan kepada Senat Universiti Putra Malaysia sebagai memenuhi keperluan untuk ijazah Doktor Falsafah

PENAIKTARAFAN MODEL SINARAN TERMA BAGI BAHAN API GAS DAN CECAIR

Oleh

MICHAEL CHONG VUI SAN

Julai 2024

Pengerusi : Mohd Zahirasri bin Mohd Tohir, PhD
Fakulti : Kejuruteraan

Kajian ini menilai prestasi model sinaran terma dalam kejuruteraan keselamatan kebakaran untuk meningkatkan kebolehgunaannya dalam pelbagai senario kebakaran, dengan matlamat membangunkan model sinaran terma yang lebih baik bagi bahan api gas dan cecair. Penyelidikan ini disusun dalam tiga bahagian. Bahagian pertama menilai keberkesanan model sinaran terma sedia ada untuk kebakaran gas propana, menggunakan data eksperimen sekunder dari kajian-kajian terdahulu. Penemuan ini menekankan keperluan untuk pengesahan menggunakan fasa bahan api yang berbeza bagi mempertingkatkan kebolehpercayaan model, memandangkan hanya bahan api cecair yang diuji dalam kajian ini. Dalam bahagian kedua, penilaian diperluaskan kepada kebakaran kolam bahan api cecair yang menggunakan etanol dan isopropil alkohol. Melalui beberapa siri eksperimen khusus, ketepatan model sinaran terma dinilai, memberi pandangan mendalam dalam menangkap kerumitan yang berkaitan dengan sinaran terma dalam kebakaran

bahan api cecair. Penemuan dari bahagian pertama dan kedua penyelidikan ini menyediakan asas yang kukuh bagi pembangunan model baharu yang mampu menangkap fenomena sinaran terma daripada nyalaan dengan lebih baik. Justeru, bahagian ketiga penyelidikan ini menumpukan pada pembangunan model sinaran terma baharu melalui pemodelan semi-a priori. Dengan mempertimbangkan tingkah laku terma kedua-dua kebakaran gas dan cecair, model ini bertujuan untuk memperbaiki ketepatan dengan menggunakan data penyesuaian daripada eksperimen kebakaran gas propana serta ujian kebakaran kolam etanol dan isopropil alkohol. Penemuan utama kajian ini menunjukkan bahawa model sumber titik tunggal memperlihatkan prestasi terbaik bagi senario kebakaran gas dan cecair. Di samping itu, penilaian terhadap model baharu ini menunjukkan potensinya dalam menangkap sifat kompleks fenomena sinaran terma. Pengesahan model baharu ini menggunakan data eksperimen dan simulasi yang belum diuji, dan dibandingkan dengan model sumber titik tunggal untuk menilai ketepatan dan keberkesanannya. Penyelidikan ini menyediakan pandangan yang bernilai dalam pemodelan sinaran terma, menawarkan alat kepada penyelidik dan pengamal dalam memilih model sinaran terma yang sesuai untuk sistem perlindungan kebakaran. Dengan meningkatkan ketepatan dan kebolehpercayaan pemodelan sinaran terma, kajian ini bertujuan untuk memajukan pembangunan langkah-langkah perlindungan kebakaran yang lebih selamat dan berkesan.

Kata Kunci: Titik Sumber Tunggal, Fluks Haba Radiasi, Model Radiasi Terma, Pemindahan Haba, Pemodelan Separuh A Priori

SDG: MATLAMAT 9: Industri, Inovasi dan Infrastruktur

ACKNOWLEDGEMENTS

I would like to express my sincere gratitude and appreciation to the following individuals and organisations who have contributed to the successful completion of my thesis. First and foremost, I am deeply grateful to my main supervisor, Associate Prof. Dr. Mohd Zahirasri Bin Mohd Tohir, for his invaluable guidance, support, and advice throughout my Ph.D. journey. I am especially thankful for the opportunity to work under his supervision, which has enriched my knowledge and research skills. I would also like to extend my thanks to my co-supervisors, Prof. Dr. Abd. Rahim Bin Abu Talib and Dr. Syamimi Binti Saadon, for their valuable input and assistance in shaping the direction of my research. Their expertise and guidance have been instrumental in the development of my thesis.

I am indebted to the faculty of engineering at Universiti Putra Malaysia for granting me access to the combustion laboratory. I am particularly grateful to Mr. Ismail Abdullah, the assistant engineer of the combustion laboratory, whose assistance and cooperation have been indispensable during my experimental work. Furthermore, I would like to express my heartfelt appreciation to the undergraduate students, Nor Syamimi Amalina Robane, who provided valuable assistance in conducting the experiments.

Finally, I would like to express my deepest gratitude to my parents for their unwavering support, love, and encouragement throughout my academic journey. Their belief in me and their constant motivation has been the driving force behind my accomplishments. I am truly fortunate to have received the

guidance, support, and assistance from these individuals and organisations, and I am humbled by their contributions to my academic and personal growth.

I certify that a Thesis Examination Committee has met on 2 July 2024 to conduct the final examination of Michael Chong Vui San on his thesis entitled "Development of a Refined Thermal Radiation Model for Gas and Liquid Fuels" in accordance with the Universities and University Colleges Act 1971 and the Constitution of the Universiti Putra Malaysia [P.U.(A) 106] 15 March 1998. The Committee recommends that the student be awarded the Doctor of Philosophy.

Members of the Thesis Examination Committee were as follows:

Siti Aslina binti Hussain, PhD
Associate Professor Ir.
Faculty of Engineering
Universiti Putra Malaysia
(Chairman)

Thomas Choong Shean Yaw, PhD
Professor Ir.
Faculty of Engineering
Universiti Putra Malaysia
(Internal Examiner)

Dayang Radiah binti Awang Biak, PhD
Senior Lecturer
Faculty of Engineering
Universiti Putra Malaysia
(Internal Examiner)

Grunde Jomaas, PhD
Professor
Department for Fire-safe Sustainable Built Environment
Slovenian National Building and Civil Engineering Institute
Slovenia
(External Examiner)

RUSMAWATI BINTI SAID, PhD
Professor and Deputy Dean
School of Graduate Studies
Universiti Putra Malaysia

Date: 26 February 2025

This thesis was submitted to the Senate of Universiti Putra Malaysia and has been accepted as fulfilment of the requirement for the degree of Doctor of Philosophy. The members of the Supervisory Committee were as follows:

Zahirasri bin Mohd Tohir, PhD
Associate Professor
Faculty of Engineering
Universiti Putra Malaysia
(Chairman)

Abd. Rahim bin Abu Talib, PhD
Professor Ir.
Faculty of Engineering
Universiti Putra Malaysia
(Member)

Syamimi binti Saadon, PhD
Senior Lecturer
Faculty of Engineering
Universiti Putra Malaysia
(Member)

ZALILAH MOHD SHARIFF, PhD
Professor and Dean
School of Graduate Studies
Universiti Putra Malaysia

Date: 13 March 2025

Declaration by the Graduate Student

I hereby confirm that:

- this thesis is my original work;
- quotations, illustrations and citations have been duly referenced;
- this thesis has not been submitted previously or concurrently for any other degree at any institutions;
- intellectual property from the thesis and the copyright of the thesis are fully-owned by Universiti Putra Malaysia, as stipulated in the Universiti Putra Malaysia (Research) Rules 2012;
- written permission must be obtained from the supervisor and the office of the Deputy Vice-Chancellor (Research and innovation) before the thesis is published in any written, printed or electronic form (including books, journals, modules, proceedings, popular writings, seminar papers, manuscripts, posters, reports, lecture notes, learning modules or any other materials) as stated in the Universiti Putra Malaysia (Research) Rules 2012;
- there is no plagiarism or data falsification/fabrication in the thesis, and scholarly integrity is upheld in accordance with the Universiti Putra Malaysia (Graduate Studies) Rules 2003 (Revision 2015-2016) and the Universiti Putra Malaysia (Research) Rules 2012. The thesis has undergone plagiarism detection software

Signature: ________________ Date: 16/4/2025

Name and Matric No.: Michael Chong Vui San, GS62787

Declaration by Members of the Supervisory Committee

This is to confirm that:

- the research and the writing of this thesis were done under our supervision;
- supervisory responsibilities as stated in the Universiti Putra Malaysia (Graduate Studies) Rules 2003 (Revision 2015-2016) are adhered to.

DR. MOHD ZAHIRASRI BIN MOHD TOHIR
Pensyarah Kanan
Jabatan Kejuruteraan Kimia & Alam Sekitar
Fakulti Kejuruteraan
Universiti Putra Malaysia
43400 UPM Serdang
Selangor, Malaysia

Signature: ______________________
Name of Chairman of
Supervisory Committee: Mohd Zahirasri bin Mohd Tohir

PROF. Ir. Ts. Dr. ABD. RAHIM ABU TALIB
Ketua
Jabatan Kejuruteraan Aeroangkasa
Fakulti Kejuruteraan
Universiti Putra Malaysia

Signature: ______________________
Name of Member of
Supervisory Committee: Abd. Rahim bin Abu Talib

Jabatan Kejuruteraan Aeroangkasa
Fakulti Kejuruteraan
Universiti Putra Malaysia

Signature: ______________________
Name of Member of
Supervisory Committee: Syamimi binti Saadon

TABLE OF CONTENTS

LIST OF TABLES

LIST OF FIGURES

LIST OF ABBREVIATIONS

χ_r	Radiative fraction
A	Area of flame base (m^2)
D	Diameter of flame base (m)
T_f	Flame temperature (K)
T_a	Ambient temperature (K)
w	Width of flame base (m)
b	Breadth of flame base (m)
n	Number of multi cuboid flames/ multi cylinder flames
H_f	Height of flame (m)
H_t	Height of target (m)
H_m	Mean flame height (m)
H_i	Elevated height for the base of multi cylinder from the surface of fuel (m)
Δz	Height of multi cylinder (m)
L	Horizontal distance from the centre of the base of the fire to the target (m)
$\dot{Q}$	Total heat release rate (kW)
$\dot{Q}_r$	Radiative heat output (kW)
τ	Atmospheric transmissivity
r	Radius (m)
E	Emissive power of flame (kW/m^2)
E_{max}	Equivalent black body emissive power (kW/m^2)
E_s	Emissive power of smoke (kW/m^2)
S	Extinction coefficient (m^{-1})
F_i	Configuration factor from fire to target

$\dot{q}''$	Radiant heat flux (kW/m^2)
ε	Emissivity
θ	Angle between normal and line of sight from target to flame source (rad)
R	Displacement from the receiving target to the centre of flame (m)
σ	Stefan-Boltzmann constant (5.67×10^{-8} W/m^2K^4)
dA	Target element
κ	Effective flame emission/absorption coefficient (m^{-1})
MAPE	Mean Absolute Percentage Error
MdAPE	Median Absolute Percentage Error
FDS	Fire Dynamics Simulator

CHAPTER 1

INTRODUCTION

1.1 Background of Study

Globally, building fires had become an established norm and no longer an unforeseeable irregularity in day-to-day lives. Due to urbanisation, the emergence of multistorey or high-rise buildings increases the likelihood of fire and is often accompanied by the loss of properties and life (Fu, 2021). With no favouritism towards the country of origin, building fire could manifest at just about any building worldwide, making it one of the most prominent fire scenarios reported annually. For instance, according to National Fire Protection Association (NFPA) data for reported fire loss in the United States during 2020, more than half (55%) of the total fire occurrences were associated with building fires, with residential structure fires contributing up to 40% and non-residential structure fire made up the remaining of the building fires statistic (Ahrens & Evarts, 2021), while according to Fire and Rescue Department of Malaysia statistical report for 2018, an amount of 5,368 building fires were reported throughout the whole nation within that year alone, numerically emphasising building fires as the third most common types of fires scenarios in the country (JBPM, 2018).

Uncontrolled building fires are highly detrimental and life-threatening due to their rapid development in a compartment (Ye et al., 2016; Zainudin et al., 2003). Besides causing a fatality, the uncontrolled spread of fire from one compartment to another will certainly result in structural failure of a building, aggravate fire outbreak, and in extreme instances can overwhelm firefighting capacity (Gibson et al., 2019; Kodur et al., 2019; Walls et al., 2017; Zainudin et al., 2003). Henceforth, fire safety has been made one of the prerequisite requirements for all types of buildings (Ibrahim et al., 2011; L. Wang et al., 2021).

The evolution of fire regulations shows that fire safety control in buildings will initially be regulated by a systematic framework of code of practices, primarily prescriptive in nature (Kodur et al., 2019; Tsui, 2004). The codes for design is mainly drafted based on past major fire incident, whereby the identified contributing factors are codified into regulation in coherence to insurance preconditions, industry customs or common company practices (Huang et al., 2019; Hurley & Rosenbaum, 2015; Zainudin et al., 2003). Despite having excellent past records in fire protection performance, the prescriptive-based approach lacks flexibility in terms of acceptable functional design features on top of the unquantified safety margin (Ezekoye et al., 2013; Kodur et al., 2019).

As the underlying principles for fire science develop and are validated by research, the fire regulations have gradually incorporated performance-based fire protection design to optimise the functionality, aesthetics and cost of a building. Many jurisdictions around the world already have, or are progressing towards, the acceptance of a performance-based design approach for fire safety in buildings. The performance-based design provides a structured approach to the preservation of life and property through an engineering approach in response to possible fire incidents within buildings (James M., n.d.). This approach allows flexibility in obtaining a desired level of safety while retaining unique design aspects and without losing any of the pre-defined design objectives since the individual characteristics of a building are taken into consideration during the conceptual phase (Begley, 2004; IFEA, 2018). In other words, performance-based fire design allows the design team to decipher building performance in the event of fire buildings by taking and preserving the intended level of fire protection without compromising the unique feature of the building. (Ezekoye et al., 2013).

While guaranteeing the intended characteristic of the building to be tailored, performance-based fire design also permits the finest available engineering knowledge to be incorporated into fire protection tools and processes. It allows buildings to be designed based on the prediction of what would happen in the event of a fire, mainly achieved through model-based fire design (Ezekoye et al., 2013; Huang et al., 2019). According to Sayin (2015), the evaluation of performance-based design through the quantification method will determine whether the proposed design is able to meet the designated performance during a fire incident or the contrary. This approach speeds up design procedure, boosts productivity, enables comparison of several possible design performances, as well as provides a more ideal solution.

Following the evolution in quantitative understanding of fire, the sophisticated and highly dynamic structural fire analysis is made probable through the application of modern commercial software for fire scenarios simulation, such as Fire Dynamic Simulator (FDS), as well as finite element packages such as ANSYS and OpenSees (Fu, 2021; Hurley & Rosenbaum, 2015). There is a broad selection of models available for the simulation of fire phenomena depending on the needs and requirements.

Generally, a prescriptive approach offers a definite means of achieving an acceptable fire safety level, while a performance approach describes the mandatory response of buildings should a fire manifest (Tsui, 2004; Zhou et al., 2016). According to Ezekoye et al. (2013), the transition from the traditional prescriptive approach to performance-based fire design has been the impetus for the development and utilisation of fire models in the fire protection engineering field.

In coping with the demanding efficiency of design performance prediction and risk mitigation processes, the usage of performance-based design calls for a well-defined fire model (Seo et al., 2013; Zhou et al., 2016). The selection of the model is highly influenced by the uncertainties that need to be addressed. Since fire protection of buildings deals exclusively with the heat release rate, ignition of burnable, flame propagation, and flashover probability, thermal radiation, as the dominant mechanism of fire transfer, appeared as the perfect panacea for the problem (Fu, 2021; L. Wang et al., 2021).

For years, researchers have been studying the thermal radiation mechanism due to its rapid heat transfer rate in a high-temperature environment, where chemical energy is transformed during combustion to heat energy (Ji et al., 2019). A large amount of heat is inevitably transmitted via thermal radiation at such temperature. Thermal radiation is a mechanism by which energy is released by a heated surface or object in the form of electromagnetic radiation and passes directly to its point of absorption at the speed of light. Unlike conduction or convection, thermal radiation does not require any intermediate medium to transfer energy from one point to another. The temperature of the emitting surface governs the strength and distribution of radiant heat transfer.

1.2 Problem Statement and Research Gap

A number of models have been developed to characterise radiant heat transfer, each with its own degree of complexity that depends on an assumption of the flame geometry. The importance of using an accurate model in fire protection cannot be emphasised enough. An accurate model captures the intricacies of fire phenomena, including heat transfer, combustion, and smoke movement. It empowers engineers and fire safety professionals to simulate diverse fire scenarios and evaluate the effectiveness of different fire protection measures and systems before their actual implementation. Consequently, identifying the best-performing model is crucial as it enhances the overall efficacy of fire protection strategies by proactively identifying and addressing potential weaknesses or deficiencies. By selecting the most suitable model, fire safety professionals can ensure accurate fire analysis and improve the overall outcomes of fire safety measures.

The challenge, however, lies in the fact that there is no universal model that can comprehensively address the complexities of all fire scenarios. This has led to the continuous development of thermal radiation models, each focusing on specific applications or assumptions. Among the existing models, those derived from gas burner experiments have gained prominence due to their extensive use in laboratory fire studies. These experiments have formed the basis for semi-empirical models like the cuboid flame model (Huang et al., 2020; Wan et al., 2018) and line source model (Zhou et al., 2016; Zhou & Jiang, 2016), where propane gas is commonly used as the experimental fuel.

Despite their widespread application, there has been limited research focused on direct benchmarking of these gas burner-based models against other types of fire scenarios, particularly in terms of their performance in capturing thermal radiation accurately. Fleury et al. (2011) attempted to address this by evaluating six different radiation models using propane gas burner experiments, concluding that the single point source model was the best-performing. However, the analysis is now over a decade old, and the outcomes have not been revisited to reflect advancements in radiation model development. This creates a research gap, as the continuous improvement in fire modelling technologies suggests that newer models may outperform the single point source model identified by Fleury et al. (2011). Thus, there is a need for an updated and comprehensive assessment to determine whether these newer models can provide more accurate and reliable estimations for gas fires.

Moreover, while gas fire experiments have been extensively studied, there remains a significant gap in the research concerning thermal radiation models for liquid fires. Most available literature on liquid fire primarily focuses on scenarios such as liquid fuel spill fires during storage or transportation, specifically focusing on flame propagation modelling (Y. Li et al., 2015; Liu et al., 2021), as well as the studies of duct fire modelling, and duct fire modelling for tunnel fires (Comitis et al., 1996; H. Y. Wang & Joulain, 2007). These studies often emphasize flame propagation rather than a direct assessment of radiation models. Complex sub-models integrated into main radiation models have been utilised in research by Fukumoto et al. (2020) and Stewart et al. (2021), but their focus was not on evaluating thermal radiation model performance across different liquid fuels. Given that liquid fuels are prevalent in many building fires, which can include scenarios such as kitchen fires involving cooking oils, pool fires resulting from the ignition of common liquid combustibles, or hospital fires caused by alcohol-based sanitisers, it is critical to address this research gap by conducting direct assessments of thermal radiation models using liquid pool fire data. This would ensure that models used in performance-based fire design are adequately validated for liquid fire scenarios.

In addition to gas and liquid fires, thermal radiation modelling for closed-compartment fires has not progressed at the same pace as other fire scenarios. The development of models for closed-compartment fires is often hindered by the challenge of fuel-dependent correlations derived from experimental data (Palazzi et al., 2017; Raj, 2007). This has led to limited publications investigating the performance of existing thermal radiation models for enclosed spaces. The disparity in progress indicates a need for a versatile model that can be reliably applied across various types of fires, including those occurring in enclosed environments. A universally applicable and economically feasible model would address the underdevelopment of closed-compartment fire modelling and ensure consistency in predicting fire behaviour across different settings.

Currently, the fire safety industry faces significant challenges in accurately modelling radiant heat transfer due to these existing gaps. For instance, building designers and safety engineers rely on precise thermal radiation predictions to determine safe evacuation routes, assess the need for fire-resistant materials, and design effective suppression systems. Inaccurate models can lead to misjudgements in these areas, potentially compromising safety and leading to property damage or loss of life. While it is true that smoke analysis is more common in fire safety engineering, particularly for assessing factors such as visibility and smoke layer height, radiation analysis plays a crucial role in specific performance-based scenarios. For instance, non-compliance issues in staircase discharge designs may require both smoke and radiation analyses to prove tenability during escape. Therefore, this study aims to provide an updated evaluation of thermal radiation models, leveraging recent advancements to develop a more comprehensive model capable of accurately predicting radiant heat transfer across different fuel types and scenarios, thus addressing these critical safety needs.

The goal of this research is to bridge these identified gaps by conducting comprehensive assessments of existing thermal radiation models. By utilising experimental data from propane-based fire experiments (gas fires) and liquid pool fire experiments, this study will offer a more holistic view of model performance. The research will address the need for an updated evaluation of gas fire models, while also extending the analysis to liquid fires and closed-compartment scenarios. Through this approach, the study aims to develop a model that reflects the latest advancements and can provide a more comprehensive understanding across various types of fire incidents, contributing to improved fire protection strategies.

1.3 Research Objectives

The research gap presented in the research by Fleury et al. (2011) has created an alluring starting point for further investigation into the assessment of radiation model performance. Building upon this research gap, the present study aims to expand the scope by evaluating a wider range of thermal radiation models and considering variations in fuel sources. This expansion serves as the foundation for the current research, contributing to its originality. The general objective of this research is to establish a benchmark for assessing the performance of thermal radiation models, incorporating a broader range of models and fuel variations. Moreover, the novelty of this research lies in the development of a new thermal radiation model, adding to the existing body of knowledge in this field. By addressing these objectives, this research seeks to enhance our understanding of thermal radiation behaviour and improve the accuracy and effectiveness of radiation modelling techniques.

This can be achieved by completing the following specific objectives:

I) To assess the performance of established thermal radiation models for gas fire experiments.

II) To evaluate the accuracy of thermal radiation models in predicting liquid fuel burning behaviour.

III) To formulate a semi-empirical thermal radiation model based on the single point source approach.

1.4 Scope and Limitation of Studies

1.4.1 Scope of Experimental Work

Experimental work is required to bring forth a complete and all-inclusive set of radiant heat flux data for assessment and comparison with the prediction obtained from radiation models. In order to determine which model is the best performing in terms of predicting radiant heat flux, the knowledge of radiative heat flux received by an ignited object is necessary. Ideally, the experiment's fire source should be burning an office desk or other common solid items. Nevertheless, the fire from these sources is highly unstable in the sense of the shape of the fire, the height of the fire, as well as the heat release rate. This results in difficulties during data comparison between the calculated data and the experimental data. For instance, the repeatability of the experiment is hardly possible due to the drastic changes in data attained. For these reasons, the research does not involve heat flux data from solid fire experiments.

In addition, it is important to consider the significant capital expenditure associated with setting up a gas burner fire experiment. Such experiments involve substantial costs due to the need for specialised equipment, safety measures, and controlled environments. As a cost-effective alternative, this research utilised heat flux data from previous studies conducted by Fleury et al. (2011), which focused on propane gas burner experiments, while only the liquid pool fire experiments were conducted in this research. Consequently, the findings and conclusions of the study are limited to the performance of thermal radiation models in the context of gas and liquid pool fires.

The major drawback of this alternative is the challenge of fully representing real-life fire scenarios within compartments. Common combustible materials found in buildings often consist of a combination of different fuel variants, forming hybrid fuel sources. Furthermore, conventional flammable liquids and gases within buildings rarely exist in their purest form. Therefore, the applicability of the research findings to real-world fire scenarios involving hybrid fuels or other types of sophisticated fires may require additional validation and careful consideration.

1.4.2 Other Research Scope

In addition to the aforementioned experimental work, several other research scopes are considered:

- Direct radiative impact from flame: This investigation focused solely on the direct radiative impact from the fire source. It specifically examined the radiation received by the target solely from the burning object without considering the contribution of radiation from the hot upper gas layer or the surfaces of the compartment. The scope is limited to understanding the direct radiative effects of the fire source itself.
- Single fire experiment: The measurement of heat release rates is confined to scenarios representative of typical fires originating from a single-item compartment source. The research primarily utilised a single gas burner or pool fire to represent the source of the fire. As a result, the findings may not be applicable to fire incidents involving multiple separate-compartment fires. The scope focused on understanding the characteristics of fires originating from a single source within a compartment. Even so, the assumption of a

single fire at one location aligns with standard fire engineering practices, as fire engineers typically assume a single ignition source in performance-based design to simplify analysis and ensure a conservative approach to fire safety assessment.

- Geometry of flame base: The experiments are conducted assuming that the rectangular burner (for gas fires) and square pan (for liquid pool fires) adequately represent the geometry of a circular flame in models that assume cylindrical shape. This assumption is based on the equivalent diameter correlation described in Equation 2.5. The research assumed that the chosen geometries could effectively capture the essential characteristics of circular flames.

1.4.3 Limitation

The research prioritises comparing hand calculation-based thermal radiation models, rather than evaluating computational fluid dynamics (CFD) tools like FDS against experimental data. Since the experimental fuels differ from those used in FDS simulations, direct comparison would not yield consistent insights within this study’s scope.

Instead, the study focuses on comparing the performance of thermal radiation models using data from gas and liquid pool fires, which are widely used in standard fire safety experiments due to their stability, high repeatability, and controlled combustion characteristics. While solid fuel fires are significant in fire safety engineering, gas burner and liquid pool fires provide specific insights into flame behaviour, heat release rate, and combustion dynamics, essential for understanding radiative heat transfer mechanisms.

To broaden the study's scope, this research incorporates widely recognised propane gas burner data (i.e., research by Fleury et al. (2011)) alongside conducting pool fire experiments using both sooting and non-sooting fuels. This combination allows for a more comprehensive assessment of radiative properties under varying combustion conditions.

However, in conducting pool fire experiments, physical constraints, such as the total fuel supply available and laboratory dimensions limit the achievable fire size. Several specific limitations impacting the scale of liquid pool fire experiments include:

- Laboratory Space Constraints: The combustion laboratory serves various research functions and accommodates various equipment, inherently limiting the available space for fire experiments. Nevertheless, the laboratory setting offers essential advantages, including an exhaust fan, suction hood, a controlled environment, safety measures, and technical expertise. To address spatial limitations, the experimental setup has been optimized through strategic reconfiguration, allowing for testing flame sizes up to 0.4 m x 0.4 m, representing small-scale fire scenarios. While these experiments may not capture the full scale of large fires, they offer valuable insights into fire behaviour relevant to practical applications and preliminary model validation.

- Exhaust Hood Height Limitation: The exhaust hood's height can impede full flame height visibility, particularly with larger flames, posing challenges for video capture and analysis. However, the exhaust hood is essential for effective ventilation and capturing combustion by-products, ensuring a safe and controlled experimental environment. To mitigate this limitation, video recording devices have been strategically positioned to capture as much of the flame as possible within the given constraints, ensuring reliable data collection and analysis despite the visibility restrictions.
- Weighing Scale Capacity: The choice of the OHAUS Ranger Count 4000 series weighing scale was made based on its durability, large enough surface to support the fuel pan, and seamless integration with the computational system for data transfer. However, the scale's maximum capacity of 15 kg limits its use for larger pool fires with heavier fuel pans. This restriction means that larger-scale experiments involving higher fuel volumes or larger pans are not feasible within the current laboratory setup.
- Safety considerations: Conducting larger-scale fires may raise safety concerns that need to be evaluated and approved by the responsible authority overseeing the laboratory. While large fires pose increased risks, the use of smaller flames ensures compliance with safety regulations and helps mitigate potential hazards. Future studies may need to explore alternative approaches or facilities that allow for larger-scale experimentation under strict safety protocols.

1.5 Significance of Research

Predicting thermal interaction between the source of ignition and receiving element has been a crucial part of fire engineering knowledge in providing better fire protection for buildings. To estimate whether an object at a distance from a fire source can attain adequate heat transfer and start to ignite, one must be able to distinctively predict the thermal radiation field surrounding the fire. This requires the calculation of radiant heat flux for the fire ignition source (Yang et al., 2023). In combusting flows, radiative heat transfer is a significant origin of energy devaluation. Wan et al. (2018) and (Parot et al., 2022) emphasised that the radiant heat flux is one of the key predominant parameters governing fuel surface heating, fire initiation, fire sustenance and spread hazard in free space.

According to Fleury et al. (2011) and (Li et al. (2021), a full understanding of radiative heat transfer would allow for the following:

- Prediction of the possibility and time taken for an adjacent object to ignite
- Prediction of the degree of damage from fire and ignition hazard
- Estimation of safe separation distances (fireproofing distance) between objects (combustible) or individuals from a fire source
- Prediction of activation of thermal detectors or sprinkler system
- Estimation of the total amount of heat transfer from one object (flame) to another (nearby target)
- Prediction of misfunction of the structural element

From a theory-wise point of view, the key contribution of this research is that it points out the limitation of various models in providing an effective measurement of radiant heat flux while subsequently providing supporting data and a theoretical basis for the selection of the most suitable model(s) for mitigation of loses for different possible fire circumstances. The reasonable prediction of radiation heat towards a receiving target would lead to a higher level of safety and protection, better estimation of safe distance with the implementation of correct models, and the reduction of risk for latent energy dissipation (Ji et al., 2019).

From the practicality perspective, it is envisaged that the credibility and novelty of this research could be translated into decision support for the higher implementation of performance-based fire design in buildings, which acts as a trigger for the evolution of the global fire safety approach. It is known that modelling complexity is often the inhibiting factor in the widespread use of performance-based fire design. Therefore, the breakthrough from this research would undoubtedly trigger the transition from conventional means of fire safety design into adopting the performance-based fire design, which is a more efficient, less labour-intensive, timesaving, and more contemporary approach for the region which are still implementing the prescriptive method as the main mode for building fire safety design.

If properly harnessed, the foundation for the established thermal radiation model would surely strengthen technological capabilities and ensure sustained economic growth since the loss of assets usually accompanies uncontrolled fire incidents. Nevertheless, the fundamental aim of fire safety is not only confined to property loss mitigation but also the preservation of life. Besides the secure evacuation of occupants, life safety is also concerned with the risk imposed on the fire rescue team. Therefore, sufficient fire resistance levels are needed to facilitate safe fire annihilation operations to safeguard evacuation procedures. The structural design must be able to withstand both internal and external progressive collapse of the building during the time interval for complete suppression of fire. The precision of design simulation plays a major role in determining whether fire safety features and desired performance goals are achievable, especially during this sort of fire incident.

1.6 Hypothesis

With a manifold sequence of fire experiments performed on different types of fuel variants, it is envisioned that the whole range of experimental data would be sufficient to draw attention to the shortcomings of present radiation models. Determining existing models' limitations will mark the first step in the grand effort to formulate a superior thermal radiation model specifically for tackling the ceaseless applicability predicament regarding predicting a building fire. It is also the intention of this research to provide as close as possible replication of actual building fire incidents by including some of the most common burnable found in buildings as the fuel tested in this research to further boost the credibility of this research to a whole new level. Hence, the completion of this research would surely contribute the required information for the continuous evolution of performance-based fire design as well as provide answers to the following questions:

I) Does the single point source model remain relevant for predicting heat flux from gas fires?

II) Is the single point source model suitable for predicting heat flux from liquid fires?

III) Is it possible to surpass the performance of the single point source model?

1.7 Chapter Layout

The thesis is structured to align with the specific objectives outlined in Section 1.3. It consists of seven major chapters, each serving a specific purpose. The overview of the thesis is as follows:

Chapter 1 introduces the project, encompassing the background of studies, problem statement, research objectives, and the gaps in current research. Additionally, it outlines the scope and limitations of the study and highlights the significance of the research. The chapter wraps up by presenting a hypothesis regarding the potential outcomes of the research.

Chapter 2 serves to clarify several common terms used throughout the thesis, facilitating a better understanding of the subsequent sections and subsections. Moreover, this chapter provides justification for the selection of thermal radiation models and the types of fuel tested in the investigation. The literature review within this chapter explains how the chosen models and fuels address the existing research gap.

Chapter 3 explains the general methodology used to achieve all specific research objectives. This chapter encompasses the statistical analyses required to assess the performance of thermal radiation models, which include mean analysis, median analysis, and sensitivity analysis. Furthermore, this chapter details the experimental and simulation setups used to achieve the research objectives.

Chapter 4 presents the performance assessment of several recently developed models. These models include the weighted multi-point source model, cuboid flame model, multi-cuboid flame model, multi-cylinder flame model, and single point source model. The assessment is conducted using propane gas burner experiments.

Chapter 5 highlights the performance assessment of various models, including the models examined in Chapter 4 as well as several conventional models, such as the Shokri and Beyler correlation, Shokri and Beyler detailed method, Mudan method, Dayan and Tien method, and rectangular planar model. The assessment is carried out utilising ethanol and isopropyl alcohol pool fire experiments.

Chapter 6 outlines the final phase of the research, where novel semi-empirical thermal radiation models are developed based on the experimental data collected in Chapters 4 and 5. This chapter also compares the heat flux estimation performance between the proposed models and the single point source model. Untested experimental data (acetone and methanol pool fires) and Fire Dynamic Simulator (FDS) simulation data (heptane and methane pool fires) are employed for the comparison.

Chapter 7 concludes the findings derived from Chapters 4, 5, and 6. It summarises how each chapter has successfully achieved the designated research objectives and offers several recommendations for future research endeavours.

CHAPTER 2

LITERATURE REVIEW

This chapter encompassed a whole range of affiliated information and all decision support compiled from a wide collection of publications. The content will begin with the introduction of several important terms applied in the contemporary field of fire science, followed by a decision-making process for selecting thermal radiation models in evaluating heat flux values and fuel variants experimented in this particular study.

2.1 General Terms in Fire Science Community

Several common terms that are employed repeatedly throughout the domain of fire protection society will be further clarified in this subsection. The radiation heat transfer section would explain explicitly how heat is transferred from a burning object towards the target at a distance without being in direct contact with one another, while the radiant heat flux section introduced the most prominent element in the assessment of thermal radiation models. In relation to this, the interrelationship between radiant heat flux and radiative energy output, as well as atmospheric transmissivity, will also be discussed clearly in the subsection.

2.1.1 Radiation Heat Transfer

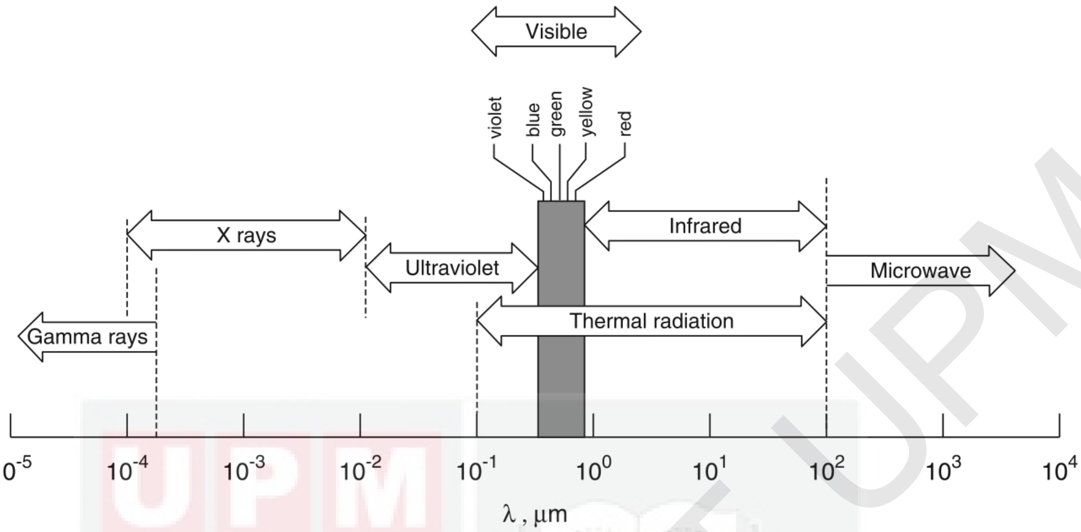

Figure 2.1: Electromagnetic Spectrum
(Source: Bahrami, 2005)

Thermal radiation, spanning from 0.1 μm to 100 μm, encompasses ultraviolet, visible, and infrared spectra, as shown in Figure 2.1. Visible light falls within the 0.4 μm to 0.7 μm range, while infrared thermal radiation ranges from 0.7 μm to 100 μm, and ultraviolet thermal radiation occurs between 0.1 and 0.4 μm (Bahrami, 2005).

Like other forms of electromagnetic radiation, thermal radiation demonstrates both wave and particle characteristics and can be understood as the propagation of electromagnetic waves. Taking into consideration the molecular vibrational and rotational movement of particles, any physical body with finite temperature disregards the state of matter able to emit energy in the form of electromagnetic radiation (Hurley et al., 2016).

Heat energy can be transmitted through gas, liquid, solid, or even in the absence of any medium (in a vacuum) and can travel over distances much greater than the typical reach of flames (Filkov et al., 2023). In the case of thermal radiation transfer involving an intermediary medium, the radiation energy might be absorbed, reflected, or distributed by the molecules and atoms of the medium. However, the circumstances are different for transmission through a vacuum; the radiation energy is not attenuated by any means and, thus, is completely transmitted to the receiving target. Hence, thermal radiation is clearly a more efficient and dominant means of heat transfer between two separated bodies (Ganji et al., 2017).

Radiation heat transfer is the process of transferring thermal energy from one body to another through the emission and absorption of electromagnetic waves. According to Stefan-Boltzmann Law, the radiation heat transfer from a body to its surroundings is proportional to the fourth power of the absolute temperature. It can be expressed by the following equation:

$$\dot{q}'' = \varepsilon \sigma T_a^4 \qquad 2.1$$

where

$\dot{q}''$ is the radiant heat flux (kW/m^2)

ε is the emissivity

σ is the Stefan-Boltzmann constant (5.67×10^{-8} $W/m^2 K^4$)

T_a is the ambient temperature (K)

2.1.2 Radiant Heat Flux

According to the Glossary of Fire Science Terminology, radiant heat flux is typically calculated or measured for a specific surface to determine the heat transfer at that surface. Since any object with a temperature above absolute zero radiates thermal energy, the net radiant heat transfer between two objects of the same radiation characteristic would depend on their temperature difference. The following equation describes the factors that determine the radiant heat flux from radiative source incident at the target surface:

$$\dot{q}'' = F_i \varepsilon \sigma T_a^4 \qquad 2.2$$

where

$\dot{q}''$ is the radiant heat flux (kW/m^2)

F_i is the configuration factor from fire to target

ε is the emissivity

σ is the Stefan-Boltzmann constant (5.67 x 10^{-8} W/m^2 K^4)

T_a is the ambient temperature (K).

2.1.3 Radiative Heat Output

The amount of heat transferred through radiation to objects adjacent to the source of flame affects the danger posed by the specific fire and determines how quickly the fire spreads. The radiative fraction, a significant parameter indicating the proportion of heat released as radiation, is the product of the radiative fraction and total heat release rate such that:

$$\dot{Q}_r = \chi_r \dot{Q} \qquad 2.3$$

where

χ_r is the radiative fraction

$\dot{Q}$ is the total heat release rate (kW).

The fraction of total heat transfer due to radiation increases with combustor size, as noted by Viskanta and Mengüç (1987). This aligns with the findings of J. Liu and Zhou (2019), who suggest that the radiative fraction is primarily affected by the formation of soot and flame volume, both of which are dependent on surrounding pressure. Additionally, Beyler (2016) provides a more specific approach for fire with diameter less than 50 m, indicating that the radiative fraction, χ_r for these smaller fires can be deduced using the curve fit linear equation shown in Figure 2.2.

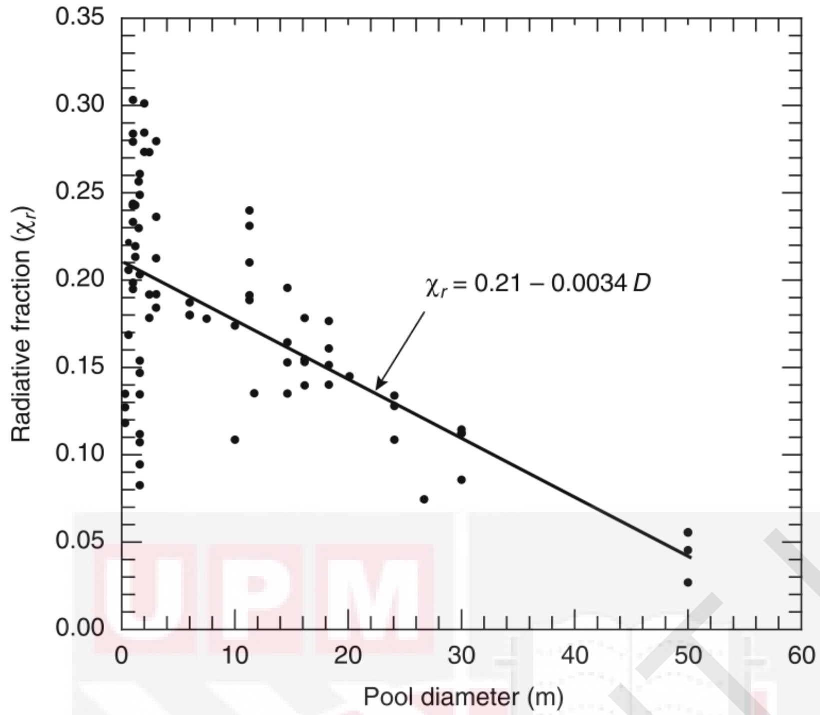

Figure 2.2: Radiative Fraction as a Function of Flame Diameter
(Source: Beyler, 2016)

From Figure 2.2, the radiative fraction, χ_r is a function of flame diameter and can be estimated as:

$$\chi_r = 0.21 - 0.0034D \qquad 2.4$$

where

D is the diameter of flame base (m), while for non-circular flame, an equivalent diameter correlation could be implemented to make radiative fraction correlation applicable. The equivalent diameter is given by:

$$D = \sqrt{\frac{4A}{\pi}} \qquad 2.5$$

where

A is the area of the flame base (m^2)

2.1.4 Atmospheric Transmissivity

A well-known term introduced in this section, atmospheric transmissivity factor, τ , signifies the effect brought upon by atmospheric absorption as well as atmospheric scattering towards the transmission of radiative heat flux (Gavelli, 2021; Paquet et al., 2019). The absorption and scattering nature of not only smoke around the burning flame but also water vapour and carbon dioxide in the surrounding area have the possibility to lessen the total thermal radiation emitted by a burning source towards a target. Factors such as the diameter of the burner would indirectly affect the relative absorption and scattering of thermal radiation by altering the amount of smoke produced. On the other hand, this would greatly affect the effective emissive power of the flame burner (Shen et al., 2019).

The determination of the transmissivity factor involves tedious calculations involving a number of parameters. According to Wan et al. (2019), the attenuation of thermal radiation from the atmosphere can be omitted for a small fire spacing. Jie Ji et al. (2020), in their research, pointed out that, for distances less than 10 m between the flame source and the receiving target at normal atmospheric conditions, the atmospheric absorption effect can be neglected. Hence, for simplicity of this work, the atmospheric transmissivity is assumed to be τ = 1. Similar assumptions have also been used in the research by Huang et al. (2020) and Beyler (2016).

2.1.5 Flame Morphology

The amount of heat transfer between two surfaces depends on the geometry and orientation of the surfaces and the distance between them. The configuration factor is the dimensionless quantity that represents the fraction of radiation leaving one surface that directly reaches another surface. In the case of a flame, the configuration factor will be a function of the size and shape of the combustion zone.

According to Audouin et al. (1995), the flame manifested from either a pool fire or a controlled gas burner comprises three different flame zones with varying characteristics. The three zones are the continuous flame zone, the intermittent flame zone, and the plume zone. The continuous zone is the region of flame established above the burner or surface of the pool fire, and it consists of visible flame that continuously presents during burning. The intermittent zone consists of the irregular flame pocket, which diverges away from the continuous flame zone and forms the maximum flame height, while the plume zone consists of the region with no presence of visible flame. The distribution of the flame zone is represented in Figure 2.3.

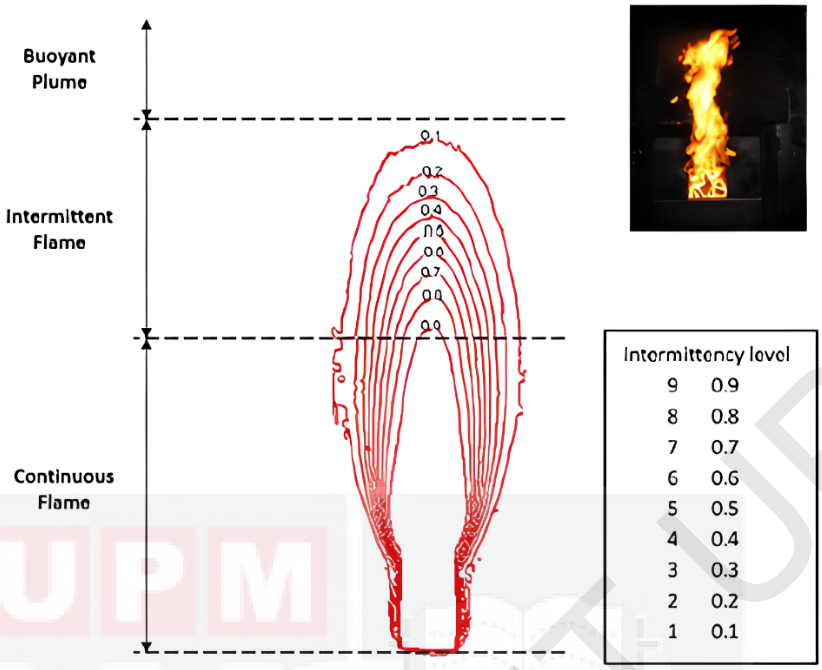

Figure 2.3: Schematic Representation of Three Flame Zones
(Source: Tang et al., 2012)

From the figure, it is noted that the visible portion of flame corresponds to the continuous flame and intermittent flame zones. Typically, it is assumed that the continuous flame extends from the base of the flame up until the region with the intermittency level of 0.95, while the intermittent flame is located between the 0.95 and 0.05 intermittency levels. The region beyond the intermittency level of 0.05 represents the buoyant plume (Q. Wang et al., 2013).

In relation to Figure 2.3, the intermittency level of 0.5 also corresponded to the mean flame height (Fleury et al., 2011; Tang et al., 2012). Due to the constantly fluctuating nature of the flame’s highest point, it is, therefore, more practical to define the flame height based on its mean value, as suggested by Fleury et al. (2011). Notably, correlations have been developed for estimating the height of the flame, including the well-known Heskestad’s correlation (Heskestad, 1983). However, in evaluating models' heat flux estimations for this research, the flame height information is derived from measured data, i.e., the information obtained from video image analysis.

2.2 Screen for Model Inclusion

As aforesaid, there are several different thermal radiation calculation methods available for predicting fire behaviour; nevertheless, delving into an exhaustive exploration of every existing flame radiation prediction method would be an extremely arduous and time-consuming task. Following the compilation of relevant literature, screening of radiation models ought to be carried out in contemplating the completion of research within the stipulated time frame through the most practical means possible. A rational way is to screen thermal radiation models that correspond to two inclusion criteria. The first is model accuracy, which determines the reliability in actual fire protection implementation, coupled with the model's universal compatibility or model complexity, which determines the real-life practicality.

The prediction of flame radiation is conventionally segregated into three primary categories: field model, empirical model, and semi-empirical radiation model (Li et al., 2023). Field models refer to thermal radiation models that require mass balance, energy balance, and momentum differential equation decoding to ascertain the complete course of combustion. Since this model requires Navier-Stokes equation resolution, field models are periodically known as computational fluid dynamics (CFD) models. On the contrary, the second cluster of models, the analytical model (empirical model), is developed from a simple fire experiment to sidestep the burdensome confrontation with sophisticated software in exchange for a prominently lower accuracy thermal radiation evaluation. The last grouping of models as well as the category of interest for this research, the semi-empirical model, is the thermal radiation model, which delivers the exquisite balance between results accuracy and model complexity (Rew et al., 1997; Zhou & Wang, 2019).

The purpose of this early screening is to weed out models inapplicable to the established criterion set beforehand. Thus, any CFD models and empirical models would be excluded from the studies. The main justification for the exclusion of field models is due to the inconsistency present for the type of software required to decipher the desired results, as well as the demanding and lavish computational resources, time, and expertise (Palazzi et al., 2017; Raj, 2007). The above vindication is also supported by Loy et al. (2018), which stated that the eradication of the geometrical assumption of flame had cost the CFD simulation greatly in the aspect of simulation duration, especially when multiple fire scenarios are considered.

On the other hand, the simplest type of model, the empirical model, is a regression analysis that relies on measuring a quantity based on one or multiple parameters without any predetermined trend. Predictions made by this type of model heavily rely on the available measurements, and any extrapolation beyond the experimental setup can result in significant errors (Bal, 2018). Nevertheless, the empirical fire behavior models continue to be employed in fire simulators (Castillo Soto et al., 2022). The oversimplified models are often used as sub-models to yield crucial boundary condition information for the simulation of fire dynamics using CFD fire tools. According to Sikanen and Hostikka (2016), conditional and time-dependent boundary conditions such as surrounding temperature, radiative degree, ambient wind drift, atmospheric condition, and periodic burning rate necessitate the involvement of empirical model(s) in fulfilling simulation preliminary standards. The highly circumscribed application, as well as the non-standalone flaw of empirical models, are undoubtedly the major exclusion criteria for the model itself.

In accordance with the process of elimination, the semi-empirical model is clearly the best-suited radiation model category to be assigned as the domain of interest in this study. Semi-empirical thermal radiation models are basically the arrangement of mathematical correlation derived from the extensive number of experimental results obtained through great series of fire experiments to understand fire behaviour (Zhou & Wang, 2019). This model simplifies the mass and energy balance, incorporating the measured data to refine and adjust the constants involved (Bal, 2018). This model outclassed both the field and empirical models in terms of suitability for the implementation in thermal radiation models' performance study due to its highly sensible approximation of fire deportment with minimal expenditure of effort and time. Flame geometry, complete combustion chemistry, and total radiative output are some of the quality parameters taken into consideration in the course of developing a semi-empirical model (Raj, 2007). Given the user-friendly and readily applied features, semi-empirical models are more favourable in most risk assessments, albeit the employment is only limited to predicting radiative heat from fire (Rew et al., 1997).

2.3 Semi-Empirical Thermal Radiation Models

As clarified in Section 2.2, the genre for models of interest in this research is those in the spectrum of semi-empirical thermal radiation models. Thermal radiation models hold a pivotal role in the realm of performance-based building design. These models serve as fundamental components both for manual calculation as well as within advanced fire simulation software, affording engineers and researchers the ability to comprehensively assess the thermal impact of fires on structures, occupants, and the surrounding environment. In performance-based design, thermal radiation models are used to predict heat flux, temperature distributions, and fire spread patterns within a building or a specific environmental setting. To achieve this, the models rely on input data encompassing variables such as fuel types, fire sizes, and prevailing environmental conditions. Through these estimations, thermal radiation models offer invaluable insights into fire behaviour across diverse scenarios. Such insights are indispensable in the design of fire protection systems, the evaluation of structural fire resistance and building stability, as well as the assurance of occupant safety (Nguyen & Kohno, 2023).

According to Singleton (2002) and Martínez (2019), radiation modelling is the representation of actual flame morphology using simplified geometry to predict the heat transfer process through computational analysis. The estimated morphology is commonly represented by the configuration of a plane, cylinder, cuboid, or even a set of points. In line with the assertions made by Xu et al. (2022) and Pinto et al. (2023), reinforced by the research of Palazzi et al. (2017) and Raj (2007), it is posited that semi-empirical thermal radiation models can be classified into two main categories: point source models and solid flame models. The former model treated radiative heat interaction as if it originated from a certain point(s) within the fire and regressed when the receiving target moved further from the fire. While the latter model, the solid flame model, exhibited a more substantial theoretical basis and more sensible flame geometry for representing actual fire. In relation to this, radiative heat flux emitted from each surface of the designated solid geometry is the main foundation for the solid flame model in estimating the degree of hazard emanating from the source of the fire.

In alignment with this classification, the present research incorporated a total of two point source models and eight solid flame models after critical screening from a wide range of literature spanning several years. Table 2.1 provides a detailed overview of all the models included in this study.

Table 2.1: Thermal radiation models assessed in this research

Type of Model	Solid Flame Model	Publication
Point Source Model	Single point source model	Modak (1977)
Point Source Model	Weighted multi point source model	Wan et al. (2019)
Solid Flame Model	Shokri and Beyler simple correlation	Shokri & Beyler (1989)
Solid Flame Model	Shokri and Beyler detailed method	Shokri & Beyler (1989)
Solid Flame Model	Mudan method	Mudan (1984)
Solid Flame Model	Dayan and Tien method	Dayan & Tien (1974)
Solid Flame Model	Rectangular planer model	Fleury et al. (2011)
Solid Flame Model	Cuboid flame model	Wan et al. (2018)
Solid Flame Model	Multi cuboid flame model	Huang et al. (2019)
Solid Flame Model	Multi cylinder flame model	Ji et al. (2020)

2.3.1 Single Point Source Model

One of the most common and simplest radiation models that are widely used is the single point source model. Given its simplicity, the single point source model predicts radiant heat transfer from a fire to a target by establishing a relationship between the flame heat flux and the inverse square of the separation distance between the source of flame and a target (Beyler, 2016). Rather than assuming a three-dimensional solid flame representation or a two-dimensional planar representation as the basis for the flame geometry, as the name suggests, all the radiant heat released from the fire source is assumed to originate from a single point within the flame region. The isotropic heat energy then travels in radial directions and transfers energy to any object on its path. This approach is established without the involvement of a configuration factor. The single point source model applies the relative angle between the centre point of fire and the position of the receiving target. The distance, R is given by the displacement from the centre of flame to the receiving target, as shown in Figure 2.4.

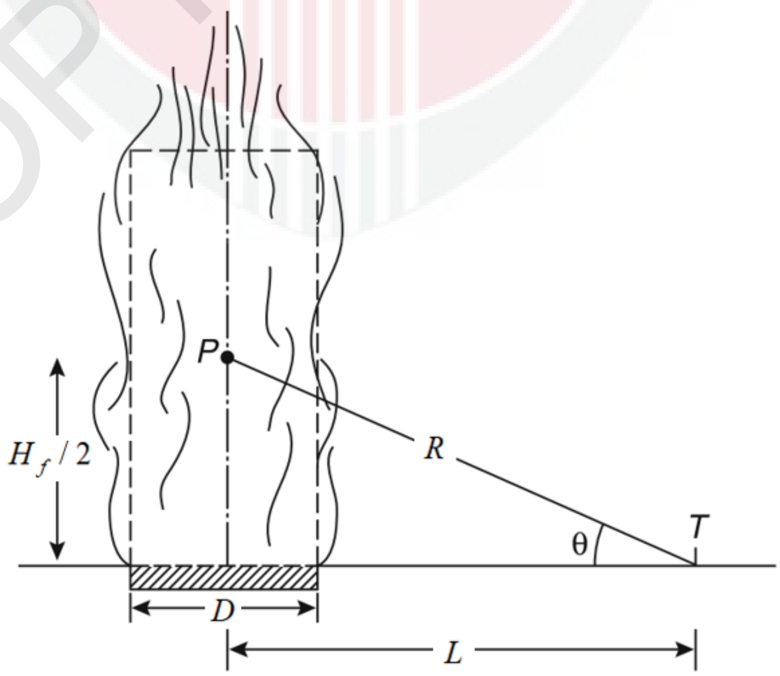

Figure 2.4: Schematic Representation of the Single Point Source Model
(Source: Beyler, 2016)

The incident radiant heat flux is given by:

$$\dot{q}'' = \frac{\dot{Q}_r \cos\theta}{4\pi R^2} \qquad 2.6$$

where

$\dot{Q}_r$ is the radiative heat output (kW), refer to Equation 2.7

θ is the angle between normal and line of sight from the target to the flame source (rad)

R is the displacement from the receiving target and the centre of flame (m)

The distance R can be calculated using the Pythagorean theorem:

$$R = \sqrt{L^2 + \left|\frac{H_f}{2} - H_t\right|^2} \qquad 2.8$$

where

H_t is the height of the target relative to the height of the equivalent point source at $H_f / 2$ (m)

L is the horizontal distance from the centre of the base of the fire to the target (m)

Beyler (2016) noted that the point source configuration, as shown in Figure 2.4, is known to be a very simplistic representation of a pool fire. It offers an acceptable heat flux prediction between a fire and a target at larger distances. Results obtained by Modak (1977) showed that when the ratio of the horizontal distance from the centre of a pool fire to the diameter of the pool exceeded 2.5, the single point source model was able to generate results within 5% of the measured incident heat flux.

2.3.2 Weighted Multi Point Source Model

According to Wan et al. (2019), the weighted multi point source model assumes that multiple point sources of fire are distributed uniformly along the entire vertical flame axis, with the weighted sum of radiation from every single point making up the total radiation directed towards the receiving target. A notable characteristic of the model is that the independence of a configuration factor enables the calculation of radiant heat flux originating from more than a single fire source.

Given the previously noted limitation of the single point source model in predicting near-field flame radiation, the weighted multi point source model aims to provide an appropriate estimation for both near-field and far-field scenarios. Assuming that *N* point sources are uniformly distributed vertically along the flame axis, the overall radiation heat flux emitted by a flame source is given by:

$$\dot{q}'' = \sum_{j=1}^{N} \frac{w_j \dot{Q}_r \cos\theta_j}{4\pi R_j^2} \qquad 2.9$$

where

θ_j is the angle between normal and line of sight from target to flame source (rad)

R is the displacement from the receiving target and the centre of flame (m)

w_j is the weight of the jth point source

$\dot{Q}_r$ is the radiative heat output (kW)

$\dot{Q}_r$ can be determined using Equation 2.3, while w_j always satisfies $\sum_{j=1}^{N} w_j = 1$.

The weight distribution of point sources for a flame is always uniform with the vertical radiation distribution. Since the vertical radiation distribution can be segregated into the continuous zone (T_f is constant throughout) and intermittent zone (increases with decreasing height), the specific weights are greatly affected by the shape of the flame, as shown in Figure 2.5.

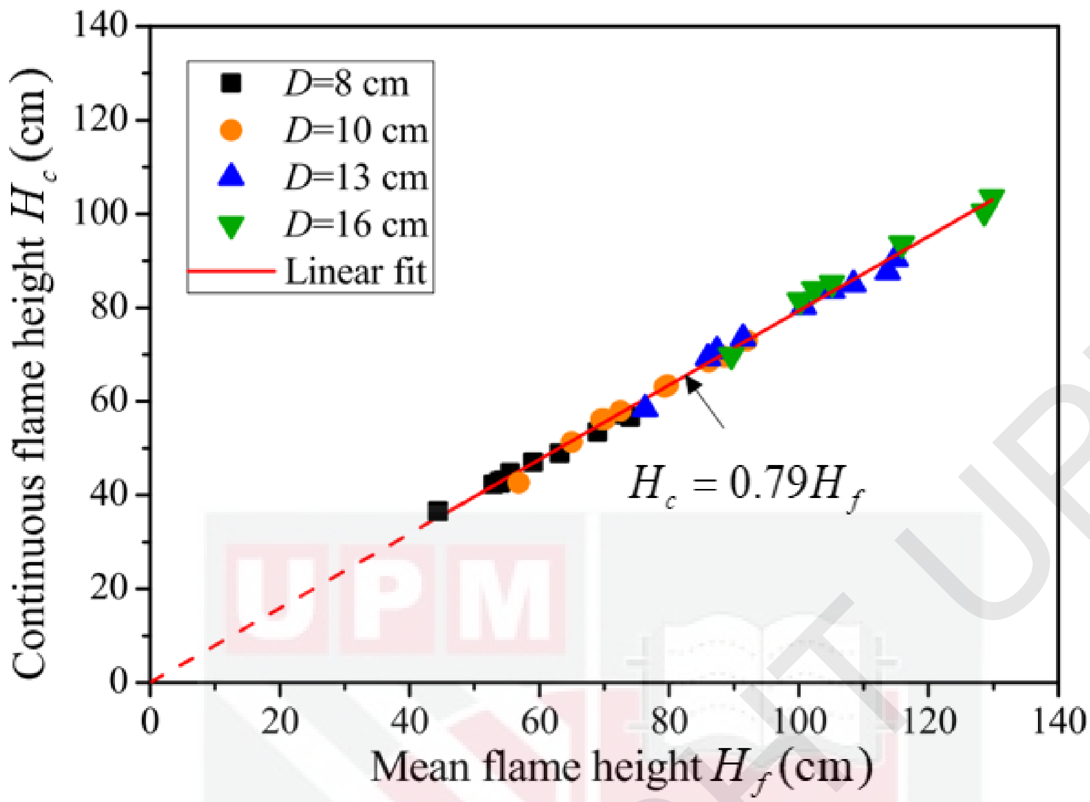

Figure 2.5: Relationship between Continuous Flame Height and Intermittent Flame Height
(Source: Wan et al., 2019)

Figure 2.5 shows the relationship between flame height in the continuous zone and flame height in the intermittent zone, where the data represent the linear function of $H_c = 0.79H_f$. Wan et al. (2019) assumed that the continuous zone and intermittent zone flames took the shape of a cuboid and cone, respectively, the calculated flame volume fraction for the continuous zone is 0.92, while the remaining (0.08) is for the intermittent zone.

This information later led Wan et al. (2019) to an assumption that a total of 10 point sources (N=10) are distributed evenly along the flame axis. Reciprocally, a similar assumption will also be applied for this research, where the visible portion of the flame is assumed to consist of ten different points within the fire. Therefore, the receiving target receives heat flux emitted by ten different points, which differ in values depending on the relative distance and angle between the receiver and emitter. The positioning of point sources is shown in Figure 2.6.

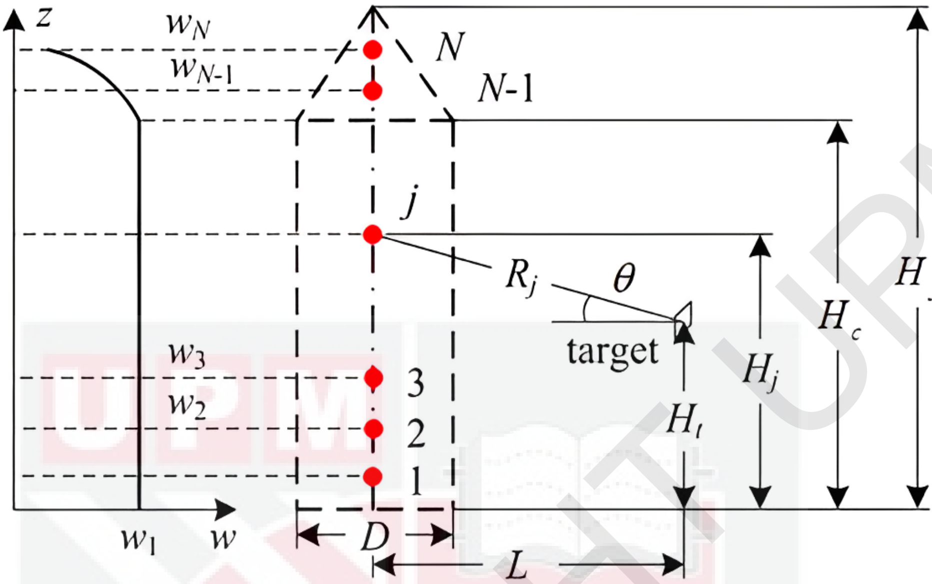

Figure 2.6: Schematic Representation of the Weighted Multi Point Source Model
(Source: Wan et al., 2019)

Figure 2.6 shows two point sources are allocated at the cone-shaped intermittent flame zone, while the remaining eight point sources are included in the cuboid-shaped continuous flame zone. By computing the flame volume fraction for each point source, the specific weight, w_j is given by:

$$\text{Continuous zone: } w_j = 0.115,\ j = 1, 2, \ldots, 8 \qquad \text{Intermittent zone: } w_9 = 0.07,\ w_{10} = 0.0.1 \qquad 2.10$$

For simplicity, Equation 2.8 can be expressed as:

$$\dot{q}'' = \sum_{j=1}^{N} \frac{w_j \dot{Q}_r \cos\theta_j}{4\pi R_j^2} = \frac{\dot{Q}_r}{4\pi} \sum_{j=1}^{N} \frac{w_j L}{R_j^3} \qquad 2.11$$

where

$$R_j = \left(L^2 + \left(H_j - H_t\right)^2\right)^{1/2},\quad H_j = \frac{2j-1}{2N} H_f,\ N = 10 \qquad 2.12$$

2.3.3 Shokri and Beyler Correlation

Shokri and Beyler (1989) established a basic correlation based on large pool fire experimental results. This approach measures the radiant heat flux at the ground level, which is greatly affected by the vertical target's radial location. The term 'ground level' represents the height of the flame in relation to the base of the fire. The correlation which calculates the radiant heat flux is given by the equation below:

$$\dot{q}'' = 15.4\left(\frac{L}{D}\right)^{-1.59} \quad 2.13$$

where
$\dot{q}''$ is the radiant heat flux (kW/m^2)
L is the horizontal distance from the centre of the base of the fire to the target (m)
D is the diameter of the flame base (m)

This expression, however, is only recommended for vertical targets with flame height equal to ground level (flame base). Nevertheless, the model is still useful for preliminary assessments despite its limited generality. Besides the limitation mentioned previously, the method is also limited to luminous flame and might not be suitable for non-luminous flame. In addition, Fleury et al. (2011) also reported that the correlation systematically over-predicted the results for larger flame diameters.

2.3.4 Shokri and Beyler Detailed Method

The methods mentioned in the previous section are known to suffice only as basic screening methods and might not be adequate if high-precision analysis is required. Apart from the simple correlation, Beyler (1989) also introduced more comprehensive and detailed methods for predicting radiant heat flux. The model is based on a basic but practical flame model with the usage of appropriate assumptions. For this, the flame shape is speculated to take the form of a cylindrical black body with constant radiation and homogeneous emissive power throughout the whole flame.

Thermal radiation is assumed to be emitted from the visible portion of the cylindrical flame surface. Similar to the previous simple correlation, this method is developed using pool fire experimental data. Shokri and Beyler (1989) have treated radiant heat transfer from a source to a target based on the concept of the angle factor, also variously known as the shape, configuration, geometrical, or view factor.

The incident radiative flux to the target from the fire source is given by:

$$\dot{q}'' = EF_i \qquad 2.14$$

where

$\dot{q}''$ is the radiant heat flux (kW/m^2)

E is the emissive power of flame (kW/m^2), refer to Equation 2.15

F_i is the view or configuration factor from fire to target

The configuration factor always takes a value between zero and one, depending on the target location, flame height, and flame diameter. When the target is at a close distance to a fire source, the view received by the target would consist mostly of the flame, thus, the configuration factor approaches unity.

Figure 2.7 and Figure 2.8 provide the explicit schematic and nomenclature for Shokri and Beyler detailed method for vertical and horizontal targets located at both the ground level and above ground level.

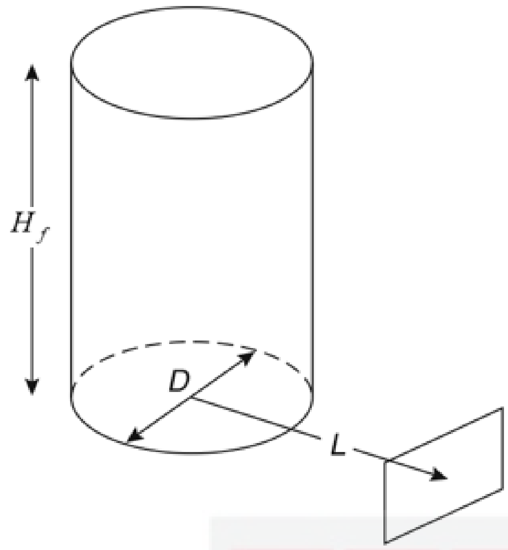

Figure 2.7: Cylindrical Flame-Shape Configuration Factor Geometry for Vertical and Horizontal Targets at Ground Level
(Source: Beyler, 2016)

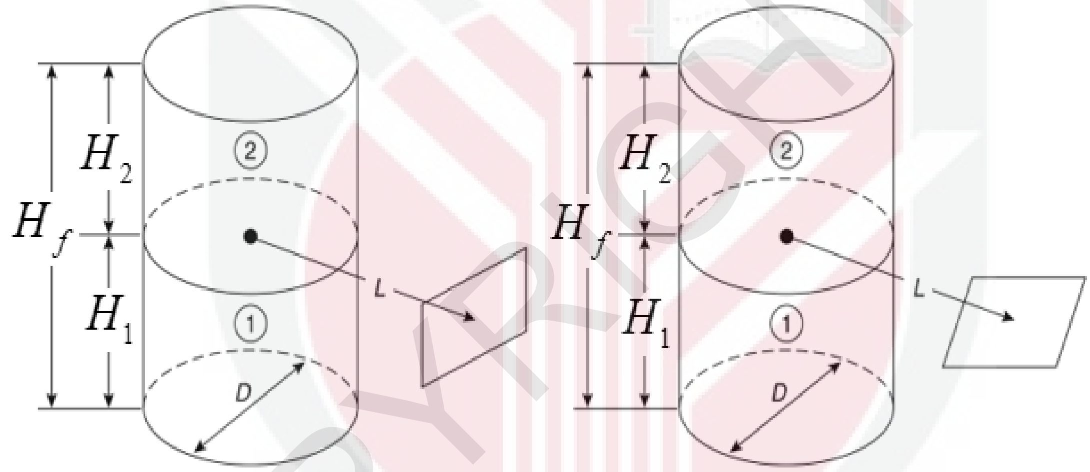

Figure 2.8: Two-Cylinder Configuration Factor Geometry for Vertical and Horizontal Targets Above Ground Level
(Source: Beyler, 2016)

In this case, one cylindrical flame model is used to represent the flame for a target at ground level, while the cylinder is broken down into two individual cylinders for the target above ground level. From Figure 2.7 and Figure 2.8, the flame is constructed with a diameter equal to the diameter of the pool, D and a height equal to the height of the flame, H_f. Using the flame height and diameter information, the configuration factor for horizontal $F_{i,H}$ and vertical targets $F_{i,V}$ can be determined with the equation below:

$$F_{i,H} = \frac{\left(B - \frac{1}{S}\right)}{\pi\sqrt{B^2 - 1}} \tan^{-1}\sqrt{\frac{(B+1)(S-1)}{(B-1)(S+1)}} - \frac{\left(A - \frac{1}{S}\right)}{\pi\sqrt{A^2 - 1}} \tan^{-1}\sqrt{\frac{(A+1)(S-1)}{(A-1)(S+1)}} \qquad 2.16$$

$$F_{i,V} = \frac{1}{\pi S} \tan^{-1}\left(\frac{h}{\sqrt{S^2 - 1}}\right) - \frac{h}{\pi S} \tan^{-1}\sqrt{\frac{(S-1)}{(S+1)}} + \frac{Ah}{\pi S\sqrt{A^2 - 1}} \tan^{-1}\sqrt{\frac{(A+1)(S-1)}{(A-1)(S+1)}} \qquad 2.17$$

where

$$A = \frac{h^2 + S^2 + 1}{2S}, \quad B = \frac{1 + S^2}{2S}, \quad S = \frac{2L}{D}, \quad h = \frac{2H_f}{D} \qquad 2.18$$

The maximum configuration factor F_{max}, is given by the vector sum of the horizontal and vertical components:

$$F_{max} = \sqrt{F_{i,H}^2 + F_{i,V}^2} \qquad 2.19$$

Equation 2.15 is applied for vertical targets, both for ground level as well as above ground level targets. In the case of vertically oriented targets located above ground level, the equation must be applied for both sections of the cylinder (see Figure 2.8), yielding two configuration factors, $F_{i,V1}$ and $F_{i,V2}$. The sum of the configuration factor is thus given by the equation below:

$$F_{i,V} = F_{i,V1} + F_{i,V2} \qquad 2.20$$

On the other hand, horizontal targets only necessitated one equation (Equation 2.14), both for above-ground targets and ground-level targets. This is due to the assumption that only one side of the target can absorb radiation at a time. Thus, only one of the two cylinders (see Figure 2.8) would act as the radiation source. For calculation purposes, one must determine which surface is needed, either the surface facing upwards or the one facing downwards, depending on the actual fire scenario.

By fitting experimental heat flux data from a pool fires experiment, Shokri and Beyler (1989) established the method of calculating the effective emission power from a given burning source. The effective emissive power in terms of effective pool diameter is given by the following equation:

$$E = 58\left(10^{-0.00823D}\right) \qquad 2.21$$

This correlation represents the average emissive power brought upon by the entire flame rather than being the local emissive power depicted at a specific point in space. It is necessary to note that the ‘effective’ power of flame is defined only in terms of a homogeneous radiation model and not the local emission power, which is depicted directly from a heat flux gauge. Unarguably, the emissive power is significantly less than the actual attained value due to the formation of black smoke outside the flame, which greatly affects the radiation from the luminous flame.

2.3.5 Mudan Method

Mudan (1984) has introduced an alternative to understanding radiant heat flux from fire sources for both no-wind conditions as well as for wind-blown conditions of flames. Nevertheless, only the wind-free condition would be a concern in this investigation, while wind-blown flame models are excluded. The radiant heat flux from the fire source on the target can be estimated using the equation below:

$$\dot{q}'' = EF_i\tau \qquad 2.22$$

where
$\dot{q}''$ is the radiant heat flux (kW/m^2)
E is the emissive power of flame (kW/m^2)

F_i is the view or configuration factor between the target and the burning source
τ is the atmospheric transmissivity factor

The Mudan method also revolves around the theory that the flame behaves and takes the shape of a cylinder. In relation to this, some important parameters, such as the height of the flame and flame diameter, must be known before calculating radiant heat flux. The correlation based on the mean visible height of the flame, H_f, of turbulent diffusion flames (wind-free condition) formed the basis for the flame height correlation, which would be implemented in this method.

Similar to the previous section, factors such as the shape of a flame, the separation distance between the fire source and the receiving target, as well as the positioning of the target greatly influenced the radiation heat transfer between the source and target. Therefore, the same principle in determining the configuration factor, F_i (Equation 2.14 - 2.18) can be implemented in this section.

The effective emissive power, E however, is dissimilar compared to the previous section. For the Mudan method, the effective emissive power, E is determined as below:

$$E = E_{max} e^{(-sD)} + E_s \left(1 - e^{(-sD)}\right) \qquad 2.23$$

where
E_{max} is the equivalent black body emissive power (kW/m^2)
s is the extinction coefficient (m^{-1})
D is the diameter of the flame base (m)
E_s is the emissive power of smoke (kW/m^2)

2.3.6 Dayan and Tien Method

Similar to the Shokri and Beyler detailed method and the Mudan method, the basis for the Dayan and Tien method is done by assuming that the flame source took the shape of a cylinder. The homogeneous cylinder with uniform temperature is considered a vertical surface with radius, $r = D/2$ and height equivalent to the mean flame height. The shape geometry and differential area specification are shown in Figure 2.9.

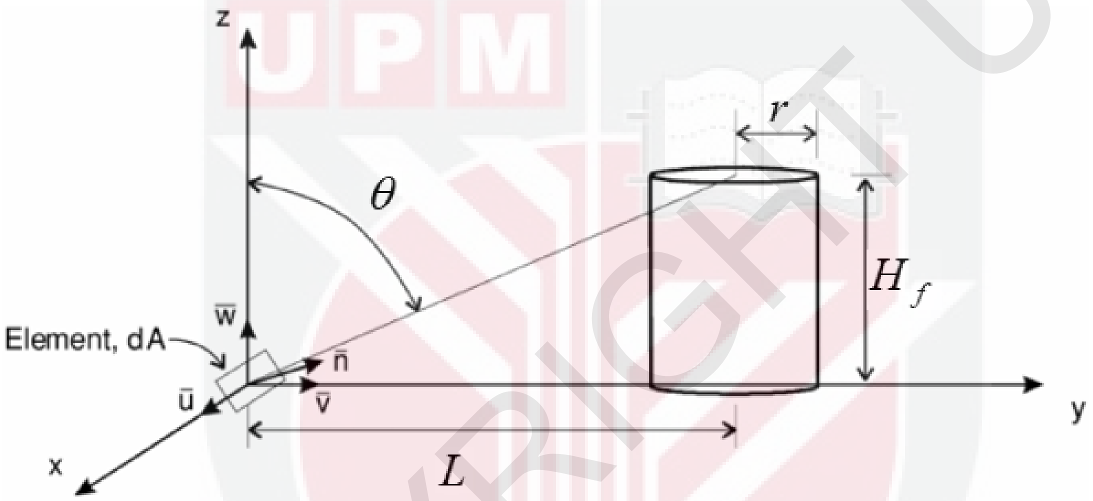

Figure 2.9: Schematic Diagram of Radiation Exchange Between a Homogeneous Cylindrical Flame Towards the Target Element
(Source: Fleury et al., 2011)

The unit vector at normal to a target element, dA (at [0,0,0]) in Figure 2.9 is denoted by the subscript u, v, and w along x, y, and z coordinates, respectively. The unit normal vector follows that:

$$\bar{n} = u\bar{i} + v\bar{j} + w\bar{k} \qquad 2.24$$

and,

$$\sqrt{u^2 + v^2 + w^2} = 1 \qquad 2.25$$

The expression for calculating the radiant heat flux to the target is as follows:

$$\dot{q}'' = \sigma\varepsilon T_f^4 \left(F_1 + F_2 + F_3\right) \qquad 2.26$$

where

$$\varepsilon = 1 - e^{-0.7\mu} \qquad 2.27$$

$$\mu = \frac{2r\kappa}{\sin\beta} \qquad 2.28$$

$$\beta = \frac{\theta + \frac{\pi}{2}}{2} \qquad 2.29$$

$$F_1 = \frac{u}{4\pi}\left(\frac{r}{L}\right)^2 \left(\pi - 2\theta + \sin 2\theta\right) \qquad 2.30$$

$$F_2 = \frac{v}{4\pi}\left(\frac{r}{L}\right) \left(\pi - 2\theta + \sin 2\theta\right) \qquad 2.31$$

$$F_3 = \frac{w}{\pi}\left(\frac{r}{L}\right) \left(\cos^2\theta\right) \qquad 2.32$$

κ is the effective flame absorption coefficient (m^{-1})
β is the mean value for θ (rad)
θ is the angle between the line of sight (target to centre-top of the cylinder) and the z-axis (rad)

Coherent to Shokri and Beyler detailed method, this method can be applied to the calculation of both ground-level and above-ground-level targets. Similarly, the flame model must be separated into two different cylinders in the case of the target located at an elevated position. Thus, the target is assumed to achieve total radiant heat flux from the sum of heat emitted from the upper cylinder and lower cylinder (refer to Figure 2.8).

According to He (2001), the main benefit of the method proposed by Dayan and Tien is the mathematical simplicity presented by the technique over the exact method; this advantage diminishes the estimation of computerised engineering. In addition, the calculation using this method often underestimates the maximum configuration factors between the source of fire and the target element when the interval is large. However, the errors are usually capped at 3.5% for both great flame height and further distance targets.

Equation 2.24 holds true when the target element, in the orientation posing for maximal configuration factor, does not induce changes in the geometry of the finite companion viewed from the position of the target element. The restriction of validity for the particular configuration discussed in this research is that the ratio of the distance between the flame axis and the differential area must be greater than 1.07 (He, 2001).

2.3.7 Rectangular Planar Model

The rectangular planar model is one of the attempts by Fleury et al. (2011) to develop an original radiation model for predicting heat flux. The goal is to step away from the traditional ideology of cylindrical flame form with the emergence of a more modern model. Myriads of different versions of the cylindrical flame model have been introduced previously; however, the normal occurrence of fire scenarios seldom involves a circular object as the base of the fire. For instance, during fire emission in a building, the burning item frequently revolved around standard-size furniture, which takes the shape of a rectangular cross-section object rather than the unusual round-shaped unit. Therefore, Fleury et al. (2011) came up with a different model that permits the estimation of radiant heat flux from non-circular fires; the geometry of the model is shown in Figure 2.10.

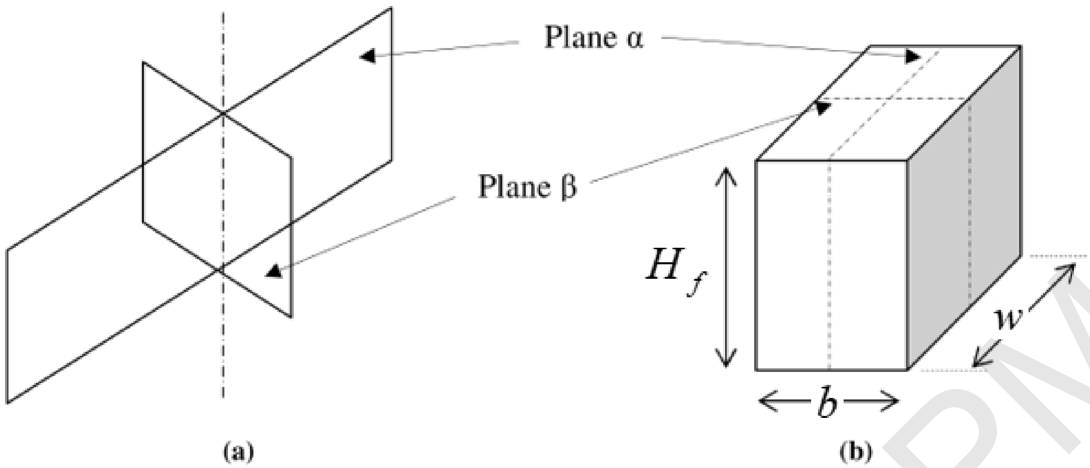

Figure 2.10: (a) Two Intersecting Planes Forming a Line (b) Rectangular Cuboid Formed from Two Intersecting Planes
(Source: Fleury et al., 2011)

The theory behind this model is that the flame resembled two intersecting planes perpendicular to one another. From the centre of the flames, the line of intersection between these two planes stretches vertically. As shown in Figure 2.10, the centreline planes for the rectangular cuboid are illustrated by the intersection between the two planes. The main objective of the assumption is to provide a more general flame geometry as an alternative to the common cylindrical flame model.

According to Fleury et al. (2011), the plane α has a length, w (m), and the plane β has a width, b (m) which is equivalent to the base length of the fire source and base width of the fire source, respectively.

The radiant heat flux towards a target element can be calculated below:

$$\dot{q}'' = F_i \sigma \varepsilon T_f^4 \qquad 2.33$$

where

$$F_i = \frac{2}{\pi XY}\left[\begin{array}{l} X\sqrt{1+Y^2}\tan^{-1}\left(\dfrac{X}{\sqrt{1+Y^2}}\right)+Y\sqrt{1+X^2}\tan^{-1}\dfrac{Y}{\sqrt{1+X^2}} \\ -X\tan^{-1}\left(X\right)-Y\tan^{-1}\left(Y\right)+\ln\left[\dfrac{\left(1+X^2\right)\left(1+Y^2\right)}{1+X^2+Y^2}\right]^{1/2} \end{array}\right] \quad 2.34$$

$$X = \frac{H_f}{L} \qquad Y = \frac{b}{L} \quad 2.35$$

σ is the Stefan-Boltzmann constant (5.67E-8 W/m^{2}K^4)
ε is the flame emissivity
T_f is the flame temperature (K)

The existing configuration factor formula by Ivanova and Muneer (2017) can be implemented into this method. Equation 2.32 allowed the calculation of the configuration factor for two directly opposite rectangular surfaces parallel to one another. The configuration factor formula enabled the orientation of the differential element to be done at any parallel angle with respect to the burning source. This is especially helpful for calculating configuration factors using a computer-programmed heat radiation model, given any parameter changes. This can be described more efficiently in Figure 2.11.

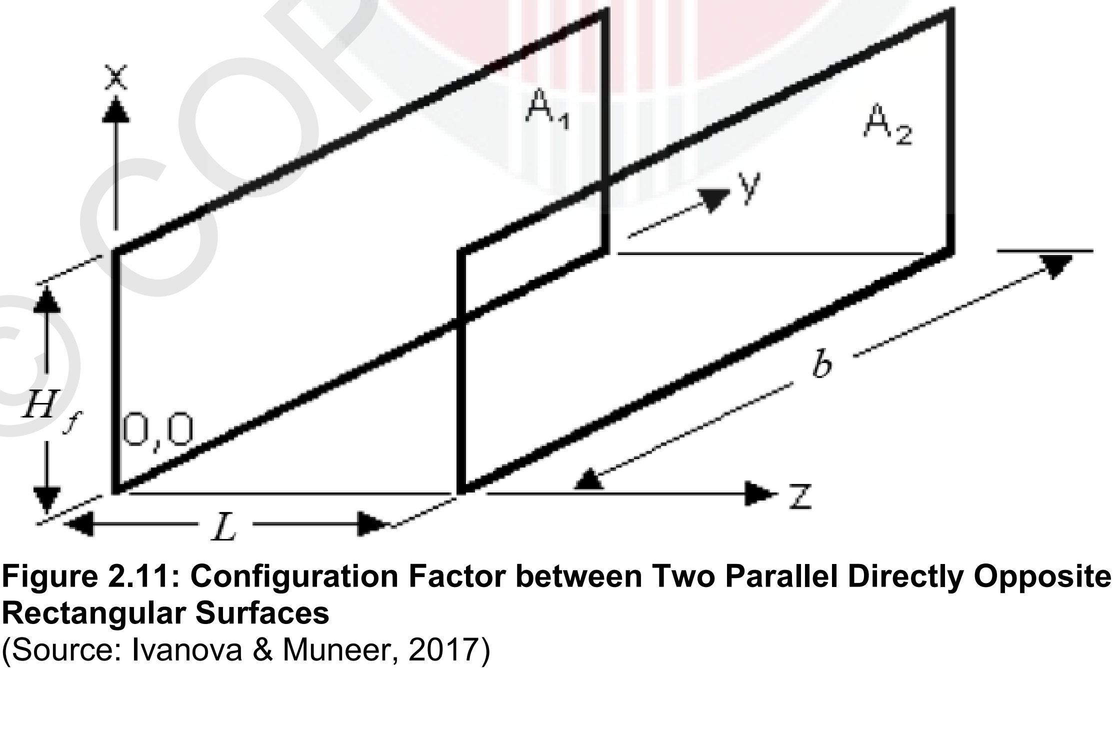

Figure 2.11: Configuration Factor between Two Parallel Directly Opposite Rectangular Surfaces
(Source: Ivanova & Muneer, 2017)

The figure above indicates that the target must be in a position that is parallel to that rectangular plane while being separated by distance, L from one face of the rectangular burner. If this requirement is fulfilled, the demand for formula can be considerably reduced. Nevertheless, such condition is rarely satisfied for real-life fire scenarios since possible combustion targets would be positioned all across the space. To address this matter, different components that constructed the overall configuration factor need to be added or taken down.

The flame emissivity can be determined through the following formula:

$$\varepsilon = 1 - e^{-\kappa D} \quad 2.36$$

where
κ is the effective flame absorption coefficient (m^{-1})
D is the diameter of the flame base (m)

2.3.8 Cuboid Flame Model

According to Wan et al. (2018), the cuboid flame model provides a better option than both the single point source model and the Mudan method in calculating radiant heat flux from a rectangular propane gas burner with a width-to-breadth aspect ratio equal to 2. Since the conventional cylindrical flame model (Mudan method) yields sizeable errors for propane gas flames of larger aspect ratios, extensive studies have been established to improve the shortcomings. In relation to this, Wan et al. (2018) developed a cuboid flame model to predict radiant heat flux to a target. The model is initially targeted for the ignition of everyday household furniture, which is more commonly found as cuboidal shapes rather than cylindrical or spherical. Huang et al. (2020) have also examined the cuboid flame model, and a comparison of heat flux estimation between the cuboid flame model and single point source model has highlighted the improvement presented by the cuboid flame model. The cuboid flame model assumes that both the top and side surfaces of the cuboid emit radiation with equivalent intensity to the surroundings, as shown in Figure 2.12.

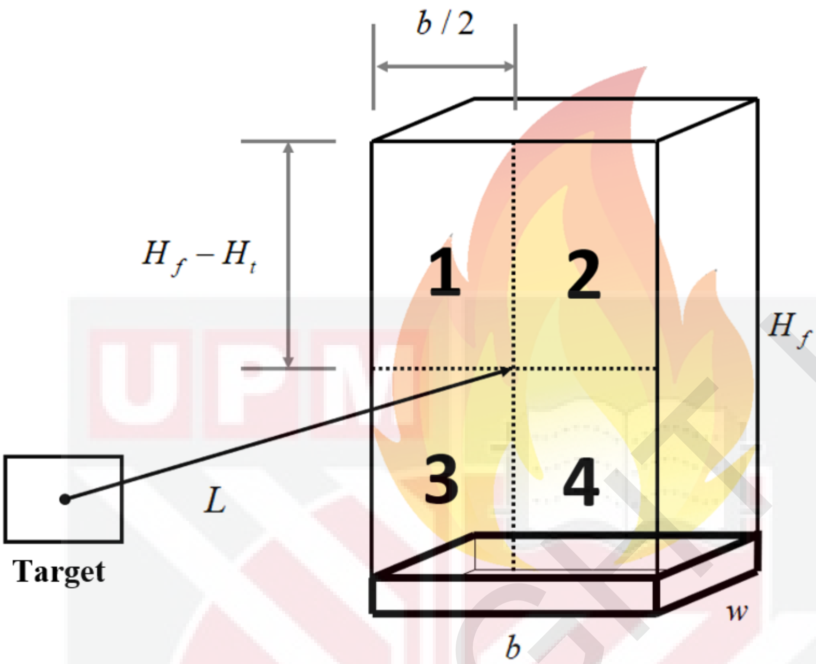

Figure 2.12: Schematic Representation of the Cuboid Flame Model

Using the four imaginary partitions of the cuboid flame model with respect to the position of the target, as shown in Figure 2.12, the calculation of heat flux is given by:

$$\dot{q}'' = \frac{\tau F_i \chi_r \dot{Q}}{2bH_f + 2wH_f + wb} \quad 2.37$$

where

$$F_i = F_{O-F} = \sum_{i=1}^{4} F_{O-F,i} = F_{O-F,1} + F_{O-F,2} + F_{O-F,3} + F_{O-F,4} \quad 2.38$$

and

$$F_{O-F,j} = \frac{1}{2\pi}\left[\frac{H_j}{\sqrt{H_j^2+L^2}}\tan^{-1}\left(\frac{W_j}{\sqrt{H_f^2+L^2}}\right)+\frac{W_j}{\sqrt{W_j^{\,2}+L^2}}\tan^{-1}\left(\frac{H_j}{\sqrt{W_j^2+R^2}}\right)\right]$$

$$\begin{aligned} & j = 1,2,3,4 \\ & W_1 = W_2 = W_3 = W_4 = b/2 \\ & H_1 = H_2 = \begin{cases} H_f - H_t & for\ \ H_t < H_f \\ H_f & for\ \ H_t \geq H_f \end{cases} \\ & H_3 = H_4 = \begin{cases} H_t & for\ \ H_t < H_f \\ 0 & for\ \ H_t \geq H_f \end{cases} \end{aligned} \qquad 2.39$$

2.3.9 Multi Cuboid Flame Model

According to Huang et al. (2019), for a conventional solid flame model, differences in the flame morphology greatly influence the total radiant heat flux transfer from the point of burning to the receiving target. When dealing with fuel sources of varying aspect ratios or diameters, both the flame's height and the flame's division (i.e., by the formation of sub-flames) are impacted by the changes arise from different levels of air entrainment in various directions. This influence is particularly pronounced in the case of a rectangular burner with a high aspect ratio, where the longer sides are more exposed to air entrainment. Notably, the original cuboid flame model does not consider this factor. Recognising this limitation, Huang et al. (2019) introduced the multi cuboid flame model, which assumes that every sub-flame originating from a single fire source is treated as a distinct cuboid flame unit, as shown in Figure 2.13. Huang et al. (2019) asserted that the multi cuboid model outperforms the cuboid flame model for burners with an aspect ratio greater than 2.

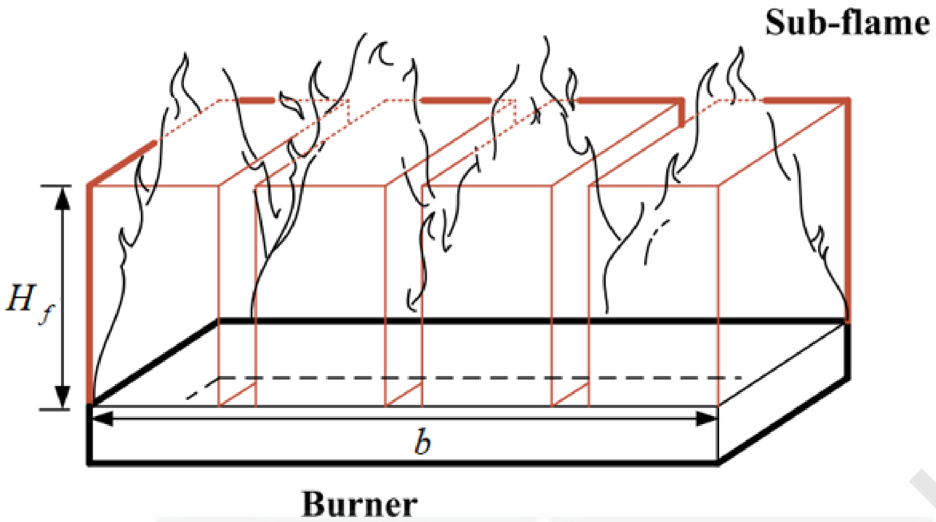

Figure 2.13: Schematic Representation of the Multi Cuboid Flame Model
(Source: Huang et al., 2019)

By noting the ability of flame to split into smaller sub-flames, as shown in the figure above, the total number of sub-flames that would be used for this work is n = 3 since the experimental results only revolve around laboratory-scale combustion. According to the concept of Huang et al. (2019), a flame produced by a burning source is comprised of several cuboid sub-flames that are uniform in terms of firepower as well as volume, as shown in Figure 2.13. Therefore, the total radiant heat flux emitted can be estimated as below:

$$\dot{q}'' = \sum_{i=1}^{n} \frac{\tau F_i \chi_r \dot{Q}}{2bH_f + 2nwH_f + wb} \qquad 2.40$$

where

F_i is the configuration factor from fire to target
τ is the atmospheric transmissivity
χ_r is the radiative fraction
$\dot{Q}$ is the total heat release rate (kW)
H_f is the height of the flame(m)
b is the breadth of the flame base (m)
w is the width of the flame base (m)
n is the number of multi cuboid flames

The configuration factor for individual sub-flames is calculated using Equations 2.36 and 2.37. During this research, the performance of the multi cuboid flame model was tested using various numbers of sub-flames along the longer side of the burner. The results indicated that the model performed best when configured with three cuboid flames. Therefore, despite Huang et al. (2019)'s depiction of four sub-flames in Figure 2.13, this research will assess the multi cuboid flame model's performance using three flame divisions.

2.3.10 Multi Cylinder Flame Model

By considering flame emissivity, Ji et al. (2020) proposed a new radiation model by taking the conventional cylindrical flame model as its basis. Besides emissivity, the model also makes allowances for the variation in flame temperature and diameter. The main assumption is that the flame is considered to be made up of multiple identical thin cylinders with height Δz and diameter D as shown in Figure 2.14.

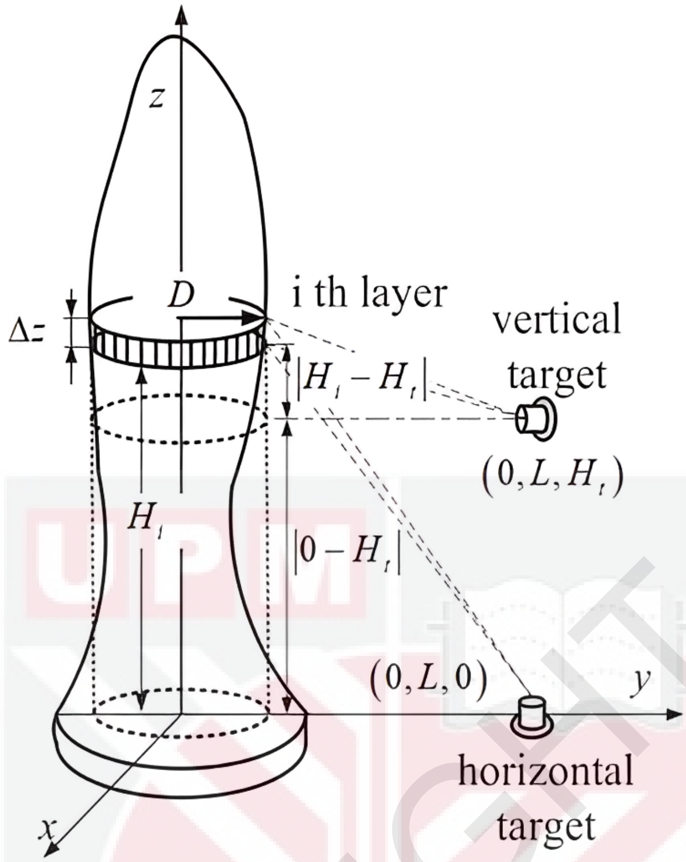

Figure 2.14: Schematic Representation of the Multi Cylinder Flame Model
(Source: Ji et al., 2020)

For this work, the fire is assumed to be made up of four identical cylinders. This number is obtained after testing the model with several number of cylindrical flame model configuration. The total radiant heat flux emitted is thus equivalent to the sum of the heat flux of all cylinders and can be calculated as below:

$$\dot{q}'' = 0.80\varepsilon\sigma \times \sum_{1}^{n} \tau F_{f(i)-f(t)} \left(H_i / H_m\right)^{-0.32} \left(\left(T_f - T_a\right)_z + T_a\right)^4 \qquad 2.41$$

where
N is the number of cylinders
τ is the atmospheric transmissivity
σ is the Stefan-Boltzmann constant (5.67 x 10^{-8} W/m^2 K^4)

Ji et al. (2020) stated that emissivity, ε can be determined using the method proposed by Babrauskas (1983), as expressed by the following equation:

$$\varepsilon = 1 - \exp(-\kappa\beta D) \qquad 2.42$$

where κ is the effective emission/absorption coefficient, while (Zalosh, n.d.) noted in his study that the mean equivalent beam lengths, β are influenced to some extent by flame geometry but are approximately equivalent to the flame radius.

The view factor of the i[th] cylinder from the vertical target element is given by:

$$F_{f(i)-f(t)} = F\left(\left|H_i - H_t\right| + \Delta z, D, L\right) - F\left(\left|H_i - H_t\right|, D, L\right) \quad 2.43$$

Using the flame height, flame diameter, and distance from the flame to the target, the configuration factor for a vertical target $F_i\left(H_t, D, L\right)$ can be determined by:

$$F_i = \frac{1}{\pi S}\tan^{-1}\left(\frac{h}{\sqrt{S^2-1}}\right) - \frac{h}{\pi S}\tan^{-1}\sqrt{\frac{(S-1)}{(S+1)}} + \frac{Ah}{\pi S\sqrt{A^2-1}}\tan^{-1}\sqrt{\frac{(A+1)(S-1)}{(A-1)(S+1)}} \quad 2.44$$

(2.41)

and

$$A = \frac{h^2 + S^2 + 1}{2S}, \quad S = \frac{2L}{D}, \quad h = \frac{2H_t}{D} \quad 2.45$$

The configuration factor always takes a value between zero and one, depending on the target location, flame height, and flame diameter. When the target is close to a fire source, the view received by the target would consist mostly of the flame, thus, the configuration factor approaches unity.

2.3.11 Summary of Model

Chapter 3: Given that the study in this chapter is based on the dataset obtained from the research by Fleury et al. (2011), conducting the reassessment of older models using the same set of propane gas experiment data would likely lead to the same conclusion. As a result, out of the six models tested by Fleury et al. (2011), only the single point source model, which has already been established as the best-performing model, is included in the testing along with the four newly developed models. The models selected for the assessment in this chapter are the single point source model, the weighted multi point source model, the cuboid flame model, the multi cuboid flame model, and the multi cylinder flame model.

Chapter 4: As the assessment no longer involves propane gas fire experiments, the results of older models may vary when assessed using liquid pool fire experiment data. Hence, all of the models mentioned in the literature review will be tested in this chapter. This includes the six conventional models examined in the study by Fleury et al. (2011) (Shokri and Beyler simple correlation, Shokri and Beyler detailed method, Mudan method, Dayan and Tien method, the rectangular planar model, and the single point source model), as well as the four recently developed models (the weighted multi point source model, the cuboid flame model, the multi cuboid flame model, and the multi cylinder flame model).

Chapter 5: Since the best-performing model (single point source model) has already been determined in Chapter 4 and Chapters 5, this chapter of the research will focus on assessing the performance improvements offered by the newly developed models in comparison to the single point source model.

Table 2.2 shows the summary of radiation models assessed in this research.

Table 2.2: Summary of thermal radiation models

Research Section	Radiation Models	
Chapter 5	Shokri and Beyler Correlation	$\dot{q}'' = 15.4\left(\frac{L}{D}\right)^{-1.59}$
	Shokri and Beyler Detailed Method	$\dot{q}'' = EF_i$
	Mudan Method	$\dot{q}'' = EF_i\tau$
	Dayan and Tien Method	$\dot{q}'' = \sigma\varepsilon T_f^4\left(F_1 + F_2 + F_3\right)$
	Rectangular Planar Model	$\dot{q}'' = F_i\sigma\varepsilon T_f^4$
Chapter 4 Chapter 5	Weighted Multi Point Source Model	$\dot{q}'' = \sum_{j=1}^{N}\frac{w_j\dot{Q}_r\cos\theta_j}{4\pi R_j^2} = \frac{\dot{Q}_r}{4\pi}\sum_{j=1}^{N}\frac{w_jL}{R_j^3}$
	Cuboid Flame Model	$\dot{q}'' = \frac{\tau F_i\chi_r\dot{Q}}{2bH_f + 2wH_f + wb}$
	Multi Cuboid Flame Model	$\dot{q}'' = \sum_{i=1}^{n}\frac{\tau F_i\chi_r\dot{Q}}{2bH_f + 2nwH_f + wb}$
	Multi Cylinder Flame Model	$\dot{q}'' = 0.80\left(1-\exp\left(-1.1D\right)\right)\sigma \times\sum_{1}^{n}\tau F_{f(i)-f(t)}\left(H_i / H_m\right)^{-0.32}\left(\left(T_f - T_a\right)_z + T_a\right)^4$
Chapter 4 Chapter 5 Chapter 6	Single Point Source Model	$\dot{q}'' = \frac{\dot{Q}_r\cos\theta}{4\pi R^2}$

2.4 Selection of Fuel

General fire hazards could be discovered at any section of the buildings with no regard to the specification of occupancy. Common heat-producing appliances, static electricity, flammable chemicals, and miscellaneous human behaviour (smoking, etc.) are proven to have either direct or indirect linkage to the origin of fire calamity (Abbott, 1942). Nevertheless, the fundamental trigger for a major fire often lies in the initial ignition of a significant amount of combustible or flammable material within a building or structure. This initial ignition serves as the starting point that sets in motion a series of consequential and potentially devastating fire-related events. For this reason, the research schemes to incorporate some of the common fuel sources for collecting heat flux data.

This research prioritises the selection of fuels that not only provide controlled conditions for testing thermal radiation models but also represent common fire hazards in building environments. Propane, ethanol, and isopropyl alcohol were chosen specifically to test the adaptability and accuracy of radiation models across different fuel types (i.e., gas and liquid) while covering both non-sooting and sooting combustion characteristics. These fuels are commonly encountered in fire safety engineering standards and provide a practical basis for model assessment in real-world building fires.

2.4.1 Gas Fuel Consideration

In line with the first research objective, propane is chosen to replicate stable and predictable gas fire behaviour for calibrating and evaluating radiation models. Propane's consistent combustion characteristics make it ideal for assessing model performance, allowing for clear comparisons across different fire safety studies. Additionally, propane is widely used in standardised fire tests, such as the Single Burning Item (SBI) test, which supports the Euroclasses fire classification standards (EN13823) (Gossiaux et al., 2021).

Furthermore, propane is highly relevant for fire safety engineering as it serves as a representative gas fuel commonly found in building environments, such as in heating systems, refrigeration, and aerosol applications (Rostamzadeh et al., 2021). It is commonly encountered as a propellant in everyday essentials such as edible food aerosol sprays, shaving creams, and air fresheners (Kulkarni & Shaw, 2016; Varlet et al., 2014).

By using propane, this research leverages a fuel that not only meets laboratory standards for stability and repeatability but also aligns with realistic fire hazards in buildings. The fuel specification is shown in Table 2.3.

Table 2.3: Gas fuel used for experimental data collection

Gas Fuels	Propane
Item represented	Aerosol propellant, combustion fuel, refrigerant
Autoignition Temperature	287°C
MSDS Reference	(Airgas, 2005)

2.4.2 Liquid Fuel Consideration

In selecting liquid fuels, this study focuses on ethanol and isopropyl alcohol due to their wide applicability in building environments and unique combustion characteristics. These fuels enable the examination of radiation models under both non-sooting (ethanol) and sooting (isopropyl alcohol) conditions, capturing a broader range of radiative behaviours critical for model validation.

Ethanol and isopropyl alcohol are ubiquitous in modern buildings, especially with increased use in cleaning and disinfection post-COVID-19. These fuels are present in various forms, from hand sanitisers to cleaning agents, making them realistic representations of fire risks associated with everyday products. Ethanol and isopropyl alcohol also contribute to a diverse understanding of pool fire dynamics, which are known for producing large radiant heat fluxes, a key aspect for testing radiation models. Given the high relevance of these substances as potential ignition sources in buildings, using them in this research provides practical insights into fire dynamics and risk assessment.

Additionally, previous studies often overlook liquid fuels in radiation model testing, focusing instead on gas fires. This research, therefore, addresses a gap in fire safety literature by evaluating radiation models with both non-sooty and sooty pool fires. This dual focus supports a comprehensive approach to fire safety modelling, equipping engineers with better tools for assessing real-life building fires.

Given the prevalence of these items, it is only fitting that both isopropyl alcohol and ethanol are favoured for experimental work in this research. The summary and specification of the liquid fuels tested are shown in Table 2.4.

Table 2.4: Liquid fuel used for experimental data collection

Liquid Fuels	Isopropyl Alcohol (2-Propanol)	Ethanol
Item represented	Hand sanitiser, surface disinfectant, antiseptics, detergents	Aerosol propellant, alcoholic beverages, wine, engine fuels, solvent, cosmetics
Autoignition Temperature	399°C	362.8°C
MSDS Reference	(Lab-Chem, 2016)	(Thermofisher, 2022)

2.5 Summary

In this chapter, it is clarified that there are three major classifications for thermal radiation estimations: CFD models, empirical models, and semi-empirical. While complexity is the main issue for CFD models, the shortfall in terms of accuracy for empirical models has promoted the focalisation towards the study of semi-empirical models' performance. A total of ten thermal radiation models are introduced in this section, each with its limitations and advantages. Hence, in determining the best-performing model, the performance of all models will be assessed using experimental data obtained from laboratory works as an accuracy benchmark.

In addition, the section also highlighted that experimental work relied heavily on the manipulation of variables to produce a meaningful research outcome. Therefore, the fuel tested must be the best-suited material for representing an actual building fire scenario. In accomplishing these, propane gas represents gas fires, while ethanol and isopropyl alcohol represent liquid fires.

The correct inclusion criteria for models' selection and fuel choice will ensure not only the viability of research but also the credibility of findings. It is envisioned that the data amassed from evaluated data and experimental data will engender a definite answer for finding the best-performing model for building fire.

CHAPTER 3

GENERAL METHODOLOGY

Each of the specific objectives outlined in Section 1.3 and Figure 3.1, while interconnected, represents a distinct study that can stand alone. Consequently, the research methodology differs significantly between them. To accommodate the variations in fuel specifications and experimental or simulation parameters required to address each objective, specific details about these parameters are provided in their respective results and discussion chapters. This chapter, however, furnishes the general methodology applicable to all three research objectives.

The general methodology encompasses a data analysis section, which elucidates how primary and secondary experimental data are employed in model assessment in Chapters 4, 5, and 6. It includes an experimental setup section that outlines the procedures for primary data measurement from pool fire experiments for model assessment in Chapter 5 and model validation in Chapter 6. Additionally, it includes a simulation setup section that details the procedure for configuring a Computational Fluid Dynamics (CFD) model for model validation in Chapter 6.

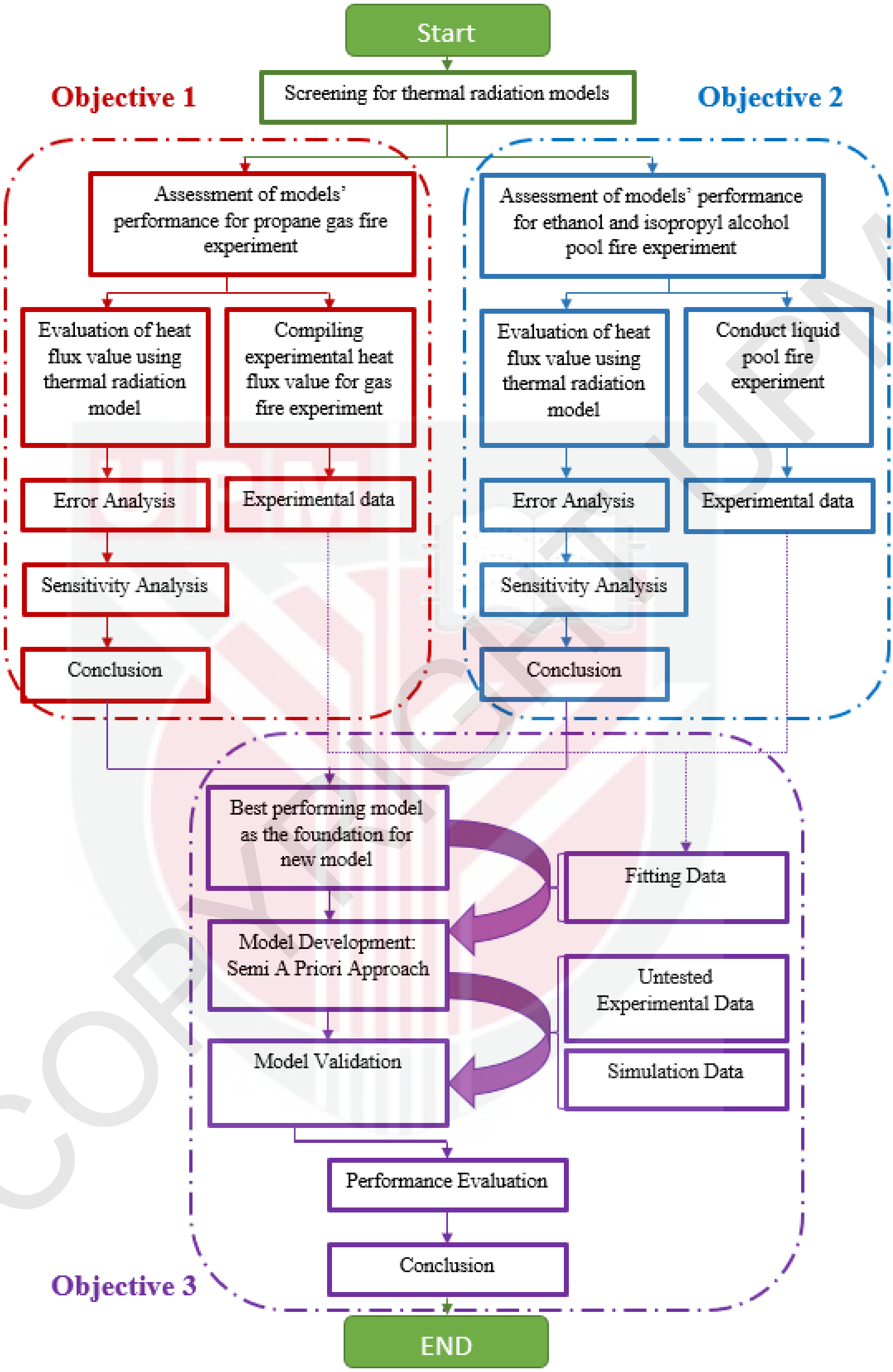

Figure 3.1: Research Flowchart

3.1 Data Analysis

The primary approach for evaluating the performance of various thermal radiation models is to determine the degree of proximity between the estimated radiative heat flux values and the actual measured heat flux values obtained from experiments. Calculated heat flux values are obtained by substituting the values required by the radiation models under investigation in accordance with the parameter combination of each experiment. Data are then analysed using mean absolute percentage error and median absolute percentage error analyses.

3.1.1 Mean Absolute Percentage Error (MAPE) Analysis

The MAPE is a statistical measure of the precision of a model. It expresses the precision as a percentage and can be calculated as the average absolute percentage error for the calculated heat flux value minus the measured heat flux value divided by the measured heat flux value. The equation for MAPE analysis is given by:

$$\% = \frac{1}{n}\sum_{i=1}^{n}\left|\frac{\dot{q}''_T - \dot{q}''_E}{\dot{q}''_E}\right| \times 100 \qquad 3.1$$

where

$\dot{q}''$ is the calculated heat flux value

$\dot{q}''_E$ is the experimental heat flux value

n is the total number of experiments

The total number of experiments is contingent on the various combinations of experimental parameters, including data collected at specific flame magnitudes (in terms of heat release rate and flame area) for each horizontal distance from the flame centre, conducted at various vertical measurement locations. On the other hand, the individual absolute percentage error for the heat flux resulting from every experimental parameter combination is calculated for each of the models under investigation. A comparison of model performance is made using the difference between the theoretical and experimental heat flux values in the form of MAPE. A lower average error implies a lower deviation between the estimated heat flux by the model in comparison to the measured heat flux value. The model with the lowest average mean percentage error indicates that it is able to register the most reliable estimation for a wider range of circumstances and can, therefore, be rated as the best-performing radiation model. This mean analysis will be applied throughout Chapter 4, 5, and 6.

3.1.2 Median Absolute Percentage Error (MdAPE) Analysis

In obtaining a more comprehensive understanding of the data, it is beneficial to complement MAPE analysis with another statistical approach, i.e., MdAPE analysis. The median, which represents the middle value in a sorted dataset, is employed to measure central tendency in MdAPE analysis. By considering the median, MdAPE is less influenced by extreme outliers or skewed distribution, making it a valuable complementary analysis to gain insights into the performance of thermal radiation models.

The median is the centreline for the specified group of data, which separates the entire range of statistics into two equivalent regions. A MdAPE analysis is performed by arranging the absolute percentage errors in ascending order, and the middle value of the dataset is identified as the median if the number of values is an odd number. For an even number of values, the average of the two middle percentage error values is taken as the median.

A median analysis is more robust towards outliers as it omits all elements, excluding the middle value, hence, the median can provide a more practical presentation of data that exhibit skewed distributions. This complementary analysis approach enhances the validity and interpretability of the results, enabling researchers to make more informed conclusions about the performance and suitability of the models assessed in this study.

3.1.3 Sensitivity Analysis

In the analysis of fire modelling, the simulation outcomes heavily rely on the values assigned to input variables. Typically, these input variables are determined through engineering judgment or referenced from experimental data and handbooks. Considering the inherent uncertainty associated with these input variables, it is essential for fire modelling analysts to conduct sensitivity analyses. These sensitivity analyses involve systematically testing and evaluating the impact of varying input variable values within a reasonable range (Kim et al., 2022). The sensitivity analysis tested in this research includes horizontal and vertical separation distance sensitivity tests, fire size sensitivity analysis, and heat release rate sensitivity tests.

Sensitivity analysis plays a vital role in fire modelling as it helps identify the influence of specific input variables on the overall simulation results. Analysts gain insights into how changes in these variables affect the model's predictions by systematically varying the input variable values. This information is valuable for understanding the robustness and reliability of the fire model and assists in making informed decisions regarding fire protection strategies and designs. An understanding of the model's sensitivity enhances confidence in its performance and allows for a more accurate interpretation of the simulation results.

Overall, conducting sensitivity analysis on input variables is crucial in fire modelling analysis. It helps address uncertainties, assess the impact of variable changes, and provide valuable insights into the reliability and applicability of the model. By incorporating sensitivity analysis, fire modelling analysts can enhance the credibility and effectiveness of their analyses, leading to improved fire safety practices and decision-making processes.

3.2 Gas Burner Experimental Set Up by Fleury et al. (2011)

Fleury et al.'s (2011) dataset is one of the most extensive and rigorous collections of experimental results for propane-based fire scenarios, offering high-quality, consistent data that is crucial for a reliable assessment of thermal radiation models. data serves as a benchmark in the field, being widely recognized and referenced in other studies. This makes it an ideal basis for conducting a comparative assessment of newer radiation models, as it ensures consistency in evaluating their predictive performance.

3.2.1 Gas Burner Instrumentation

Fleury et al. (2011) utilised three rectangular gas burners with different aspect ratios (length to width ratio), representing typical furniture configurations better than circular burners of varying diameters. The rationale is that most commercially available furniture, such as desks and cabinetry, typically have a rectangular shape rather than circular geometry. The aspect ratios tested in their experiments were 3:1, 2:1, and 1:1.

In Fleury's experiments, oxygen depletion calorimetry was used to analyse the combustion products. The tests were conducted beneath a large extraction hood designed to trap and collect these products. Air was supplied exclusively through passive louvered vents, reducing disturbances that could alter the flame shape and, consequently, the total radiated heat flux. A Universal Data Logging (UDL) system was employed to continuously monitor radiant heat flux, flame temperature, and gas analysis data, with readings taken every second throughout the experiments. Figure 3.3 provides a 2-D schematic layout illustrating the positions of the heat flux gauge trolley and gas burner.

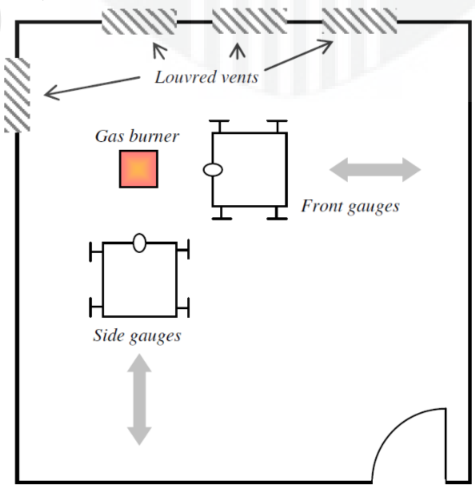

Figure 3.2: Summary of Gas Burner Experimental Procedure
(Source: Fleury et al., 2011)

3.2.2 Temperature Measurement

A thermocouple tree with a length of 1.52m, containing four ANSI type K, 24-gauge thermocouples spaced at 0.38m intervals, was placed at the centre of the burner to measure flame temperatures at different heights. The temperature data were used to estimate the mean flame height. The ambient flame temperature recorded was 1173K.

3.2.3 Heat Release Rate Measurement

Heat release rate was determined using oxygen depletion calorimetry, a technique based on the principle that the heat released per unit of oxygen consumed is consistent for organic gases and liquids. By measuring the oxygen consumption during combustion, the heat release rate could be calculated. To accurately perform this analysis, all combustion products were collected and removed via the extraction hood exhaust.

Fleury's experiments regulated the fuel mass flow rate using a pair of MKS Digital Mass Flow Rate Type 1579A controllers connected to a power supply. By adjusting the fuel mass flow rate, the heat release rate could be varied. The tested heat release rates were 100.0kW, 150.0kW, 200.0kW, 250.0kW, and 300.0kW.

3.2.4 Radiant Heat Flux Measurement

The heat flux gauges were positioned to record not only heat flux at different heights but also the horizontal distance relative to the fire. The trolley's horizontal displacement allowed measurement of heat flux at various distances from the flame. Distances from the centre of the fire tested were 0.5m, 0.75m, 1.0m, 1.5m, and 2.0m, while the vertical heights tested were 0.0m, 0.5m, 1.0m, and 1.5m. The gauges used were Medtherm Schmidt-Boelter types, with cooling water supplied via ¼ inch OD flexible tubing. The gauges detected radiant heat and produced electrical signals (mV) that were converted to heat flux readings through a calibrated conversion factor.

3.3 Pool Fire Experimental Set Up

Primary heat flux data for Chapter 5 and 6 were obtained through an extensive series of liquid pool fire experiments. Figure 3.3 provides a summary flowchart of the pool fire experimental procedure, and the complete laboratory manual can be found in Appendix A. The subsequent subsections offer comprehensive explanations of the instrumentation used for data collection.

3.3.1 Pool Fire Instrumentation

This experimental setup involved the utilisation of square SS 304 pans, chosen for their high melting point, thermal stability, corrosion resistance, ease of fabrication, and non-reactivity. These pans are of varying sizes, as elaborated in the corresponding results and discussion chapters (refer to Section 4.2 and Section 5.2). These pans are characterised by a uniform wall thickness of 0.005 m and an internal height of 0.045 m, as depicted in Figure 3.4. The pans are not mounted and placed on weighing scales to ensure independence from other surfaces.

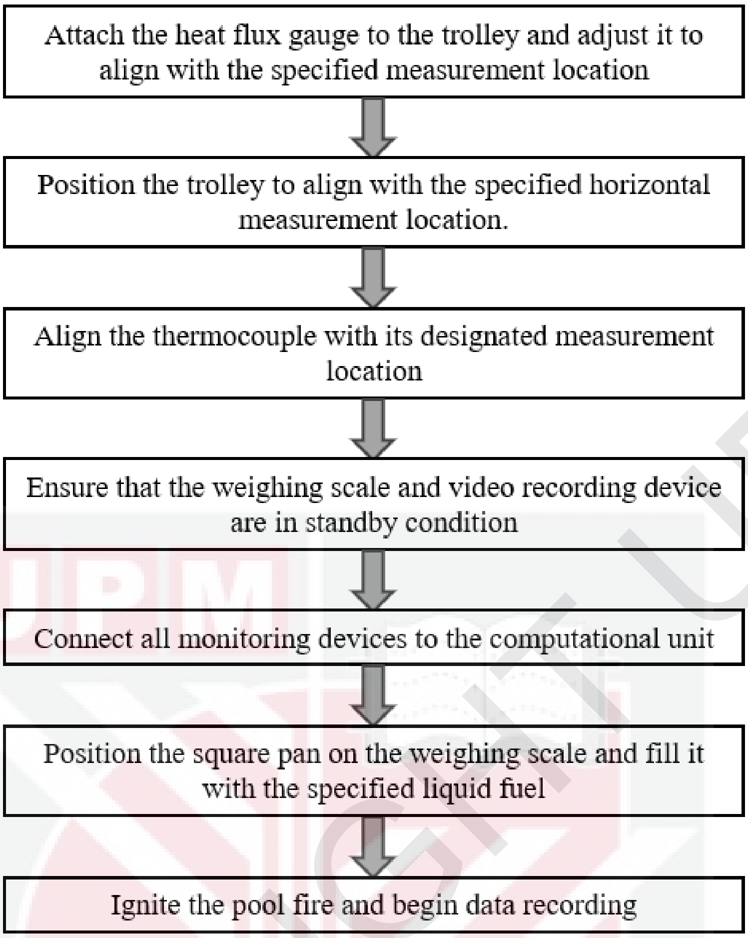

Figure 3.3: Summary of Pool Fire Experimental Procedure

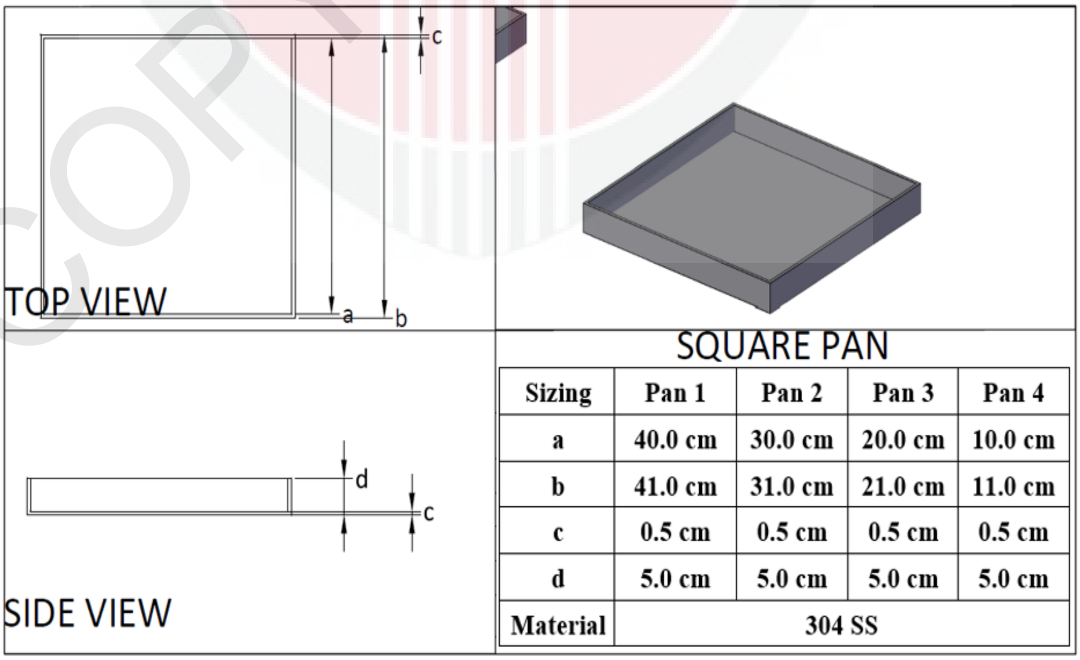

Sizing	Pan 1	Pan 2	Pan 3	Pan 4
a	40.0 cm	30.0 cm	20.0 cm	10.0 cm
b	41.0 cm	31.0 cm	21.0 cm	11.0 cm
c	0.5 cm	0.5 cm	0.5 cm	0.5 cm
d	5.0 cm	5.0 cm	5.0 cm	5.0 cm
Material	304 SS			

Figure 3.4: Geometry of the Square SS 304 Pans Used in the Experimental Setup

Square geometries have been previously used in studies by Fleury et al. (2011) and Sharma et al. (2020), offering a shape that allows the setup to approximate both circular and rectangular flame behaviours. By applying the equivalent diameter equation (Equation 2.5), the square pan can be used to approximate a circular flame profile, while its four sides also provide a realistic representation of rectangular flames. Additionally, pan size was chosen based on flame visibility and safety requirements. For instance, the 10 cm square pan was excluded for ethanol pool fires due to minimal heat flux, making it challenging for accurate detection. Conversely, the 40 cm square pan was excluded for isopropyl alcohol due to flame height, which posed potential safety risks and visibility constraints under the exhaust hood. This controlled selection of pan sizes ensures each experiment aligns with laboratory safety protocols and accurate data collection methods.

The experimental procedure involved pouring liquid fuel into the pan until the liquid reached a thickness of 1 cm, which is repeated at the beginning of each set of experiments. This setup is designed to measure the mass consumption rate of the fuel, and therefore, the fuel is not continuously replenished during the burning process. To account for the variation of fuel mass during burning, only data from the steady-state (fully developed) burning phase, i.e., excluding both the ignition and decay phase, is selected for analysis, including flame height, flame temperature, heat release rate, and radiative heat flux data. Consequently, for the entire range of measured data, only the central interval is chosen for subsequent examination. Figure 3.5 provides an illustration of the exclusion of the initial and final 1-minute segments from the analysis of heat flux data for 0.2 x 0.2 m^2 isopropyl alcohol pool fires at a distance of 0.5 m from the centre of the flame. This approach ensures that the collected data accurately represents stable and constant burning conditions, providing meaningful and reliable results for further analysis.

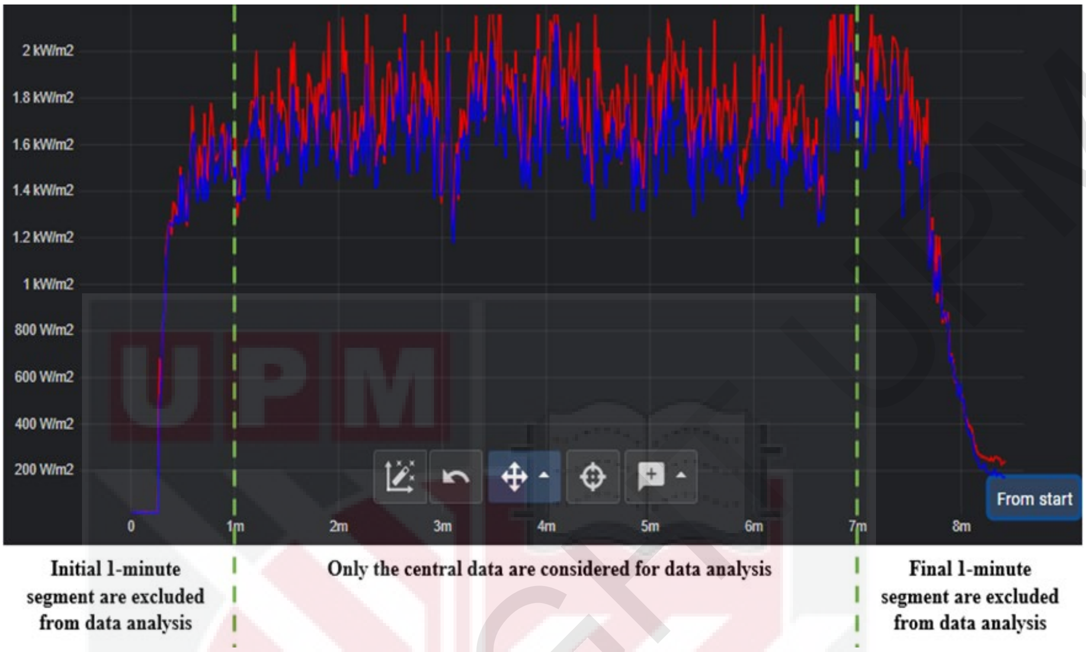

Figure 3.5: Steady State Burning Selection for Heat Flux Data at Heights 0.1 m (Blue Line) and 0.27 m (Red Line) from the Flame Base

The experiments are conducted within a controlled indoor environment, where the entire combustion process takes place under an exhaust hood, and all entrances to the combustion lab are closed to prevent any airflow disturbances caused by wind. Mechanical fans positioned at the upper wall of the laboratory are utilised to facilitate ventilation, allowing the hot gases to exit the facility and preventing the accumulation of smoke inside the laboratory. The experimental setup was designed using the experimental work of Fleury et al. (2011) and Sharma et al. (2020) as primary benchmarks, incorporating elements from both studies. The pool fire setup was based on the design by Sharma et al. (2020), though with a smaller fire, while the positioning of the heat flux gauges was adapted from Fleury et al. (2011), with the use of a pool fire instead of a gas burner. Mass loss rate calculations via a load cell were based on methods in both studies. Additionally, video capture with colour image processing for flame height estimation and the use of K-type thermocouples at various heights along the centreline to measure flame temperature were also informed by the approaches of Fleury et al. (2011) and Sharma et al. (2020). To provide a visual representation of the experimental layout for the liquid pool fire experiment, refer to Figure 3.6, which depicts the schematic layout.

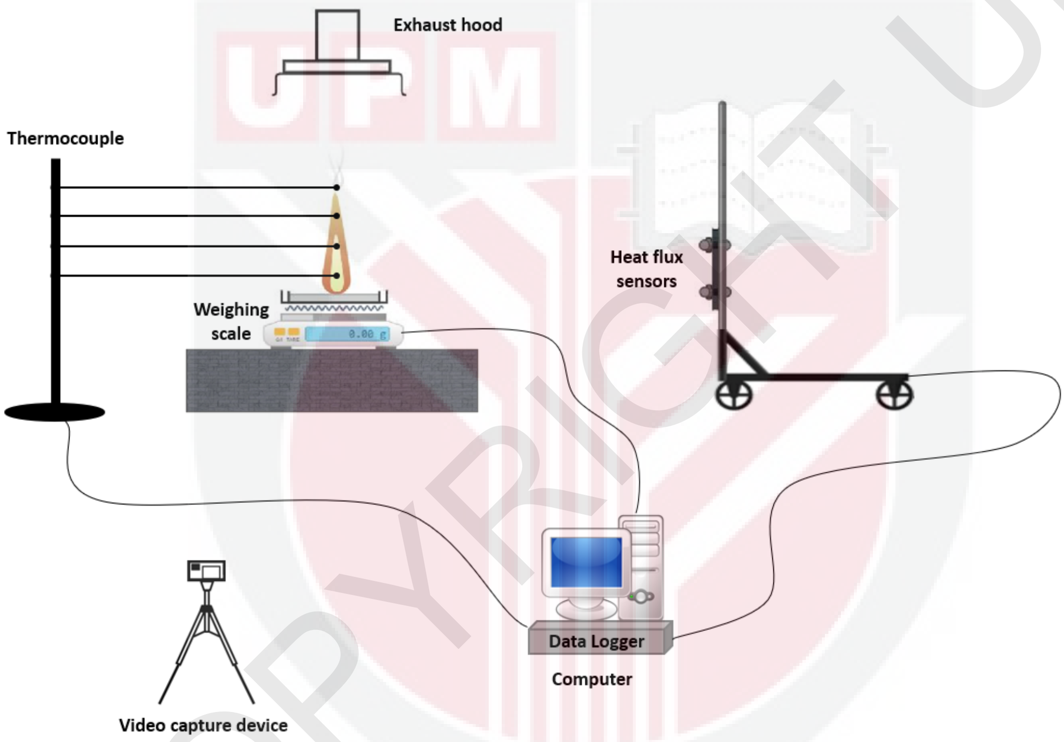

Figure 3.6: Schematic Diagram of the Experimental Setup for the Liquid Pool Fire Experiment

To address potential concerns regarding heat losses in this setup, it is worth noting that the heat flux measurements were conducted at a relatively close distance to the flame, minimising potential radiative and convective losses. Due to this proximity, any heat loss from the flame to the surroundings was minimal and therefore considered negligible. This distance ensured that the recorded heat flux values closely approximated the actual radiant output of the flame without significant interference from environmental losses.

As for flame size, although the pool fire surface area reached a maximum of 0.16 m² in this study, it aligns with previous work in fire safety research. For example, Ji et al. (2019) used heptane pool fires with a maximum fire size of 0.0896 m², and Ji et al. (2020) conducted experiments with a 0.126 m² heptane pool fire. Wan et al. (2018) utilised a propane gas burner of 0.045 m², while Huang et al. (2019) used a propane burner at 0.09 m². This comparison demonstrates that the flame size in the current study is consistent with, and even exceeds, the scale applied in other fire safety studies.

Figure 3.7: Experimental Setup for the Liquid Pool Fire Experiment (Part 1)

Figure 3.8: Experimental Setup for the Liquid Pool Fire Experiment (Part 2)

3.3.2 Temperature Measurement

Four type-K thermocouples with a diameter of 3 mm are employed to record the flame temperature. The 3 mm diameter represents a relatively large bead size, chosen for its durability in high-temperature environments but recognised to have a slower response time compared to smaller beads. This may result in slight delays in capturing rapid temperature fluctuations within the flame. All thermocouples can withstand temperatures up to 1100 ℃; each thermocouple is 2 m long with a sensitivity of 0.01 ℃. For data collection, the tip of all four thermocouples is aligned at the centre of the pool fire, with a 0.15 m interval between each thermocouple. The vertical positions of the thermocouples, calculated from the base of the flame, are 0.24 m, 0.39 m, 0.54 m, and 0.69 m. In similar flame temperature measurement setups, previous studies have employed alternative thermocouple configurations for smaller-scale fires. For instance, Sharma et al. (2020) used five type-K thermocouples with a 1 mm tip fixed at different locations above the pan rim along the centreline. Likewise, Fleury et al. (2011) positioned four type-K thermocouples over the centre of the burner in their setup. The larger bead size in this research can also introduce a minor heat loss along the stem, which could influence the accuracy of temperature readings. However, these thermocouples were positioned carefully to ensure consistent measurement along the flame's height, providing reliable overall temperature data.

Several RS PRO type-K extension cables are required to connect the thermocouples to the data logger, USB TC-08. The data logger captured the output from the thermocouples, which is then displayed as temperature data in degrees Celsius (℃) using the PicoLog 6.2.5 software. The software facilitated data recording at 10-second intervals throughout the entire combustion process. In short, the PicoLog 6.2.5 software, as depicted in Figure 3.9, serves as an open-source user interface, enabling direct interaction between computers and data-logging devices via cable. This user-friendly interface allows for efficient data collection and monitoring.

Figure 3.9: PicoLog 6.2.5 User Interface

3.3.3 Flame Height Measurement

Two major components for successfully capturing flame height are the video-capturing device and the image-processing software. The video-capturing device used for this research is a Black Shark 3 android device mounted on a tripod stand. The whole gear for the video recording procedure is arranged at approximately 1 m from the exhaust hood to enable the videotape of the entire pool fire while maintaining a safe distance to prevent damage to the device itself. To enhance the visibility of flames and minimise disturbance, which might cause difficulties during the image processing stage, the video recording setting is adjusted to the lowest brightness with 1.5 times zoom. The recorded video footage is then transferred to a computational system for flame height determination using a Python-based image processing software, i.e., Flame Tracker.

As in the studies by Fleury et al. (2011) and Sharma et al. (2020), visible flame height was recorded using a video camera placed near the vicinity of the fire, followed by image processing software. However, the image processing software used in this research differs from both of these studies. For example, Fleury et al. (2011) used Adobe Premiere Pro to break the captured video into individual still images and then processed them further using ImageStream, while Sharma et al. (2020) utilised MATLAB Image Processing to convert colour images into binary images. In selecting Flame Tracker for this research, careful consideration was given to software requirements and compatibility constraints, as different software options often have specific operating system requirements, compatibility issues, or additional dependencies, which can significantly extend processing time, especially during coding, testing, and execution.

Flame Tracker was chosen primarily due to the availability of a detailed guide provided by (Carmignana (2021), which explains the software's basic functionalities and includes a direct download link, making it both accessible and practical for experimental use. Developed by the Mechanical Engineering Department at the University of California, Flame Tracker has been validated in previous studies on flame spread by the Combustion and Fire Processes Laboratory and the Berkeley Fire Research Lab at the University of California, Berkeley, making it well-suited for capturing flame behaviour in this study.

Recognising that blue flames are generally harder to capture than yellow flames due to their lower luminosity, this study implemented specific measures to reduce uncertainties in the flame height determination process. To further enhance the accuracy of flame height determination, a black background and square pans with a black-painted surface are strategically positioned facing the video recording device during the video capturing process. By adopting this deliberate choice of colour scheme, the contrast between the blue flame and its surroundings is significantly increased, thus facilitating the precise identification of flame height during the subsequent image processing stage. This consideration proved to be crucial in elevating the performance of the Flame Tracker software, enabling it to effectively track and analyse the morphography of flames, even for weakly sooting flames.

To verify the flame height measurement methodology, a comparison of experimental flame heights for ethanol and several existing flame height correlations is depicted in Figure 3.10. While the trendline of the experimental results does exhibit deviations from both the established flame height correlations, namely Thomas's and Heskestad's correlations (Heskestad, 1983), it is noteworthy that the experimental flame heights consistently fall between these trendlines. This positioning indicates a reasonable alignment between the experimental data and the expected flame heights predicted by the correlations. The discrepancy observed might arise from factors specific to the experimental setup, fuel characteristics, or other environmental conditions not entirely captured by the established correlations. Despite these differences, the fact that the experimental results fall within the range defined by Thomas's and Heskestad's correlations reinforces the credibility of the measurement methodology.

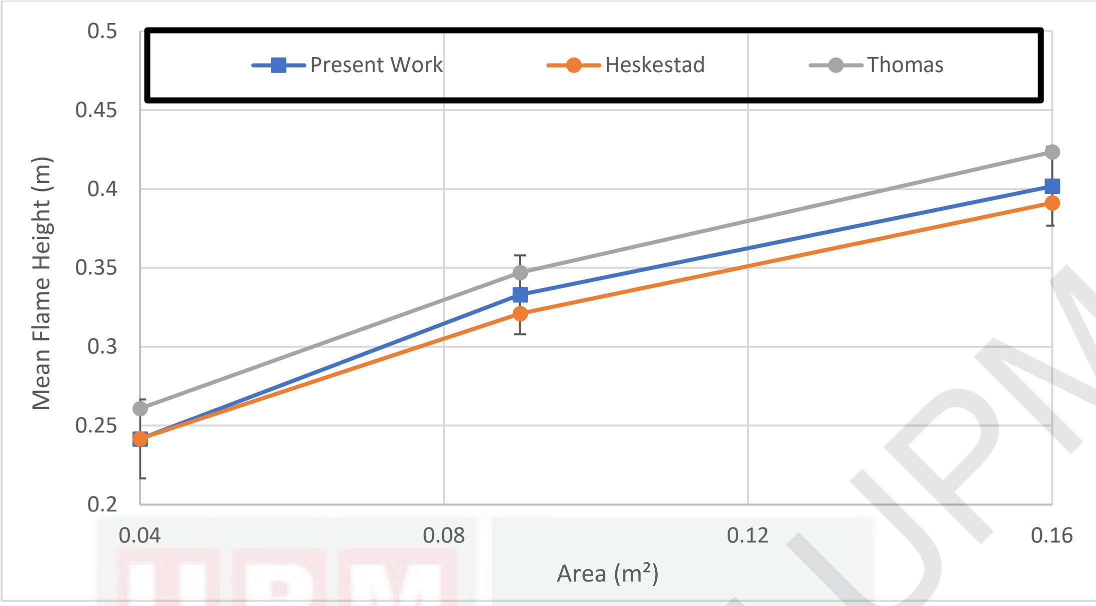

Figure 3.10: Comparative Analysis: Experimental Mean Flame Height vs. Existing Correlation

Flame Tracker is specifically designed to track the morphography of flames captured in videos and extract relevant data such as length, area, and rate of flame spreading (Carmignana, 2021). There are three basic tracking approaches: Manual tracking, Luma tracking, and Colour tracking. In this research, the Luma Tracking approach is employed. Various settings are adjusted to differentiate the flame from its background, as depicted in Figure 3.11. These settings encompass rotation, brightness, threshold, and the degree of the filter. Further specifications regarding the video recording settings and image processing settings are provided in Table 3.1 and Table 3.2, respectively.

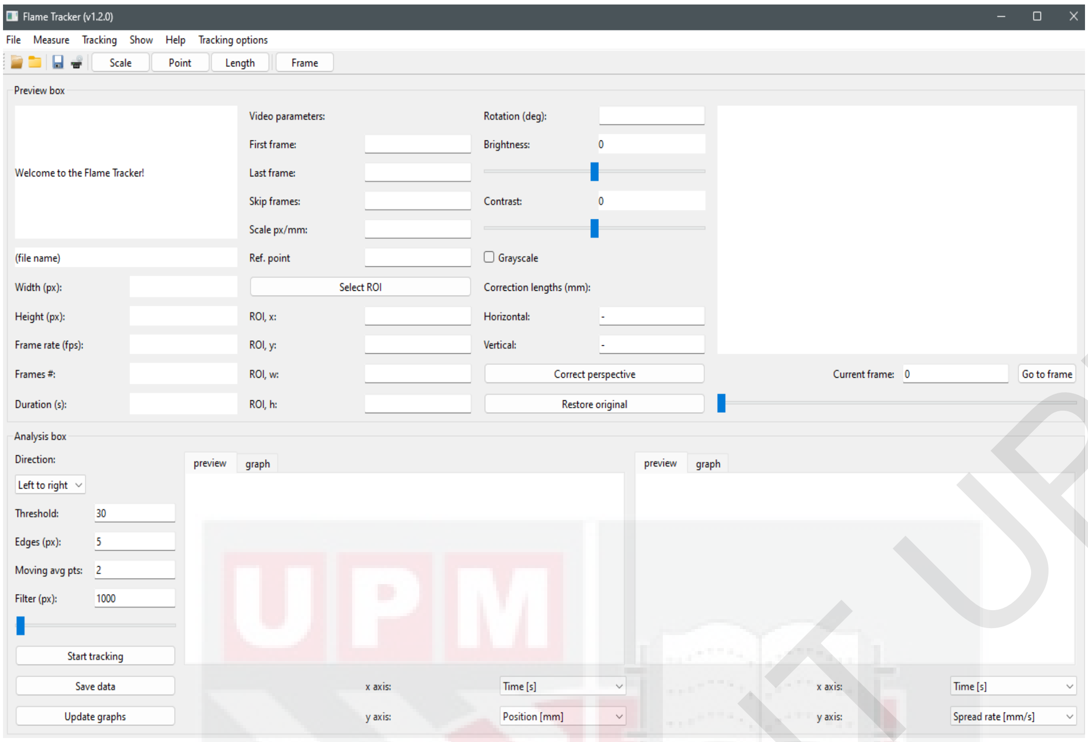

Figure 3.11: Flame Tracker Software User Interface for Luma Tracking

Table 3.1: Video recording settings

Video Recording Settings	Specifications
Video Capturing Device	Black Shark 3
Tripod Stand Distance	1 m
Brightness	Lowest
Zoom	1.5 times
ISO Value	Auto
Frame Rate	30 fps
Quality	720p
Exposure Time	Auto
Lens Aperture Settings	f /1.8
Video Resolution	3840 x 2160 pixels

Table 3.2: Image processing settings

Image Processing Settings	Specifications
Flame Tracker Software	Python-based
Tracking Approach	Luma Tracking
Rotation	-90 degree
Brightness	-2
Contrast	0
Threshold	29
Filter Degree	1000
Filter Toggle	Maximum
Skip Frames	50
Edges	5
Moving avg pts	2

The computation of flame heights involved the conversion of the image's red, green, and blue (RBG) colour spaces into YCbCr colour spaces, as shown in Figure 3.12. This conversion facilitated the subsequent calculation of flame heights for each designated video frame. Since human eyes are more sensitive towards the luminance component (Y) component rather than the chrominance component (Cb and Cr), luma tracking allowed these binary images to be analysed by differentiating the light intensity and brightness of images. From Figure 3.12, the brighter region signifies the fire, while the non-flame part is denoted as the darker background. After the tracking process, the resulting data are exported into an Excel file for further analysis and interpretation.

RGB image

YCbCr image

Figure 3.12: Digital Image Processing Procedure for Ethanol Pool Fire

3.3.4 Heat Release Rate Measurement

The calculation of the heat release rate for different sizes of liquid pool fires is based on the determination of the mass loss rate of the fuels during the combustion process. The rate of evaporation is considered negligible in this experiment because the combustion process is predominantly driven by the energy released from the liquid fuel's surface, with any evaporation quickly compensated by the combustion process itself. Additionally, the small surface areas of the pool fires and the controlled experimental environment further minimize any significant evaporation losses. This involved measuring the mass of the pan before and after combustion using a high-precision weighing scale. The heat release rate can be calculated using Equation 3.2.

$$\dot{Q} = \frac{\Delta H_c \left(m_i - m_f \right)}{t} \qquad 3.2$$

where

$\dot{Q}$ is the total heat release rate (kW)

ΔH_c is the heat of combustion for fuel (kJ/kg)

m_i is the initial mass of the pan (kg)

m_f is the final mass of the pan (kg)

t is the total duration for combustion (s)

In this study, the conventional approach of calculating mass burning rate by dividing the difference between initial and final fuel mass by the total burning time was employed, aligning with the method used by Sharma et al. (2020), who utilised a 3 kg load cell for their small-scale fire test. The mass loss rates observed in the present study align closely with those reported by Sharma et al. (2020), particularly when comparing the mass loss rate for a pool fire area of 0.03m^2 to 0.04m^2, as shown in Figure 3.13. This figure serves to validate the mass loss rate measurements by comparing them against established values from the work by Sharma et al. (2020). By presenting this comparison, Figure 3.13 highlights the reliability of the mass loss data obtained in this study and reinforces that the measurement methodology used is sound and produces results consistent with previous, respected research. This alignment is crucial for supporting the credibility of the study's experimental setup and methodology, particularly for small-scale fire experiments, where accurate mass loss rates are fundamental to calculating the heat release rate and understanding fuel consumption behaviour.

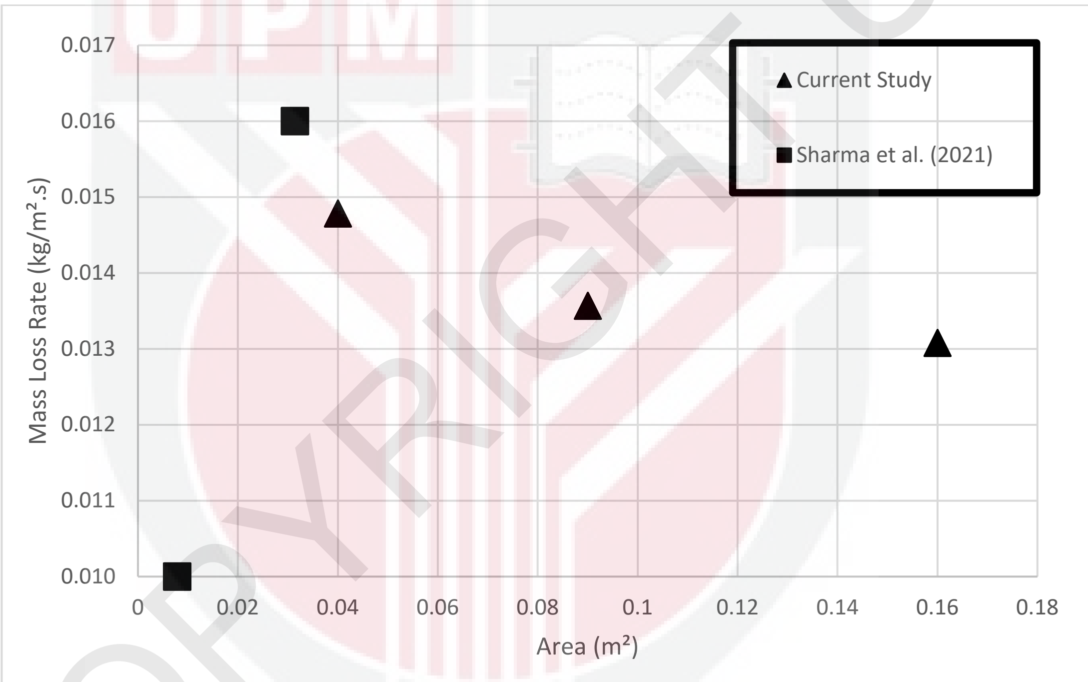

Figure 3.13: Mass Burning Rate vs. Pool Fire Area in Present Study and Literature

The weighing scale utilised for this research is the Ranger Count 4000 series from OHAUS, with a sensitivity of 0.0001 g. The weighing scale is made of a metal housing, providing extra protection against heat and mechanical damage. It is pre-equipped with an RS232 connectivity port, which allows direct linking with a computational unit. The digital reading is imported directly from the weighing scale to the Smartlux Simple Data Logger (SDL), an open-source data collection software, as depicted in Figure 3.14. Smartlux SDL enabled not only the transfer of mass loss data but also the time information at every 1-second interval. To establish a connection between the weighing scale and the SDL software, it is necessary to define the communication parameters for both devices. The COM port settings, which ensured proper communication, are outlined in Table 3.3.

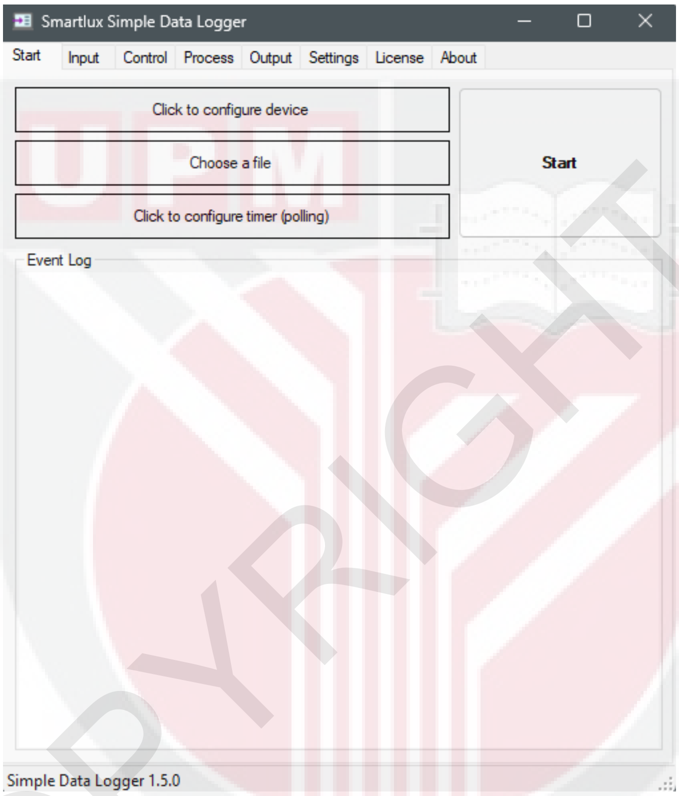

Figure 3.14: Smartlux SDL User Interface

Table 3.3: COM menu settings for connecting the weighing scale to Smartlux SDL

Ranger Count 4000	Value	Smartlux SDL
Baud Rate	9600	Bits/s
Data bits	8	Data bits
Parity	none	Parity
Stop bit	1	Stop bits
Handshake	none	Flow control

3.3.5 Radiant Heat Flux Measurement

The radiative heat flux emitted by flame is quantified using two SBG01 model heat flux sensors developed by Hukseflux. These sensors are designed with a water-cooling system and require a continuous connection to the cooling water supply during the experiment. SBG01 sensors can function with or without the water-cooling system; however, for enhanced accuracy, this research employed the water-cooling setup to prevent the sensor body's temperature from exceeding 10°C. An increase above 80°C would result in radiation emission by the sensor body itself, potentially affecting measurements.

Furthermore, the heat flux sensors have a sensing area diameter of 10 x 10^{-3} m and are designed to measure the radiation received from a 180° field of view angle. These thermal sensors are equipped with a carbon black coating that exhibits an emissivity greater than 0.95. The black coating absorbs radiation and converts it to heat, which flows through the internal thermopile sensor. The thermopile sensor generates a voltage output signal that directly corresponds to the incoming irradiance or heat flux, quantified in W/m^2. The sensors' spectrum covers a wide range from 200 to 50000 x 10^{-9} m. The SBG01 sensors incorporate a novel design that combines the advantages of both foil technology found in traditional Gardon gauges and thermopile technology used in traditional Schmidt-Boelter gauges, making them well-suited for measuring heat flux in environments where radiation is the dominant heat transfer mechanism. While Sharma et al. (2020) did not use any heat flux gauge in their study, Fleury et al. (2011) utilised Medtherm Schmidt-Boelter gauges for gas burner experiments. The current research, however, incorporated SBG01 sensors.

According to the SBG01 user manual, this water-cooled sensor is primarily used for reaction-to-fire and fire-resistance testing. It also serves as a calibration reference standard for various testing equipment, including flammability and smoke chamber tests. Compliant with ASTM and ISO test methods, the SBG01 sensor is calibrated by Hukseflux according to ISO 14934-3 standards. The calibration at Hukseflux is a secondary standard, traceably validated against the primary standard of the RISE Research Institutes of Sweden AB. This traceable calibration provided consistency with internationally recognized standards, establishing an effective benchmark for radiation measurements in this study.

For the measurements, both sensors are mounted to a trolley, which enabled heat flux readings to be taken at a different horizontal displacement from the centre of the flame. The horizontal position of the measurement location setting for this research is set at 0.5 m, 0.75 m, 1.0 m, 1.25 m, and 1.5 m. Since the SBG01 sensor uses an open detector and is not shielded, the distance of less than 0.5 m is not tested to prevent measurement error due to convective heat transport by hot gasses. On the other hand, the trolley also facilitated vertical adjustments of the heat flux sensors, with monitoring positions at 0.1 m, 0.27 m, 0.44 m, and 0.61 m calculated from the base of the flame. The heat flux sensors are directly connected to a data logging device, the USB TC-08, which records the voltage output from the sensors. The recorded voltage readings are then converted into heat flux data using PicoLog 6.2.5 software.

In measuring heat flux, it is essential to consider potential errors due to differences between calibration reference conditions and the actual experimental setup. To ensure accuracy, this study included equipment checks on all readings. The measured heat flux was cross-referenced with Equation 3.3, and the results were found to be identical, confirming the reliability of the methodology.

$$\dot{q}'' = \frac{U}{S} \qquad 3.3$$

where
$\dot{q}''$ is the heat flux reading (W/m^2)
U is the voltage output from the heat flux sensor (V)
S is the sensitivity of the heat flux sensor (V/(W/m^2))

3.3.6 Experimental Uncertainties

Identifying and defining the limitations and uncertainties associated with measuring instruments before conducting any experiment is crucial, as they can impact the results and estimations (Sharma et al., 2020). The range of uncertainties for the instruments used in this study is presented in Table 3.4. Given that all data recording is performed simultaneously, the primary method of uncertainty analysis involved comparing the heat flux values measured in the first and second run of the experiment for each specific experimental configuration. As previously explained, data collection involved the use of two heat flux gauges, allowing measurements at two distinct heights. To obtain data at all four height measurement locations for a single horizontal measurement point, experiments were repeated for an additional two height measurement locations. These procedures were conducted for every horizontal measurement point at each specific pool fire size. For the repeatability study, the entire experimental process was replicated, and standard deviations were calculated based on the same experimental parameter combination dataset, comparing results from the first and second experimental runs. The standard deviation between the recorded datasets varied according to the sizes of the flames, due to the difference in the overall oscillating behaviour of the flame. Specifically, for the 10 cm pan, the standard deviation is 10 W/m^2; for the 20 cm pan, it is 15 W/m^2; for the 30 cm pan, it is 35 W/m^2; and for the 40 cm pan, it is 55 W/m^2.

As the experiments are conducted indoors, the influence of wind is negligible. When measuring the burning rate, only the fully developed burning period is considered, disregarding the initial and final mass of the fuel. Similarly, for flame height and heat flux measurements, only data from the steady burning state are considered for data analysis.

Table 3.4: Uncertainty and sensitivity of measuring equipment

Equipment	Calibration Uncertainty	Measurement Uncertainty	Sensitivity
Heat flux gauge 1	± 1.8 x 10^{-8} V/(W/m^2)	±20 kW/m2	2.8 x 10^{-7} V/(W/m^2)
Heat flux gauge 2	± 1.7 x 10^{-8} V/(W/m^2)		2.6 x 10^{-7} V/(W/m^2)
Thermocouple (Type K)	± 1 ℃	±18 ℃	0.01 ℃
Weighing scale	± 0.001 g	±0.02 g	0.0001 g
Video capture device	± 0.02 m	±0.02 m	0.00001 m

3.4 Simulation Set Up

3.4.1 Pyrosim

To evaluate the newly proposed thermal radiation model's validity in Chapter 6, its performance is compared with results obtained from CFD simulation software. For this study, PyroSim is utilised for generating and visualising the input required for the FDS simulations. PyroSim simplifies the process of setting up FDS simulations by providing a user-friendly interface that allows users to define the geometry, specify materials and boundary conditions, and set simulation parameters. Furthermore, PyroSim also offers additional features such as advanced visualisation tools, including the ability to display smoke and temperature contours, generate animations, and analyse simulation results. In summary, PyroSim acts as an intermediary between the user and FDS, streamlining the process of setting up and running FDS simulations while providing enhanced visualisation and analysis capabilities.

3.4.2 Geometry and Mesh Generation

The simulated environment in this study comprised a fully enclosed rectangular room measuring 6 m x 6 m x 6 m (length x width x height). The simulation domain is defined within a mesh boundary of 8 m x 8 m x 8 m to account for any potential airflow and thermal effects beyond the room boundaries. In this study, the simulation is performed multiple times using varying grid resolutions, ranging from coarse to fine. The grid size is successively halved from 0.4 m until a nearly constant solution is achieved. The main objective is to examine the impact of mesh refinement on the results and determine the grid resolution at which the solution converged. The findings from the convergence and mesh independence study demonstrated that the simulation results showed a high level of independence from the grid resolution beyond a grid spacing of 0.1 m. Coarse mesh led to inaccurate results, while using a fine mesh incurred high computational costs and increased computation time. As further mesh refinement beyond 0.1 m did not significantly affect the results, a grid resolution of 0.1 m was used, resulting in a total of 512,000 grid cells. Figure 3.15 provides a visual representation of the room design, showcasing its dimensions and key features. Notably, the room featured small windows located at the upper sections of the walls, facilitating natural ventilation and preventing the accumulation of smoke, while an exhaust hood is incorporated as an integral part of the ventilation system, further contributing to the removal and dispersion of smoke within the room.

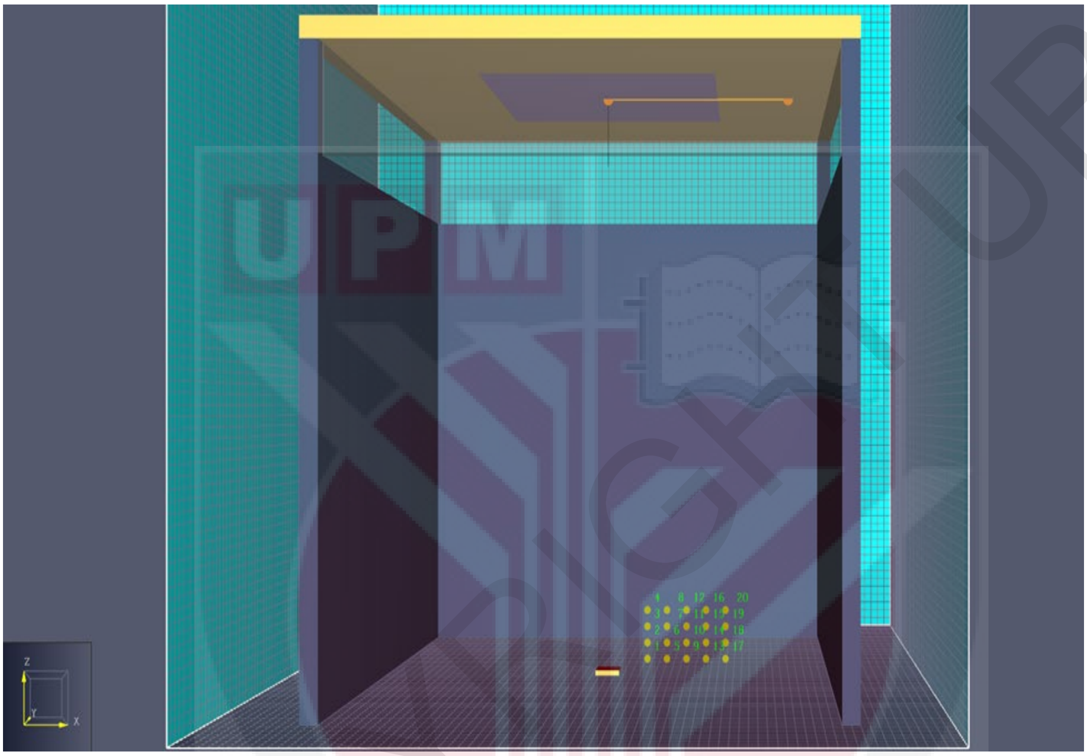

Figure 3.15: Room Design for FDS Simulation

3.4.3 Material Properties

The walls and floor of the room are constructed using 0.2 m thick concrete, providing structural stability and heat resistance. Conversely, the ceiling is made of gypsum board material, offering additional fire-resistant properties. In the simulation, the thermal conductivity, density, specific heat, emissivity, and absorption coefficient are assigned based on the default values provided by FDS. The example of materials specification is shown in Figure 3.16, where the properties of concrete used in the simulation are presented in detail.

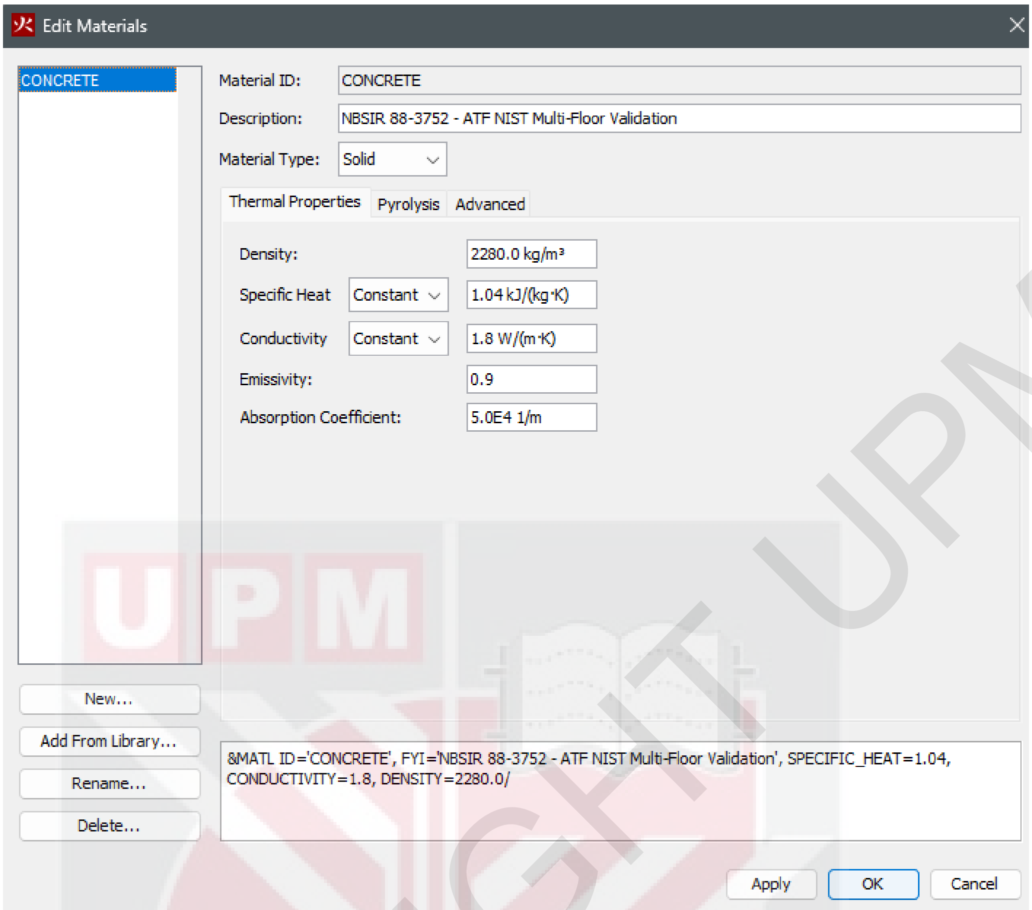

Figure 3.16: Material Description for Concrete in FDS Simulation

3.4.4 Fire Source Modelling

In this study, heptane and methane were selected as fuels for the pool fire simulations they are included as standard fuel options within PyroSim for pool fire simulations. Using these predefined fuels allowed for a straightforward setup of the simulations, as PyroSim already provides established parameters and properties for these substances. This convenience facilitated consistency across multiple simulations, enabling a reliable comparison between the thermal radiation model's performance and the CFD-based predictions generated by FDS. Additionally, by incorporating these default fuels, the study could assess the model's versatility and accuracy under conditions that closely resemble standardized pool fire scenarios. These fuels are well-documented in literature, providing reliable benchmarks for validating simulation results. Heptane is often used in fire experiments because of its consistent combustion characteristics, making it ideal for assessing the accuracy of heat flux predictions. Meanwhile, methane, being a simpler hydrocarbon, serves to simulate gas fires, allowing for comparison between the behaviors of liquid and gas fuels under similar conditions.

The data from these simulations provided a baseline to evaluate the performance of the proposed thermal radiation model. To account for different fire sizes and fuel types, six psm. files are designed, each specifying distinct pool fire configurations. Figure 3.17 shows the pool fire configurations for the 0.4 m x 0.4 m heptane pool fire used for the FDS simulations.

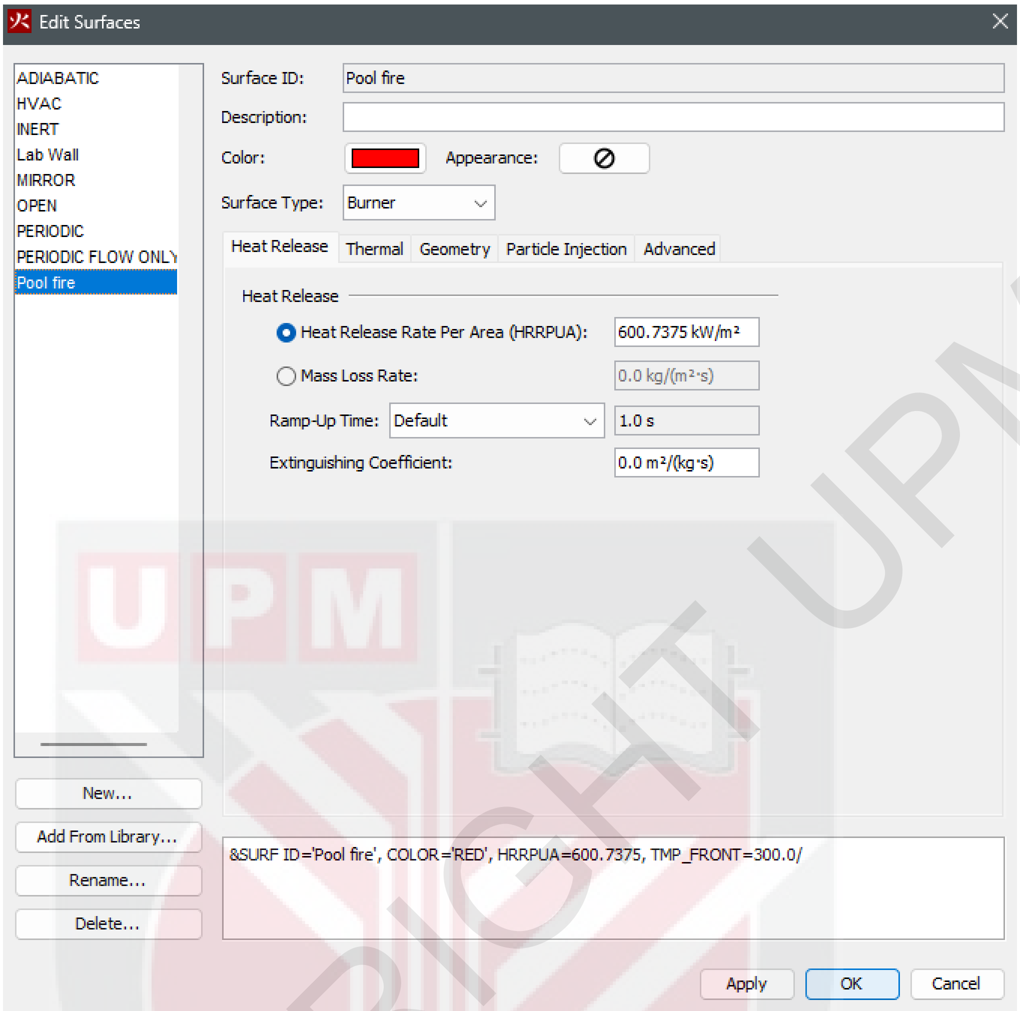

Figure 3.17: Pool Fire Configurations for 0.4 m x 0.4 m Heptane Pool Fire FDS Simulation

These variations in pool fire size and fuel type allowed for a comprehensive analysis of their impact on fire behaviour and thermal characteristics within the simulated environment. Specifically, a square pan constructed of steel is centrally positioned in the room, serving as the fire source, while the heat release rate per unit area (HRRPUA), a necessary pool fire (surfaces) information for simulation, is calculated based on the heat of combustion of the fuel used (refer to Equation 3.4). The detailed specifications of the pool fire, including its dimensions, the specific fuels tested, HRRPUA values, and corresponding heat of combustion for the other pool fires, can be found in Table 3.5.

$$HRRPUA = \frac{\Delta H_c \left(m_i - m_f\right)}{tA} \quad 3.4$$

where
ΔH_c is the heat of combustion for liquid fuel (kJ/kg)
m_i is the initial mass of the pan (kg)
m_f is the final mass of the pan (kg)
t is the total duration for combustion (s)
A is the area of flame base (m^2)

Table 3.5: Specifications of the pool fire for FDS simulations

Simulation No.	Fuel	Pan size (m^2)	HRRPUA (kW/m^2)	Heat of Combustion (kJ/kg)
1	Heptane	0.2 x 0.2	720.9	48.1 E+04
2	Heptane	0.3 x 0.3	694.2	48.1 E+04
3	Heptane	0.4 x 0.4	600.7	48.1 E+04
4	Methane	0.2 x 0.2	832.7	55.5 E+04
5	Methane	0.3 x 0.3	801.9	55.5 E+04
6	Methane	0.4 x 0.4	693.9	55.5 E+04

Note: Heat of combustion values are sourced from (Prosen & Rossini, 1944; Rossini, 1931)

3.4.5 Data Recording Devices

The simulation employed a set of 20 gas-phase heat flux gauges positioned at various horizontal measurement locations and at different vertical measurement locations relative to the flame source (as depicted in Figure 3.15). Gauges are placed at distances ranging from 0.5 m to 1.5 m away from the centre of the fire and at heights varying from 0.1 m to 0.61 m above the base of the flame. To establish a reference point, the centre of the flame is set at coordinates (4, 4, 0.05). The corresponding coordinates for the heat flux gauges are provided in Table 3.6, indicating their respective positions relative to the flame centre. Heat flux measurement at these different positions (as shown in Figure 3.18) are collected and used to validate the proposed model.

Table 3.6: Data recording devices and their positions relative to the centre of the flame

Device	Coordinate
Heat Flux Gauge 1	(4.5, 4, 0.15)
Heat Flux Gauge 2	(4.5, 4, 0.32)
Heat Flux Gauge 3	(4.5, 4, 0.49)
Heat Flux Gauge 4	(4.5, 4, 0.66)
Heat Flux Gauge 5	(4.75, 4, 0.15)
Heat Flux Gauge 6	(4.75, 4, 0.32)
Heat Flux Gauge 7	(4.75, 4, 0.49)
Heat Flux Gauge 8	(4.75, 4, 0.66)
Heat Flux Gauge 9	(5, 4, 0.15)
Heat Flux Gauge 10	(5, 4, 0.32)
Heat Flux Gauge 11	(5, 4, 0.49)
Heat Flux Gauge 12	(5, 4, 0.66)
Heat Flux Gauge 13	(5.25, 4, 0.15)
Heat Flux Gauge 14	(5.25, 4, 0.32)
Heat Flux Gauge 15	(5.25, 4, 0.49)
Heat Flux Gauge 16	(5.25, 4, 0.66)
Heat Flux Gauge 17	(5.5, 4, 0.15)
Heat Flux Gauge 18	(5.5, 4, 0.32)
Heat Flux Gauge 19	(5.5, 4, 0.49)
Heat Flux Gauge 20	(5.5, 4, 0.66)

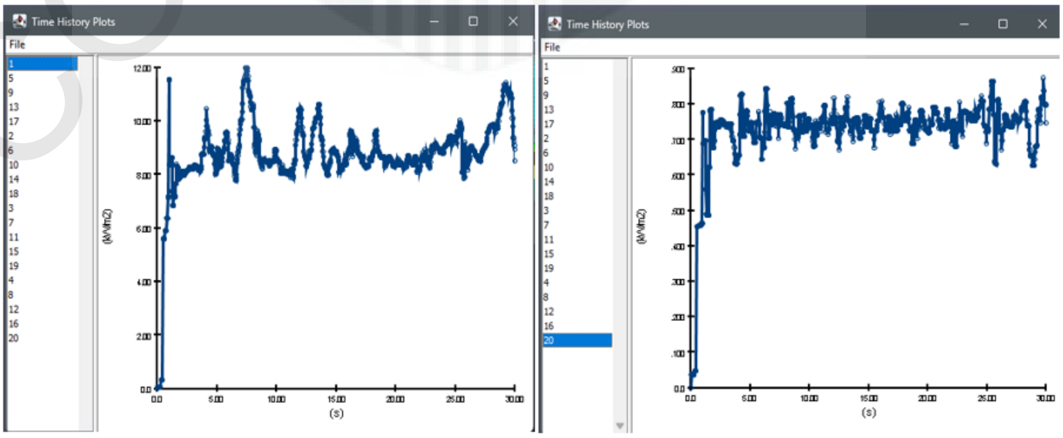

Figure 3.18: FDS Simulation Results for Heat Flux Gauge 1 (Left) and Heat Flux Gauge 20 (Right)

CHAPTER 4

RADIATION MODELS ASSESSMENT FOR GAS FIRE

4.1 Overview

The underlying principle for a large-scale fire incident is often the ignition of a small amount of combustible material, which subsequently triggers a domino effect as fire spreads from the item first ignited to other neighbouring items. Although combustion is the main concern for fire phenomena, it is the heat transfer which leads to fire propagation (Wu et al., 2022). One practical means to model this fire spread mechanism is by expressing the heat transfer using thermal radiation models, given that the primary mode of heat transfer for enclosure fire is thermal radiation (Chow et al., 2006; Ezekoye et al., 2013). Such application of thermal radiation modelling has been demonstrated by Tohir and Spearpoint (2019), in which the single point source model is integrated into the UCVFire simulation tool for the estimation of ignition time in connection with vehicle fires. Correspondingly, based on the work presented by Fleury et al. (2011), Spearpoint et al. (2020) have pointed out that the single point source model is the model of choice in the B-RISK computational tool for predicting fire spread between objects.

There is a broad selection of thermal radiation models available for the simulation of fire phenomena depending on the needs and requirements. To fully grasp the knowledge of the thermal behaviour of fire as well as the thermal interaction between adjacent items, it is imperative to ensure that the theoretical models applied have the capacity to analyse thermal response under various fire scenarios. In achieving these, the assessment of thermal radiation performance should be carried out to determine an appropriate fitting model for representing an actual fire. This chapter deals with one of the most universally used fuels for laboratory-scale fire testing, namely propane, for the assessment of thermal radiation model performance.

Previously, work that involved the evaluation of thermal radiation models for fire spread between objects using propane gas fire experiments has been carried out by Fleury et al. (2011). Embedded in that research is an investigation of the performance of six different radiation models with varying complexity. The models are the single point source model, the Shokri and Beyler simple correlation (Shokri & Beyler, 1989), the Shokri and Beyler detailed method (Beyler, 2016; Mudan, 1984), the Mudan method (Mudan, 1984), the Dayan and Thien method (He, 2001), and the rectangular planar method (Fleury et al., 2011). A number of experiments were completed, and the results obtained are used to assess the performance of these radiation models.

By comparing the measured data with the predictions made by the radiation models, Fleury et al. (2011) concluded that the single point source model is the best performing, with a MAPE value of 29%. In contrast, the MAPE values for the other models were as follows: 103% for the Shokri and Beyler simple correlation, 58% for the Shokri and Beyler detailed method, 221% for the Mudan method, 41% for the Dayan and Thien method, and 47% for the rectangular planar method. In addition, out of the six models investigated, the single point source model proved to be the most robust, being least influenced by the changes in experimental parameters. Given its performance and the previous work presented by Fleury et al. (2011), the single point source model is the only model out of the previous six assessed in Chapter 4.

The study described by Fleury et al. (2011) is limited to six common models, then available in 2011. Since 2011 to date there have been several studies on developing radiation models. Ji et al. (2019) assessed the performance of different radiation models to vertical targets and showed that a weighted multi-point model is superior for predicting radiant heat flux, as compared to the conventional single point source model. In fact, Ji et al. (2019) and Wan et al. (2019) have reached an agreement that the performance of a weighted multi point source model is considerably superior to the single point source model after finding that a weighted multi point source model is able to predict heat flux to within a 20% marginal error which could not be achieved using the single point source model. The findings by both Ji et al. (2019) and Wan et al. (2019) are derived from heptane-based experiments with diameter of fire ranging from 0.09 m to 0.34 m, evoking the question of whether the results shown by a weighted multi point model will hold true for propane-based experiments.

Conversely, Huang et al. (2020) have stated through their research that both the single point source model and the cuboid flame model are in good agreement with their propane gas fire experimental data. Nevertheless, the cuboid flame model appeared to achieve a slight improvement in terms of predicted percentage error. This finding is supported by Wan et al. (2018), who state that the cuboid flame model's precision level is far higher than the traditional single point source model when assessed against propane-based fire experiments. Both Huang et al. (2020) and Wan et al. (2018) have demonstrated a reduction in prediction error when applying the cuboid flame model as compared to the single point source model for propane flame with diameter of 0.17 m to 0.34 m; unlike with the single point source model, the estimated heat flux data evaluated using the cuboid flame model are located within ±20% error lines. The conclusions drawn by Huang et al. (2020) and Wan et al. (2018) are at odds with Fleury et al. (2011), who suggest that the best-performing model on average for propane fire heat flux estimation is the single point source model.

In assessing their upgraded version of the cuboid flame model through a series of experiments using propane as a fuel source, Huang et al. (2019) found that a multi cuboid flame model delivered a better heat flux estimation performance as compared to the single point source model. This improvement was observed for flames with diameters ranging from 0.34 m to 0.59 m. While the performance of the single point source model is found to be limited for near-field heat flux estimation, a multi cuboid flame model is shown to be superior in terms of reliability for larger radiant heat flux prediction. The standard error prediction made by the multi cuboid model is 0.505 in comparison to the single point source model, which is 0.941. Since Huang et al. (2019) have concluded that the upgraded model does indeed perform better than the single point source model, it is informative to include this model in this research.

The most recent model investigated in this research is the multi cylinder flame model developed by Ji et al. (2020) from heptane pool fires, which splits the conventional cylindrical flame model into several smaller but equal volumes of cylindrical flame geometry. Ji et al. found that the multi cylinder flame model managed to surpass the performance of most classical solid flame models. This claim is based on the apparent overestimation of radiative heat flux value for pool fires with a diameter less than 0.1 m and the underestimation of heat flux for pool fires larger than 0.2 m in diameter made by solid flame models in comparison to the results produced by the multi cylinder flame model. Taking into consideration that the single point source model is also assessed together with several classical solid flame models, it is logical that the multi cylinder model be included in this investigation.

In light of the radiation models published in the literature from 2011 up until recently, this work aims to bridge the knowledge gap by establishing a direct assessment of various recent models together with the best model determined by Fleury et al. (2011). Using the propane gas fire experimental data obtained from Fleury et al.'s work (2011), this research carries out an updated assessment of thermal radiation models' performance for propane-based fire experiments.

For this section, the performance of five thermal radiation models is investigated, including the best-performing model concluded from the findings of Fleury et al. (2011), i.e. the single point source model, as well as four recently developed models, i.e. weighted multi point source model, cuboid flame model, multi cuboid flame model, and the multi cylinder flame model. The models are assessed in terms of the horizontal distance of the target from the flame source, the height of the target from the flame base, the heat release rate of the burner and the size of the burner for propane-based experiments. The estimation of the theoretical models is then compared to the experimental data and analysed through numerical and graphical analysis.

This reassessment provides an opportunity to verify the performance of the previously identified best-performing model, the single point source model, in comparison to several newly established models. It takes into account the advancements made in fire modelling since the conclusion of the study by Fleury et al. (2011). Through this analysis, researchers can determine if the single point source model still remains superior or if the newer models offer improved accuracy and efficiency. Ultimately, this reassessment enables researchers and practitioners to make informed decisions regarding model selection, ensuring the utilisation of the most suitable and effective model for predicting thermal radiation behaviour.

4.2 Experimental Parameter

The method of analysis for the assessment of thermal radiation models in this section involves adopting the existing propane fire experimental data reported by Fleury et al. (2011) as a benchmark for the computed heat flux values using the models described above. In evaluating the radiant heat flux, the thermal radiation models require the input information from the experimental parameters shown in Table 4.1.

Table 4.1: Parameter combinations for propane fire experiments

Input parameters	Values
Distance of measurement location from centre of fire (m)	0.5, 0.75, 1.0, 1.5, 2.0
Height of measurement location from flame base (m)	0.0, 0.5, 1.0, 1.5
Area of flame base/burner (m^2)	0.3 x 0.3, 0.3 x 0.6, 0.3 x 0.9
Heat release rate (kW)	100, 150, 200, 250, 300

(Secondary data obtained from Fleury et al., 2011)

4.3 Results and Discussion

This section presents the results of the assessments. Four varying parameters are considered: horizontal distance of measurement location from the centre of the fire, height of measurement location from the flame base, aspect ratio of the flame burner, and heat release rate of the flame burner. These parameters represent the various possible interactions between different locations of the receiving target and the magnitude of the fire. By inputting the designated parameters for each test into the selected radiation models, the radiant heat flux to the target can be computed.

Given identical fire scenario (input) conditions, it is expected that the different radiation models will respond differently, thus generating different (output) heat flux estimations. By using experimental heat flux values as the benchmark for the capability of the selected radiation models, an assessment of their performance is determined by the degree of deviation between experimental and computed heat flux values.

4.3.1 Mean Absolute Percentage Error Analysis (MAPE)

This research utilised a subset of Fleury's experiments, focusing on tests (Test 7, 9, and 11) where burners were positioned vertically with heat flux gauges aligned to the longer side of the rectangular burner face. These specific test conditions differ slightly from the full range of experiments conducted by Fleury, potentially leading to differences in radiative heat transfer measurements. As such, the comparisons might differ due to these specific test conditions. Additionally, the MAPE analysis has been incorporated, showing a deviation of 31%, compared to Fleury et al.'s (2011) reported 29%, with an uncertainty margin of ± 2%.

This margin accounts for potential discrepancies, including differences in empirical assumptions, i.e., the radiative fraction assumption which might cause the divergence in results. In addition, the marginal error is also to acknowledge the original experimental uncertainty occurred in the research by Fleury et al. (2011), which noted that there exist a 0.99 coefficient of variation between to similar data sets, as well as the 900 ℃ assumption for flame temperature.

Table 4.2: Mean absolute percentage error for thermal radiation models

Performance ranking	Thermal radiation model	MAPE (%)
1st	Single point source model	30.8 ± 2
2nd	Weighted multi point source model	37.9 ± 2
3rd	Cuboid flame model	39.7 ± 2
4th	Multi cuboid flame model	56.9 ± 2
5th	Multi cylinder flame model	95.8 ± 2

Under similar fire conditions, the predictions made by the different radiation models vary between 30.8% up to 95.8%, as shown in Table 4.2. From the table, the single point source model did not only surpass the performance of the conventional models investigated by Fleury et al. (2011), but also the other recently developed models considered in this research, given the evidently lower average error. Although the single point source model can be compared to sound propagation following the Inverse Square Law, with more advanced models incorporating detailed radiation heat transfer mechanisms to enhance precision, the results for propane gas show otherwise. Table 4.2 demonstrates that the single point source model performs best among the models tested, proving its usability for accurately determining heat flux and calculating required setback distances for safe discharge paths during a fire incident. A comparison of estimated heat flux and experimental value measurements for the single point source model is shown in Figure 4.1.

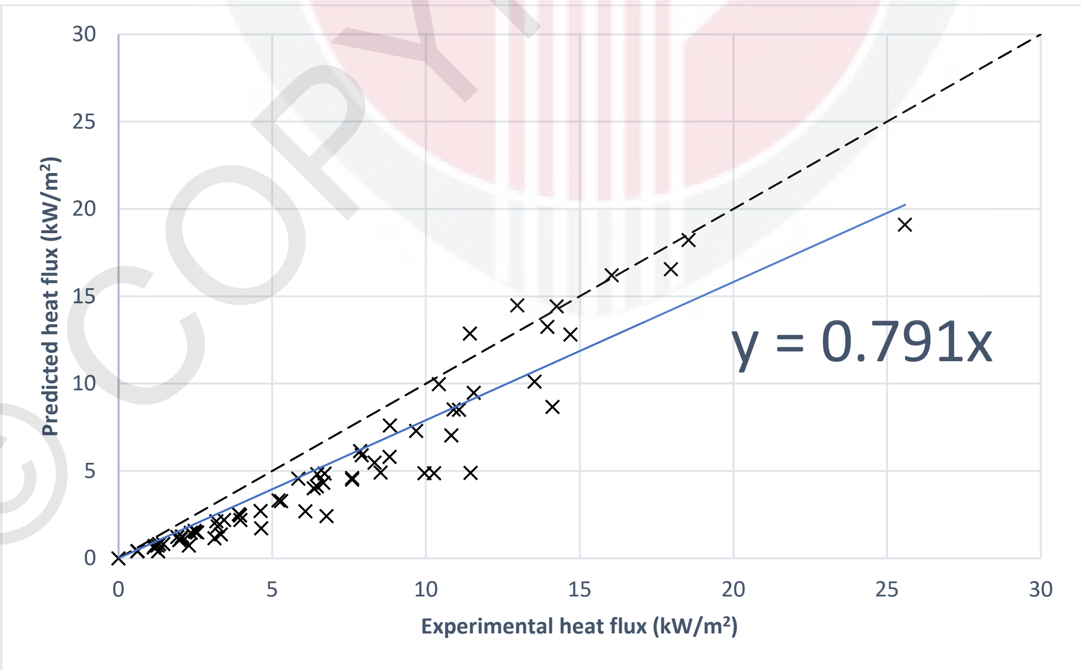

Figure 4.1: Comparison of Estimated Heat Flux and the Experimental Heat Flux Using Single Point Source Model

The scatter plot indicates a good fit between the predicted and experimental data for lower values of heat flux (< 5 kW/m^2), with the predicted values tightly clustered around the equality line. In this context, "better performing" refers to the closeness of predicted values to the equality line, which represents a 1:1 match between the predicted and experimental values. These findings align with previous research. For instance, Fleury et al. (2011) have cited Beyler (1999), which stated that the suitability of the single point source model for heat fluxes below 5 kW/m^2, while Beyler (2016) cautioned against its applicability for heat fluxes exceeding this threshold.

To better quantify the model's performance, a best-fit line was added to the scatter plot. The best-fit line represents the average trend in the model's predictions, allowing us to see general patterns, such as whether the model tends to overestimate or underestimate heat flux values across the range tested. The closeness of data points to this line can indicate the model's precision, while the closeness of the data points to the equality line reflects the model's accuracy, or "trueness," in estimating experimental values. In this case, the best-fit line has a slope less than one, indicating a general tendency of the model to underestimate heat flux values, particularly as the heat flux increases beyond 5 kW/m^2.

For heat flux values greater than 5 kW/m^2, the scatter plot reveals that while some data points remain close to the equality line, indicating that the single point source model can provide accurate estimates (trueness) in some cases, other points show increased scatter around the best-fit line, suggesting a reduction in precision as the heat flux rises. This behavior suggests that, although the model can achieve reasonable accuracy at certain higher flux levels, its precision diminishes as the flux values increase further.

By setting the intersection of the best-fit line at the origin (0,0), the analysis provides an unbiased view of the overall trend. The slope of the best-fit line being less than one reflects the tendency of the model to underestimate heat flux values at higher intensities, which could be attributed to the model's inherent assumptions and simplifications. While the model occasionally matches or exceeds experimental values at higher heat fluxes, the increased scatter indicates that these predictions become less reliable and consistent. This outcome highlights the importance of understanding the model's limitations when applied beyond its optimal range, particularly for higher heat flux values.

Of the four newer models presented in Table 4.2, following the single point source model, the best performing is the weighted multi point source model, which has an average percentage error that is 7.1% percentage points higher than the single point source model. Figure 4.2 summarises the performance of the weighted multi point source model.

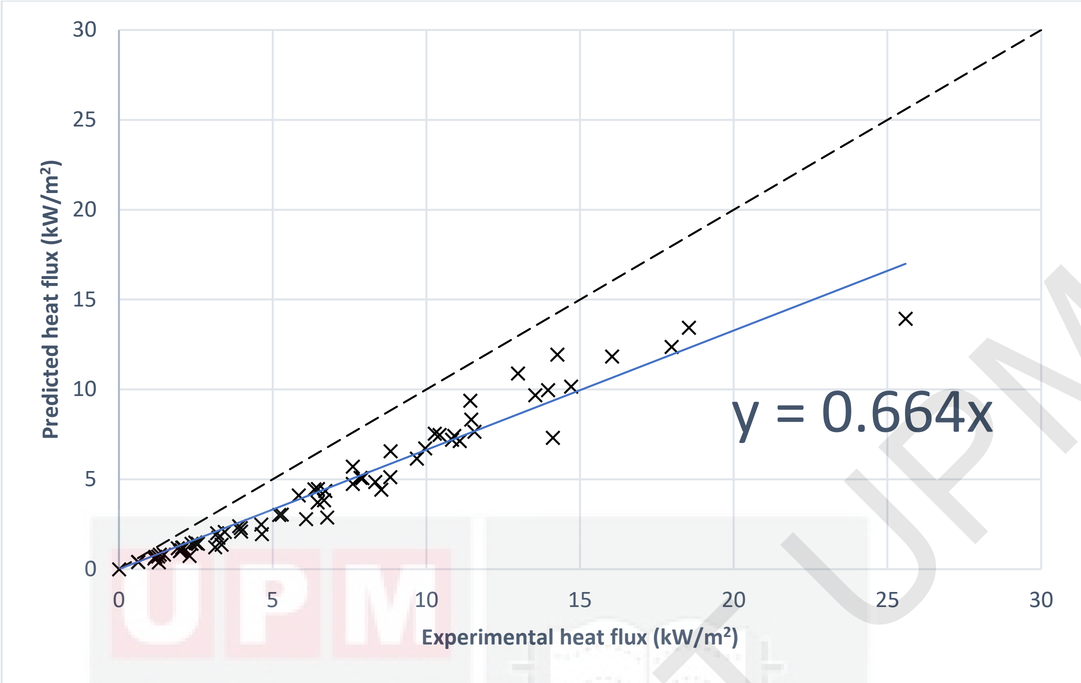

Figure 4.2: Comparison of Estimated Heat Flux and the Experimental Heat Flux Using Weighted Multi Point Source Model

As shown in Figure 4.2, the weighted multi-point source model demonstrates closer clustering of data points around the best-fit line, especially for lower heat flux values, indicating a strong precision. However, as heat flux increases, the model shows a greater tendency to scatter below the equality line, with a more pronounced underestimation at higher flux levels. This tendency is captured in the best-fit line slope, which is lower than that of the single point source model, highlighting an increased error margin as flux intensity rises. Although the weighted multi point source model shows a higher precision due to the tighter clustering of the data points around the best-fit line, the larger difference between the best-fit line and the equality line suggests a lower accuracy in predicting the actual heat flux values. In short, the accumulation of deviation error at higher heat flux values declined the overall performance of the weighted multi point source model when compared with the single point source model for propane fires.

This conflicting outcome compared to the findings by Ji et al. (2019) and Wan et al. (2019) may be explained by a combination of factors: first, both studies used heptane pool fires, which differ significantly from propane in terms of combustion properties, radiative behaviour, and sooting tendency. The heptane-based fires, as liquid pool fires, generate higher soot levels than gas fires with propane. This sooting directly impacts the radiative heat flux, as soot particles enhance radiation by emitting and absorbing in the infrared spectrum, resulting in higher and more consistent radiative intensity compared to the less sooty, non-luminous propane flames. The weighted multi-point source model may be more effective with heptane due to its design considerations for handling higher radiative emissions from soot particles.

Secondly, the experimental configurations differ between the studies. For instance, Wan et al. (2019) used both single and dual-pool fire setups. In their two-pool fire configuration, targets were placed either at the midpoint between two flames or on the side of one pool fire. Wan et al. (2019) found that the single point source model performed well for single flames and for the midpoint position in the dual-pool setup but underperformed at the side-target location. The weighted multi-point source model, on the other hand, outperformed the single point source model specifically at the side-target position. This difference in setup suggests that the weighted multi point source model may be more effective in scenarios where there are additional radiant heat contributions from multiple flame sources. Given that the propane dataset here involves a single gas burner with more uniform radiative output, this additional radiative contribution is absent, potentially diminishing the weighted multi point source model's effectiveness for propane fires.

The fuel properties directly affect several aspects of the thermal radiation models. For instance, fuels with higher sooting tendencies, such as heptane, contribute significantly to the radiative fraction due to the enhanced emissivity of soot particles. In contrast, low-soot fuels like propane exhibit lower radiative fractions, which leads to reduced radiative heat flux values. Apart from the radiative fraction, the total heat release rate ($\dot{Q}$), which is computed using the heat of combustion (ΔH_c) for specific fuel, also varies when the type of fuel changes. Fuels with higher heats of combustion, such as heptane, generally produce higher heat release rate values compared to fuels like propane. This variation in heat release rate directly impacts the model’s predictive capability, as it forms the basis for the calculation of radiative heat flux. These differences in radiative behaviour and heat release rate can influence the accuracy of the models and their predicted heat flux values.

In terms of applicability, the weighted multi-point source model shows limitations when applied to fuels with low radiative output, such as propane. This is due to the model's reliance on the radiative fraction and heat release rate, both of which are fuel-dependent and directly affect the accuracy of the heat flux estimates. Additionally, the model's effectiveness may decrease for single-flame scenarios where multiple radiant heat sources are not present. The model's assumptions, particularly regarding the weighting of heat flux contributions from multiple sources, may not align with the characteristics of single-flame propane fires.

The equations in the weighted multi-point source model are particularly sensitive to the radiative fraction term (χ_r) and the total heat release rate ($\dot{Q}$). For example, heptane pool fires typically have higher radiative fraction and total heat release rate values compared to propane fires, resulting in higher radiative heat flux estimates. If fuels such as alcohols or alkenes were used, the radiative fraction and total heat release rate values would differ further due to variations in combustion chemistry and soot production. The performance of the model may therefore vary significantly with different fuel groups, as the accuracy of the heat flux predictions is tied to the correct representation of radiative fraction and total heat release rate in the equations.

The predicted errors for each fuel group are influenced by these factors. For propane fires, the errors primarily arise from underestimation of radiative flux at higher heat flux levels due to the lower radiative fraction and total heat release rate values. For sooty fuels like heptane, errors may be smaller because the model is better suited to handle higher radiative intensities. However, fuels with unique combustion characteristics, such as alcohols with lower soot production, may introduce new error margins due to their distinct radiative and combustion behaviours.

The observed limitations of the weighted multi-point source model underscore how model effectiveness can vary significantly with fuel type and experimental setup. While this model appears particularly suited for sooty, multi-flame scenarios like heptane fires, its adaptability to single, low-soot fuel sources like propane may be limited due to differences in radiative behaviour. This highlights the potential need for refinement to enhance the model's versatility across various fire conditions.

Following the weighted multi-point source model, the cuboid flame model emerges as the third best-performing model in this research, with an average MAPE of 39.7%, 8.9% higher than the best-performing model (single point source model). Unlike the conventional solid flame model, which assumes a cylindrical geometry, the cuboid flame model utilises a cuboid shape as the basis for configuration factor calculations, significantly enhancing its performance. This approach has shown cuboid geometry to be a more effective representation of radiant heat transfer in comparison to cylindrical configurations.

Similar to the weighted multi-point source model, the performance discrepancy observed in this study, when compared to findings from multi-source setups like the two-pool fire setup used in Wan et al. (2018) studies, highlights the challenges in generalising results from multi-source fires to single-source setups. The two-pool fire setup used in Wan et al. (2018) likely introduces complex interactions between flames that could amplify the radiant heat flux experienced by any target positioned between or near the two pools. In such a configuration, the radiative zones from each fire overlap, creating enhanced regions of radiative intensity that a single fire setup would not replicate. The cuboid flame model, which assumes a simplified cuboidal geometry for radiation, may better accommodate this setup by distributing the radiative effect over a larger, more spread-out area with the combined effect of two pool fires than with a single source.

With a two-pool setup, radiant energy from each flame can intersect, and this overlapping can lead to “hot spots” of increased radiative intensity due to constructive interaction, a phenomenon that the cuboid geometry could inadvertently capture. This radiative overlap might explain why Wan et al. (2018) observed stronger performance from the cuboid flame model in a two-fire scenario for propane fire experiment, whereas, in the current study, which employs a single burner configuration, the model’s performance differs.

From a fire safety engineering perspective, a single-source fire scenario occurring at one location at a given time is often assumed to reflect the worst-case ignition location in performance-based designs, primarily to simplify calculations and avoid excessive conservatism. The single-burner setup in the current study is more aligned with such practical engineering applications, where assuming a single ignition source is standard. Thus, while a two-pool configuration may reflect a scenario with multiple ignition points, it is generally less applicable to common fire engineering practices, which prioritise single ignition scenarios for straightforward hazard assessment.

Another model with the same application of theoretical solid flame shape is the multi cuboid flame model. However, the results presented in Table 4.2 refute the claim made by Huang et al. (2019) that the multi cuboid flame model outperforms the single point source model for propane fires. This discrepancy may be partly explained by the presence of sidewalls in Huang et al. (2019)’s study, which could have influenced the model's performance by amplifying radiative heat flux. Walls surrounding a fire source often reflect and trap radiant heat, effectively creating a semi-enclosed radiative environment. This reflective effect can lead to higher radiative intensity near the flame and, consequently, may artificially enhance the accuracy of models like the multi cuboid flame model in capturing these higher flux values. In addition, it appears that the multi cuboid flame model, while developed with the intention of surpassing and enhancing the performance of the cuboid flame model, does not achieve this goal, as indicated by the outcomes of this study.

The model divides the cuboid flame model into several smaller yet identical solid flames. In the context of the propane gas fire and the range of burner sizes examined in this research, the performance of the multi cuboid flame model is assessed using different numbers of cuboids, including two, three, four, and five. The results revealed that the three-cuboid configuration achieved the best performance, with a MAPE of 39.7%. From the assessment, increasing the number of cuboids did not lead to a closer estimation, as the MAPE values for two and four cuboids are slightly higher at 49.5% and 62.4%, respectively. These findings suggest that the optimal number of cuboids may depend on the size and geometry of the flame being analysed. Considering that the maximum fire diameter employed in the work of Fleury et al. (2011) is equivalent to around 1 m, the decision to employ three cuboids offers an optimal balance between spatial resolution, computational efficiency, and model performance. The impact of sidewalls on radiative behaviour suggests that without reflective surfaces, the multi cuboid flame model may be less effective in open-air scenarios or environments lacking such boundaries, thus potentially limiting its broader applicability in predicting radiative heat flux for unconfined flames. It is important to note that further investigation is needed to determine the performance variation for different numbers of cuboids, particularly for flames with larger burning areas.

With a 66.67% increase in total surface area, it would be expected for the multi-cuboid model to transfer more heat toward the receiving target, potentially reducing the degree of underestimation observed in the original cuboid flame model. This increase in effective surface area theoretically translates to improved performance. However, contrary to the intended outcome when the multi-cuboid flame model was developed, dividing the larger single cuboid into multiple smaller cuboids has, in fact, raised the model's percentage inaccuracy. This may be due to the presence of sidewalls during model development, as discussed earlier, which could have led to amplified radiative heat flux that the current open-air setup does not replicate. The comparison between both versions of the cuboid flame model is shown in Figure 4.3 and Figure 4.4.

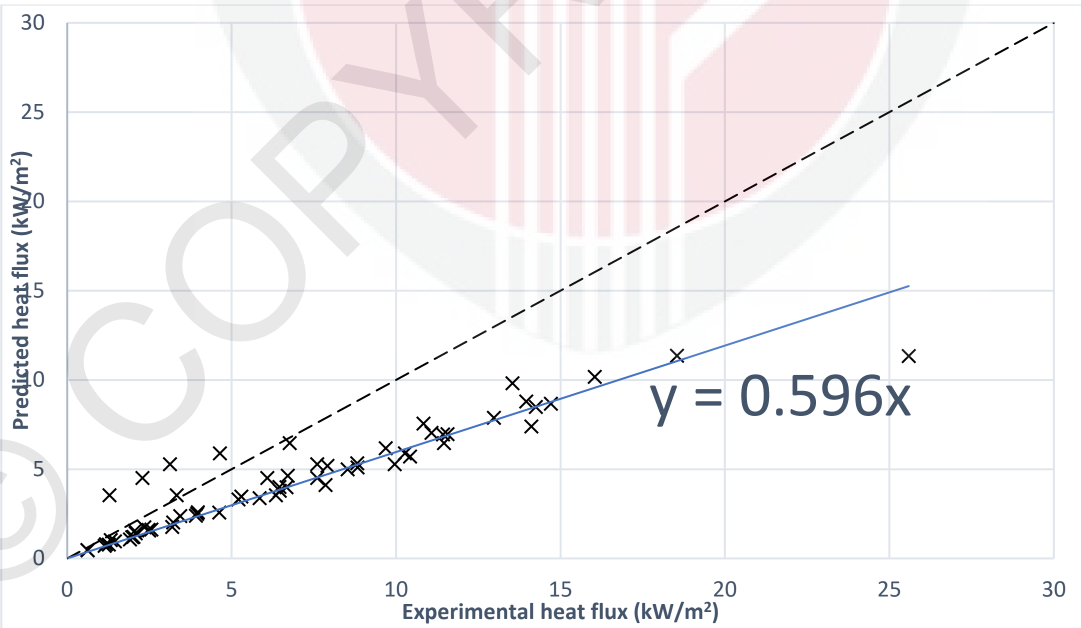

Figure 4.3: Comparison of Estimated Heat Flux and the Experimental Heat Flux Using Cuboid Flame Model

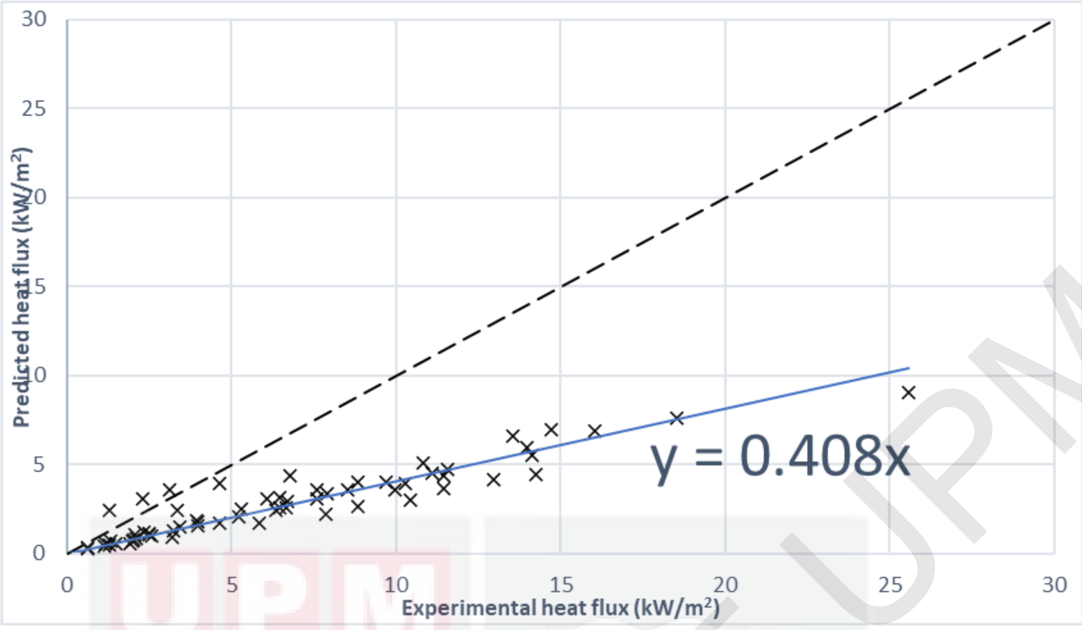

Figure 4.4: Comparison of Estimated Heat Flux and the Experimental Heat Flux Using Multi Cuboid Flame Model

Comparing Figure 4.3 and Figure 4.4, the plot for the cuboid flame model is scattered closer to the equality line, while the multi cuboid flame model is more compactly clustered at regions further below the equality line. A comparison of the slopes for best-fit lines of both models shows that the slope for the multi cuboid flame model is lower (0.408) than that for the cuboid flame model (0.596), indicating a higher degree of underestimation for the multi cuboid flame model.

These results suggest that the multi cuboid flame model, with its tighter clustering and lower slope, may be advantageous in applications where a high degree of precision is needed across distributed radiative fields over larger spatial areas. The model's consistent underestimation at high heat fluxes may make it suitable for scenarios requiring precise spatial mapping of heat flux, as it captures detailed radiative profiles with minimal deviation.

Conversely, the cuboid flame model's higher slope value brings it closer to measured values overall, albeit with slightly more scatter, making it more appropriate for situations where a conservative estimation is needed. By providing higher flux values than the multi cuboid model, it is useful in applications where slight overestimation aligns with fire safety requirements, such as in setback distance calculations. The cuboid flame model's balance between accuracy and conservatism ensures it can be relied upon for generalised scenarios where a cautious approach is essential.

Despite the differences in performance between both cuboid-based flame models, these models still outperformed the cylindrical flame model tested in this research. The most recently developed radiation model, the multi cylinder flame model, is the most mathematically sophisticated radiation model introduced for this research. Notwithstanding this, the model is the lowest-performing radiation model in this investigation. This is indicated by the average mean percentage error in Table 4.2, where the multi cylinder flame model scored the highest percentage error at 95.8%. Similar justification to the multi cuboid flame model, the multi cylinder flame model is assessed using several smaller yet identical cylindrical solid flames. Among the tested configurations, including two cylinders, three cylinders, and five cylinders, it was found that employing four cylinders resulted in the best performance for this particular set of experimental data. The MAPE for two cylinders, three cylinders, four cylinders, and five cylinders are all approximately 96.0%, with the four cylinders configuration having a slight advantage in terms of the decimal point.

It is worth noting that the impact of the number of cylinders on the model's performance is not as significant as observed for the multi cuboid flame model. Furthermore, since the maximum size of flame examined in this investigation is only limited to small-scale fire experiments, the division of cylinders beyond five is not explored. Therefore, the choice of employing four smaller cylindrical solids is deemed sufficient for capturing the fundamental flame characteristics and achieving the best predictions within the scope of the study. The heat flux estimation results are shown in Figure 4.5.

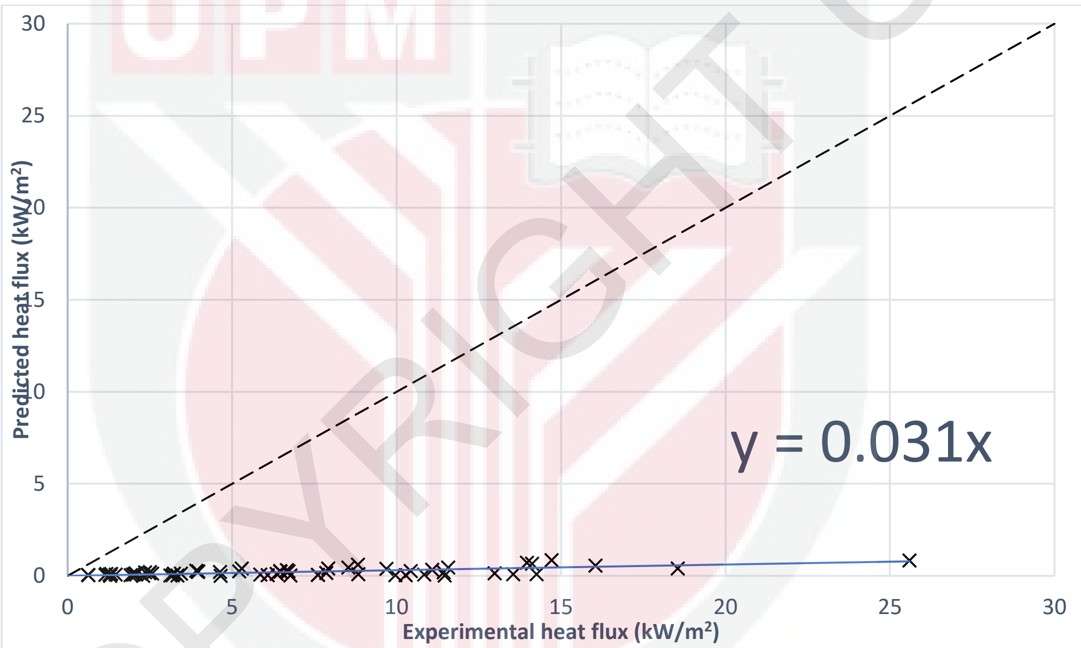

Figure 4.5: Comparison of Estimated Heat Flux and the Experimental Heat Flux Using Multi Cylinder Flame Model

A primary factor contributing to the higher mean percentage error is the lower heat flux values evaluated using the multi cylinder model compared to the experimental heat flux values. This is reflected in the scatter plot, where the predicted values are aligned far below the equality line. The slope of the best-fit line for this model is also the lowest among all models (0.138), indicating that the model is prone to significant underestimation of heat flux values. Although all models evaluated in this chapter underestimate the experimental heat flux for the propane gas fire experiment, the multi cylinder model shows the strongest bias towards underestimating the heat flux data, making it less reliable for practical applications.

This underperformance may stem from the model's design and calibration, which appear to be tailored to the radiative characteristics of heptane flames rather than propane. Klassen and Gore (1993) have shown that critical thermal and radiative properties (i.e., sooting propensity, molecular structure, and combustion dynamics), produces significant particulate emissions, emitting stronger visible and infrared radiation. In contrast, propane's radiation largely originates from non-luminous sources, resulting in lower emissivity and radiative output. Since the multi cylinder flame model accounts for fuel properties only through emissivity, this narrow parameterisation may lack the flexibility needed to accommodate propane's lower soot content and distinct radiative intensity.

A further difference lies in the treatment of heat release rates. While the single point source model incorporates fuel characteristics by adjusting the heat of combustion in calculating total heat release, the multi cylinder flame model relies solely on emissivity to account for fuel-specific properties. This approach creates a significant modelling gap for less sooty flames, where gas-phase radiation and fluctuating temperature fields play a more critical role than in sooty flames. For instance, propane's radiative output is influenced more by molecular transitions than by particulate radiation, suggesting a need for more nuanced radiative terms than those in the current multi cylinder model.

Additionally, since propane flames radiate more through vibrational-rotational transitions of gas-phase molecules than through soot particle emissions, the limited emissivity-based approach in the multi cylinder flame model lacks the complexity needed to handle propane's unique non-luminous radiative profile adequately. This highlights a potential calibration bias, where the model may have been optimised around the thermal and radiative properties specific to heptane flames and their high soot concentrations.

Furthermore, Klassen and Gore (1993) highlight that turbulence and radiative interactions significantly impact radiation intensity in turbulent diffusion flames, like those of gaseous fuels. Propane flames display dynamic, fluctuating radiative output, which the multi cylinder flame model does not account for adequately. Without variables to capture these fluctuations, the model may struggle to adapt its predictions to the varied and oscillatory nature of propane flames.

In short, the multi cylinder model's reliance on emissivity as its sole fuel-specific adjustment limits its adaptability to different fuel types, making it structurally biased toward sooty flames like heptane. While this results in lower accuracy with propane flames, the model does demonstrate the highest degree of precision among the thermal radiation models examined, as shown by the tight clustering of data points around the best-fit line. Despite its lower trueness, this precision may make the multi cylinder model a valuable option for applications where repeatability and consistency are prioritised over absolute accuracy.

4.3.2 Median Absolute Percentage Error (MdAPE)

In addition to MAPE, MdAPE offers a complementary approach to understanding the distribution of heat flux percentage errors for different radiation models. The median analysis is performed for each thermal radiation model to gain insights into the central tendencies of the model predictions, and the results are shown in Table 4.3.

Table 4.3: Median absolute percentage error for thermal radiation models

Performance ranking	Thermal radiation model	MdAPE (%)
1st	Single point source model	35.0
2nd	Weighted multi point source model	38.1
3rd	Cuboid flame model	38.6
4th	Multi cuboid flame model	58.0
5th	Multi cylinder flame model	96.2

By comparing Table 4.3 to the previously discussed Table 4.2, a consistent pattern that aligns with the findings from MAPE is revealed. Not only the best-performing models, but also the ranking performance of all other models determined through median analysis are in complete agreement in accordance with mean analysis. The single point source model exhibited the lowest MdAPE across all the tested scenarios, indicating that the model's predictions are more aligned with the central tendency of the experimental data, giving the model a greater accuracy in capturing the overall behaviour and variability of the radiative heat flux. Following closely is the weighted multi point source model and the cuboid flame model, which displayed a slightly higher MdAPE of 38.1% and 38.6% respectively, compared to the single point source model's 35.0%.

The multi cuboid flame model performed moderately with a 58.0% percentage error, while the multi cylinder flame model showed the highest MdAPE at 96.2%.

The consistency between MAPE and MdAPE across models suggests a strong alignment between the average and central tendencies in model performance. Notably, the difference between MAPE and MdAPE values is more pronounced for the single point source model, with a gap of 4.2%, while this gap narrows for models lower in the ranking. This narrowing of the gap is further reflected in the standard deviation of the error values, with the single point source model showing the highest standard deviation at 17.3, indicating greater variability in its predictions. As we move down the performance ranking, models such as the weighted multi point source model and multi cylinder flame model exhibit lower standard deviations of 10.3 and 2.5, respectively, suggesting that, although their accuracy decreases, their predictions are more consistent (i.e., have higher precision) around a central value. Thus, while models like the multi cylinder flame model are less accurate (with high MAPE), their predictions are relatively clustered around a central value, contributing to the lower deviation in MdAPE. This implies that outliers or extreme values have less influence on lower-performing models, as their error distribution is more clustered.

The alignment of results between the median and mean analysis results reinforces the findings' robustness. Both analyses indicate that the single point source model outperforms the other models in terms of heat flux estimation. Furthermore, the similar rankings observed in both analyses suggest that outliers or extreme values do not drive the performance trends but rather reflect the overall performance of the models. While mean analysis emphasises the average performance, median analysis focuses on the central tendencies for identifying potential skewness or outliers in the data. The convergence of results between the two analyses lends greater confidence to the conclusion that the single point source model is the top-performing thermal radiation model for the experiments considered.

4.3.3 Sensitivity Analysis of Input Variables

A sensitivity analysis is conducted to gain insights into how varying ranges of parameters affect the performance of different radiation models, specifically in terms of percentage error. This analysis aimed to uncover the sources of uncertainty within the thermal radiation that contributed to the overall MAPE. It is acknowledged that the use of MAPE in the calculations may result in higher deviations, especially when relying on generic data. To counter this, a categorisation approach is proposed to provide a more detailed analysis of how the data is distributed and the nature of errors introduced. By categorising the data, it becomes easier to identify outliers and the degree of variation across different experimental setups. While the MAPE and MdAPE analyses have demonstrated the accuracy of the single point source model, it remains important to assess whether these results are dependent on specific input variable ranges. Moreover, this sensitivity analysis ensures that the model is robust to variations in these parameters, offering valuable insights into identifying the most influential inputs. A detailed discussion of how each parameter affects the output, along with an analysis of the error margins and their implications, has been included in the current chapter. Further analysis of these sensitivity results will be presented in the subsequent results chapter.

4.3.3.1 Distance from the Centre of Fire

For this section, the impact of distance from the centre of fire on the performance of thermal radiation models is evaluated. The distances considered for the estimation of heat flux ranged from 0.5 m to 2.0 m (as per Table 4.1). Each thermal radiation model's performance is evaluated, and the results for each distance are shown in Table 4.4.

Table 4.4: Mean absolute percentage error at different distance parameters from the centre of fire

	Mean Absolute Percentage Error (%)				
Distance (m)	Single Point Source Model	Weighted Multi Point Source Model	Cuboid Flame Model	Multi Cuboid Flame Model	Multi Cylinder Flame Model
0.50	25.7	35.0	43.5	56.3	97.6
0.75	29.7	38.9	39.9	59.4	95.5
1.00	34.8	40.3	36.6	58.0	94.9
1.50	40.6	43.1	35.1	57.6	94.7
2.00	40.0	41.4	31.1	55.2	94.4

Based on the sensitivity analysis for the impact of horizontal distance between the burning source and target, the single point source model and the cuboid flame model are greatly affected by changes in distance with an apparent 14.3% and 12.4% mean percentage point deviation between shortest (0.5 m) and longest distance (2.0 m) examined respectively. Conversely, the changes in horizontal distance for the weighted multi point source model, multi cuboid flame model, and multi cylinder flame model have a maximum of 1.8% - 6.4% point deviation between the nearest distance examined and furthest distance tested. Despite the significant effect of distance on the performance of the single point source model, as discussed previously, it is the best-performing model over the distances examined, especially for shorter distances (under 1.25 m) from the centre of the flame, in which the error is the least.

4.3.3.2 Height of Target from Flame Base

The height of the target tested in the analysis ranged from 0.0 m to 1.5 m above the base of the fire. To perform sensitivity analysis, the evaluated heat flux data are taken as the four flame height parameters (as per Table 4.1) assessed for this research, and the results are shown in Table 4.5.

Table 4.5: Mean absolute percentage error at different target's height parameters from the base of the fire

	Mean Absolute Percentage Error (%)				
Height (m)	Single Point Source Model	Weighted Multi Point Source Model	Cuboid Flame Model	Multi Cuboid Flame Model	Multi Cylinder Flame Model
0.0	47.5	28.2	43.7	61.6	99.3
0.5	26.6	36.6	38.1	58.6	95.6
1.0	43.2	42.5	24.2	46.6	99.4
1.5	65.7	62.8	74.1	37.7	99.7

With the exclusion of the multi cuboid flame model, it is observed that all other models have increasing trend of MAPE along the vertical measurement location. Furthermore, it is also revealed that the overall outcome of the thermal radiation model performance assessment is strongly affected by the estimation made by radiation models at different heights of the measurement location, apart from the multi cylinder flame model. The mean percentage point deviation for the highest and lowest heights examined ranged from 0.4% to 34.6%, with the weighted multi point source model being the most sensitive and the multi cylinder flame model being the least affected by changes in vertical measurement location. This heightened sensitivity of the weighted multi point source model can be attributed to its assumption of multiple point sources distributed along the vertical axis of the flame, making it more responsive to relative differences between the vertical positioning of these point sources and the target's height.

One potential limitation of the analysis is that it assumes the outcome is solely determined by the target’s height, overlooking the potential influence of the heat release rate of the flames. In reality, the height of the flames is closely interconnected to the heat release rate, as higher values of heat release rate tend to result in taller flames. Consequently, the errors at specific target heights may be affected by the corresponding flame heights. Although the current analysis did not explicitly consider the combined effects of heat release rate and flame height, it is important to acknowledge this limitation. By acknowledging this limitation, the findings of the analysis can be interpreted with caution and may serve as a basis for further research exploring the interplay between heat release rate, flame height, and predictive accuracy.

4.3.3.3 Area of Burner

Different sizes of propane gas burners are involved in the experimental programme described by Fleury et al. (2011). Due to the dependency of burner geometry on the assumptions made for some of the radiation models, the flame base is partitioned in relation to the area of the burner rather than the burner diameter or burner aspect ratio. The percentage errors for the different gas burner areas are shown in Table 4.6.

Table 4.6: Mean absolute percentage error at different area parameters of burner

Mean Absolute Percentage Error (%)					
Area (m^2)	Single Point Source Model	Weighted Multi Point Source Model	Cuboid Flame Model	Multi Cuboid Flame Model	Multi Cylinder Flame Model
0.09	15.8	26.1	42.7	70.0	98.6
0.18	33.4	39.2	39.9	56.1	96.9
0.27	31.3	39.8	37.9	53.4	93.9

From Table 4.6, it can be observed that the single point source model and the weighted multi point source model exhibited an increasing trend as the area increased from 0.09 m^2 burner size, while the MAPE for the cuboid flame model, multi cuboid flame model, and the multi cylinder flame model decreased as the size of the burner increased. Based on the sensitivity analysis results, it is found that the size of the burner does have an impact on the performance of the single point source model, weighted multi point source model, cuboid flame model and multi cuboid flame model, while the multi cylinder flame model shows a high degree of robustness despite the changes in burner's size. The model that is impacted the most by the changes in the burner's size is the multi cuboid flame model, where the mean percentage point deviation between the smallest size of the burner tested (0.09 m^2) and the largest burner examined (0.27 m^2) is 16.6%, approximately 12% higher than the mean percentage point deviation for the multi cylinder flame model.

Another factor that may contribute to the observed trend is the aspect ratio of the burners. The aspect ratio refers to the ratio of width to height for the burners. In this study, the 0.09 m^2, 0.18 m^2, and 0.27 m^2 burners have aspect ratios of 1:1, 2:1, and 3:1 respectively. It is worth noting that the multi cylinder flame model exhibit less mean percentage point deviation as compared to the multi cuboid flame model when dealing with longer and narrower flame bases. The multi cylinder flame model demonstrates better consistency in scenarios with higher aspect ratios. On the other hand, the multi cuboid flame model struggles to consistently predict heat flux accurately in such cases. The robustness of the multi cylinder flame model in dealing with longer and narrower flame bases highlights its potential advantages in predicting heat flux in such configurations, especially when appropriate correction factors are applied to improve their trueness.

4.3.3.4 Heat Release Rate

The heat release rates assessed in the experimental research range from 100 kW to 300 kW. For the purpose of studying how the overall performance of radiation models is affected by the changing heat release rate, the whole range of data is partitioned into five heat release rates assessed by Fleury et al. (2011), as shown in Table 4.7.

Table 4.7: Mean absolute percentage error at different heat release rate parameters of flame

Mean Absolute Percentage Error (%)					
Heat release rate (kW)	Single Point Source Model	Weighted Multi Point Source Model	Cuboid Flame Model	Multi Cuboid Flame Model	Multi Cylinder Flame Model
100	38.7	42.0	45.8	57.9	95.4
150	34.1	40.7	43.7	57.2	96.7
200	29.6	36.9	37.9	53.6	95.3
250	27.0	34.8	37.0	55.4	97.0
300	27.5	36.4	36.9	58.6	96.8

Generally, most models assessed in this research showed consistent performance across the range of heat release rates. The single point source model and the cuboid flame model demonstrated a higher mean percentage point deviation between the highest and lowest heat release rates examined (11.2% and 8.9% respectively), while the remaining three models displayed a mean percentage point deviation below 7%. Nevertheless, it is important that the MAPE might also be affected by the height of the flames, as discussed previously in Section 4.3.3.2. The interaction between heat release rates and flame height can contribute to the overall error and should be taken into consideration for a more comprehensive analysis of the models' performance.

The sensitivity analysis reveals that the single point source model exhibits high sensitivity to changes in horizontal distance, height of measurement location, flame size and heat release rate. Since the performance of the single point source model declines with increased distance from the flame and at lower heat release rates, it is recommended to use this model within shorter distances (less than 1.25 meters) and at higher heat release rates to maintain an uncertainty margin of 2%. Any larger deviations from these conditions would likely increase the error beyond this threshold, impacting the overall consistency of the single point source model's performance. These recommended conditions were identified based on experimental calibration and sensitivity testing, ensuring that the model operates within its optimal prediction range.

In contrast, the more recent models were developed to achieve greater robustness. However, it is worth noting that the single point source model consistently outperforms the others across all ranges of flame size and heat release rate. This superiority is likely attributed to its compatibility with experimental results from propane gas fire experiments as well as the parameter tested in this research, albeit this claim is provisional until models are assessed across a broader spectrum of fuels.

4.4 Summary

The research provides insights into the basic requirements for performance-based fire design of buildings, specifically the need for an accurate and robust computational model to represent in the fire scenario simulations. The outcome of the assessment of radiation models concludes that the single point source model provides the most accurate prediction of heat flux to a target, followed by the weighted multi point source model and cuboid flame model, as determined from the experiments conducted by Fleury et al. (2011). It is worth noting that the claims made by several other researchers regarding alternative models have been examined and refuted in this study. These include Ji et al. (2019) and Wan et al. (2019), which suggested that the weighted multi point source model performs better than the single point source model, and Huang et al. (2020) and Wan et al. (2018), which advocated for the superiority of the cuboid flame model. Similarly, Huang et al. (2019) endorsed the multi cuboid flame model as a better alternative for radiant heat flux prediction. However, the comprehensive evaluation conducted in this research consistently demonstrates that the single point source model outperforms these alternatives. The single point source model's ability to achieve the lowest error through Mean Absolute Percentage Error Analysis and Median Absolute Percentage Analysis, despite the lower robustness demonstrated through sensitivity analysis, suggests it is suitable for assessing fire safety within buildings.

Acknowledging the main constraint in this research, including the limited scope of fuel tested, as well as the restricted range of heat release rates and flame dimensions, one possible improvement for heightening the credibility of the research would be to assess the performance of the radiation model for fuels of different physical states. By expanding the research to include liquid fuels as well as incorporating a wider range of flame geometries, future studies can provide a more comprehensive understanding of the radiation models' performance. This would not only complement the results obtained in this research, which focused on propane gas fires, but also provide valuable insights into the application of the models across a broader spectrum of fire scenarios.

CHAPTER 5

RADIATION MODELS ASSESSMENT FOR LIQUID FIRE

5.1 Overview

Fires can lead to various outcomes, ranging from minimal damage or loss to catastrophic consequences, depending on several factors. The characteristics of the fire, including its type, mode of occurrence, and potential for escalation, play a crucial role in determining the extent of damage and loss. In the case of a pool fire, in addition to the release of intense radiative heat fluxes and the attainment of extremely high temperatures, there are additional hazards that can have devastating consequences for both human life and structural integrity (Yuan et al., 2021). These hazards include impaired visibility along escape routes due to excessive smoke, toxicity from the release of carbon monoxide resulting from incomplete combustion, and overpressure impacts from the hot combustion gases (Pula et al., 2005). Understanding the characteristics and behaviour of pool fires becomes even more crucial in implementing effective fire safety measures and mitigation strategies, especially in industries where such incidents are more likely.

To assess fire risks and design effective protection measures, fire modelling techniques provide a valuable approach for estimating the heat transfer interaction between the flame source and the target. Over the past decades, simplified fire modelling tools derived from specific experiments and empirical correlations have been widely used to predict the harmful effects of hydrocarbon pool fires. However, Rengel et al. (2018) have pointed out the limitations of these methods, as their applicability is constrained to a limited number of fire scenarios. Therefore, identifying the best-performing thermal radiation model for predicting the thermal behaviour of pool fires remains a crucial area of investigation.

Chapter 4 builds upon and reinforces the findings of Fleury et al. (2011) by incorporating several newly developed thermal radiation models. However, it is crucial to acknowledge that the previous part of the research relied on experimental data from Fleury's work, which focused mainly on gas-based fuels. As a result, the applicability of the single point source model for liquid fuel fires remains unexplored. While the single point source model has demonstrated excellent performance in estimating heat flux for gas-based fuels, the limited availability of heat flux data collected from gas fuel experiments raises concerns about its suitability for representing fires in conventional buildings, where the main combustible materials are typically not gas fuels. Consequently, there is a need to investigate the performance of the single point source model specifically for liquid pool fuels. Chapters 5 of this research aims to address this need and identify the optimal thermal radiation model for predicting fire behaviour by conducting liquid pool fire experiments using the two most common flammable substances found in buildings, i.e., ethanol and isopropyl alcohol.

Furthermore, this chapter extends the assessment to include additional thermal radiation models that were not evaluated in the previous phase. The Shokri and Beyler correlation, Shokri and Beyler detailed method, Mudan method, Dayan and Tien method, and the rectangular planar model were excluded from the initial assessment, as they had already been assessed in previous studies specifically for propane gas fire experiments. However, following the changes of fuels tested in this chapter, these previously overlooked models are included to explore potential differences in performance for liquid pool fire experiments. In summary, this section aims to address the existing gap in model assessment for liquid fire data by conducting experiments specifically focused on ethanol and isopropyl alcohol liquid pool fires.

5.2 Experimental Parameter

This research incorporated a series of square pans with varying sizes into the experimental investigation to represent different scales of liquid pool fires. The primary aim is to gather comprehensive data on the characteristics of ethanol and isopropyl alcohol pool fires, considering the fuel properties specified in Table 5.1. To achieve this, several parameters are carefully recorded, including temperature, flame height, heat release rate, and radiative heat flux measurements. These measurements are systematically collected for each of the 120 individual experiments, all conducted with repetition, for both fuels.

Different parameters are employed to cover a wide range of fire scenarios, as illustrated in Table 5.2 and Table 5.3 for ethanol and isopropyl alcohol pool fire experiments, respectively.

Table 5.1: Fuel properties for ethanol and isopropyl alcohol

Properties	Ethanol	Isopropyl Alcohol
Boiling point (℃)	77.1	82
Flash point (℃)	13.9	12
Autoignition temperature (℃)	362.8	399
Heat of combustion (kJ/kg)	2.97×10^4	3.34×10^4

(Adapted from Thermofisher, 2022; Lab-Chem, 2016)

Table 5.2: Parameter combinations for ethanol pool fire experiment

Area of pool fires (m^2)	Distance of measurement location from the centre of the flame (m)	Height of measurement location from the base of the flame (m)
Area 1: 0.04 **Area 2: 0.09** **Area 3: 0.16**	0.50	0.1 0.27 0.44 0.61
	0.75	0.1 0.27 0.44 0.61
	1.00	0.1 0.27 0.44 0.61
	1.25	0.1 0.27 0.44 0.61
	1.50	0.1 0.27 0.44 0.61

Table 5.3: Parameter combinations for isopropyl alcohol pool fire experiment

<table>
<tr><th>Area of pool fires (m²)</th><th>Distance of measurement location from the centre of the flame (m)</th><th>Height of measurement location from the base of the flame (m)</th></tr>
<tr><td rowspan="20">Area 1: 0.01

Area 2: 0.04

Area 3: 0.09</td><td rowspan="4">0.50</td><td>0.1</td></tr>
<tr><td>0.27</td></tr>
<tr><td>0.44</td></tr>
<tr><td>0.61</td></tr>
<tr><td rowspan="4">0.75</td><td>0.1</td></tr>
<tr><td>0.27</td></tr>
<tr><td>0.44</td></tr>
<tr><td>0.61</td></tr>
<tr><td rowspan="4">1.00</td><td>0.1</td></tr>
<tr><td>0.27</td></tr>
<tr><td>0.44</td></tr>
<tr><td>0.61</td></tr>
<tr><td rowspan="4">1.25</td><td>0.1</td></tr>
<tr><td>0.27</td></tr>
<tr><td>0.44</td></tr>
<tr><td>0.61</td></tr>
<tr><td rowspan="4">1.50</td><td>0.1</td></tr>
<tr><td>0.27</td></tr>
<tr><td>0.44</td></tr>
<tr><td>0.61</td></tr>
</table>

5.3 Results and Discussion

Similar to the evaluation conducted for gas fire experiments, the performance of various thermal radiation models is assessed based on the Mean Absolute Percentage Error (MAPE) analysis, augmented by the Median Absolute Percentage Error (MdAPE) analysis. Additionally, the robustness of the models is assessed through sensitivity analysis. Notably, the conventional models examined by Fleury et al. (2011), including the Shokri and Beyler correlation, the Shokri and Beyler detailed method, the Mudan method, the Dayan and Tien method, and the rectangular planar model, have not been previously tested against the data from liquid pool fire experiments. Therefore, this chapter aims to evaluate these conventional models alongside the five models already assessed in Chapter 4. While the previous chapter relied on secondary data obtained from a propane gas fire experiment conducted by Fleury et al. (2011), Chapters 5 involves the use of ethanol and isopropyl alcohol pool fire experiments to gather comprehensive primary data for the assessment of thermal radiation models.

In this study, four pans were initially prepared for the pool fire assessments, but only three were used for both ethanol and isopropyl alcohol experiments. The smallest pan (10 x 10 cm) was excluded from the ethanol tests because it did not produce sufficient heat flux readings at greater distances, as measured by the heat flux gauge. Conversely, the largest pan was not used for isopropyl alcohol experiments because the resulting flame height exceeded the capture range of the exhaust hood, causing the flame to be partially out of the video frame and leading to measurement difficulties. These selections ensured that only the accurate and reliable data would be obtained for each assessment.

In addition to their availability and common usage in various building environments, the selection of ethanol and isopropyl alcohol (IPA) as fuels in this study was also intended to capture the distinct combustion characteristics of sooty and non-sooty fires. Ethanol was chosen to represent non-sooty combustion, while IPA served as a representative of sooty combustion. Although soot formation is generally associated with incomplete combustion due to limited oxygen, IPA will still produce a sooty flame because of its higher carbon-to-hydrogen ratio compared to ethanol. This means that during combustion, there is a greater likelihood of incomplete oxidation, leading to the formation of carbon particles (soot). The additional carbon content in IPA contributes to more complex combustion reactions, particularly under conditions such as localized cooling or disruptions in air entrainment, which can cause visible soot production. By using these two fuels, the study aims to provide a comprehensive assessment of thermal radiation behaviour across different fire scenarios.

5.3.1 Mean Absolute Percentage Error (MAPE) Analysis

This chapter evaluates the thermal radiation models applied to liquid pool fires, using experimental data from pool fire tests with varying square pan sizes (10 cm, 20 cm, 30 cm, and 40 cm). The analysis uses the Mean Absolute Percentage Error (MAPE) to compare the predicted heat flux values against the measured experimental data.

An uncertainty margin of ± 5% was introduced to account for multiple factors that may influence discrepancies in the results. Primarily, the variations in standard deviation recorded across different pan sizes reflect the fluctuating nature of the flames, as detailed in Section 3.3.6. For example, smaller pan sizes like 10 cm exhibited a standard deviation of 10 W/m² (0.01 kW/m²), while larger pans such as 40 cm showed greater fluctuations, with a standard deviation of 55 W/m² (0.055 kW/m²). For ethanol, the marginal error ranged from 3.06% for smaller pans (0.04 m²) to 7.82% for larger pans (0.09 m²). In contrast, for isopropyl alcohol (IPA), the marginal error varied between 1.50% (0.04 m²) and 9.17% (0.01 m²). These fluctuations impact the repeatability and precision of the data, contributing to the overall uncertainty in the model predictions.

The margin also accounts for inherent uncertainties in the original experimental setup, such as slight variations in measurement conditions and baseline temperature recordings. Temperature data for both fuels varied significantly across different pan sizes, affecting the radiative heat flux measurements. For ethanol, the average flame temperatures ranged from approximately 384 °C to 425 °C for smaller pans (0.04 m^2) and increased to as high as 717 °C for larger pans (0.16 m^2). This trend indicates that larger pans result in more intense burning and subsequently higher thermal radiation outputs.

Similarly, for isopropyl alcohol, the average flame temperature was recorded as lower in smaller pans (e.g., around 444 °C to 533 °C for 0.01 m^2 pans) but rose significantly for larger pans, reaching up to 743 °C in 0.09 m^2 pans. These temperature variations highlight the increased heat release rate and flame intensity associated with larger fuel surfaces, leading to higher thermal radiation outputs. Understanding these relationships provides valuable insights into the scale effects of pool fires, emphasizing how pan size directly influences heat flux and temperature readings.

Furthermore, the margin of error also considers experimental limitations such as the assumptions made regarding radiative fraction, which may not perfectly match the actual radiation characteristics across all fuel types. Environmental factors like minor temperature gradients or variations in the experimental setup could also lead to deviations from the assumed steady-state burning conditions. By acknowledging these uncertainties, the model's performance can be better contextualized, revealing both its strengths and areas for potential refinement to improve predictive accuracy in liquid fuel burning scenarios.

The thermal radiation models were evaluated against the experimental heat flux values for both ethanol and isopropyl alcohol, and the MAPE analysis results are summarised in Table 5.4. The decision to combine ethanol and IPA in the overall MAPE calculation reflects their shared role as representative liquid fuels in building fire scenarios. These fuels were chosen for their distinct radiative behaviours, i.e., ethanol as a low-soot fuel and IPA as a moderately sooty fuel. Grouping the MAPE together enabled an evaluation of the models' general applicability to liquid pool fires, irrespective of the specific fuel characteristics, while separate MAPE values provide insights into their individual behaviours. This approach ensures a thorough assessment of the models' performance, highlighting their adaptability to variations in liquid fuel properties and the associated modelling challenges.

Table 5.4: MAPE analysis results for thermal radiation models

Performance ranking	Thermal radiation model		Ethanol MAPE (± 5%)	IPA MAPE (± 5%)	Overall MAPE (± 5%)
1st	Models assessed in Chapter 4 (Advanced models)	Single point source model	12.7	32.7	22.7
2nd		Weighted multi point source model	12.2	34.9	23.5
3rd		Cuboid flame model	20.0	41.3	30.7
4th		Multi cuboid flame model	54.7	67.3	61.0
5th		Multi Cylinder flame model	87.4	88.9	88.1
6th	Models assessed by Fleury et al. (2011) (Conventional models)	Rectangular planar model	88.8	89.8	89.3
7th		Dayan and Tien method	979.3	462.0	382.6
8th		Shokri and Beyler correlation	457.3	308.0	400.3
9th		Shokri and Beyler detailed method	335.5	465.1	720.6
10th		Mudan method	922.4	1244.1	1083.3

For simplicity, all of the models that have been assessed in Chapter 4 will be grouped into the “advanced models” category, while all of the thermal radiation models assessed by Fleury et al. (2011) in the exclusion of the single point source model are grouped into the “conventional models” category. When comparing the performance of advanced models for both gas and liquid fuels (Table 4.2 and Table 5.4), consistent rankings emerge despite noticeable differences in MAPE values, particularly for the single point source model, weighted multi point source model, and cuboid flame model. For example, the single point source model shows a MAPE of 30.8% for gas fuel but a lower 22.7% for liquid fuel, while the weighted multi point source model's MAPE similarly differs, with 37.9% for gas fuel compared to 23.5% for liquid fuel. This variation in MAPE values underscores how fuel-specific characteristics impact model precision and accuracy.

Gas fuels, such as propane, combust more uniformly with faster rates, producing more consistent flame shapes and radiative behaviours conducive to stable modelling. This uniformity enables models like the single point source model to perform predictably, as fewer variations in flame characteristics occur. In contrast, liquid fuels like ethanol and IPA introduce complex radiative dynamics due to variable heat release rates, higher soot production (notably in IPA), and partial evaporation effects. Increased soot levels in liquid fuels impact radiative transfer as soot particles absorb and re-emit radiation, complicating model accuracy.

Conversely, the multi cuboid and multi cylinder flame models show relatively robust performance across both fuel types, with smaller variations in MAPE values. This robustness is attributed to their structural complexity, which incorporates detailed geometric considerations and multi-dimensional point sources, allowing them to adapt effectively to variable flame structures and emission characteristics. The multi cylinder flame model, in particular, benefits from its cylindrical geometry, which captures isotropic radiation distribution, making it less sensitive to differences in fuel phase or combustion behaviour. This adaptability renders the multi cuboid and multi cylinder models especially advantageous in scenarios with irregular flame geometries or diverse fuel types.

In terms of model performance by fuel type, the single point source model consistently achieves the lowest MAPE for both ethanol and IPA, highlighting its relative accuracy across different fuels. However, the considerable variation in MAPE values between fuels suggests that the model's precision may be more affected by fuel-specific characteristics than initially anticipated. Notably, MAPE values are generally lower for ethanol compared to IPA across most models, implying that ethanol's combustion properties may facilitate more accurate heat flux predictions, particularly with advanced models.

Comparing the performance of the advanced models and the conventional models from Table 5.4, the advanced models have shown to be the better performing groups of radiation models, given the evidently lower overall MAPE. The higher level of detail in configuration factors further differentiates advanced model from conventional models. For example, models like the cuboid flame model apply a structured view factor, which depends heavily on the relative positioning of the flame source and target. This orientation-sensitive configuration factor allows for a more refined heat flux estimation, directly influencing model accuracy. The separate MAPE values for ethanol and IPA further highlight this, as configuration-sensitive models like the cuboid flame model show heightened sensitivity to fuel type, indicating that fuel properties can directly impact accuracy.

Overall, the analysis reveals advancement and development in the level of accuracy and reliability of radiation models compared to what is achievable in the past decade. Based on the data obtained from ethanol and isopropyl alcohol pool fire experiments (as shown in Table 5.4), the best performing models are identified as follows: the single point source model, the weighted multi point source model, the cuboid flame model, the multi cuboid flame model, and the multi cylinder flame model. The consistency of the single point source model's performance across ethanol and IPA, as reflected in both its overall and fuel-specific MAPE values, further establishes it as the most adaptable model for the fuels assessed. These findings, particularly for the advanced models, align with the assessment conducted in Chapter 4. In addition, the superiority of the single point source model compared to the performance of the conventional models further corroborates the previous findings by Fleury et al. (2011), where the single point source model is also identified as the best-performing model among the six thermal radiations assessed. Figure 5.1 presents the equality graph that provides additional insights into the performance of the single point source model when compared to the liquid pool fire experiment dataset.

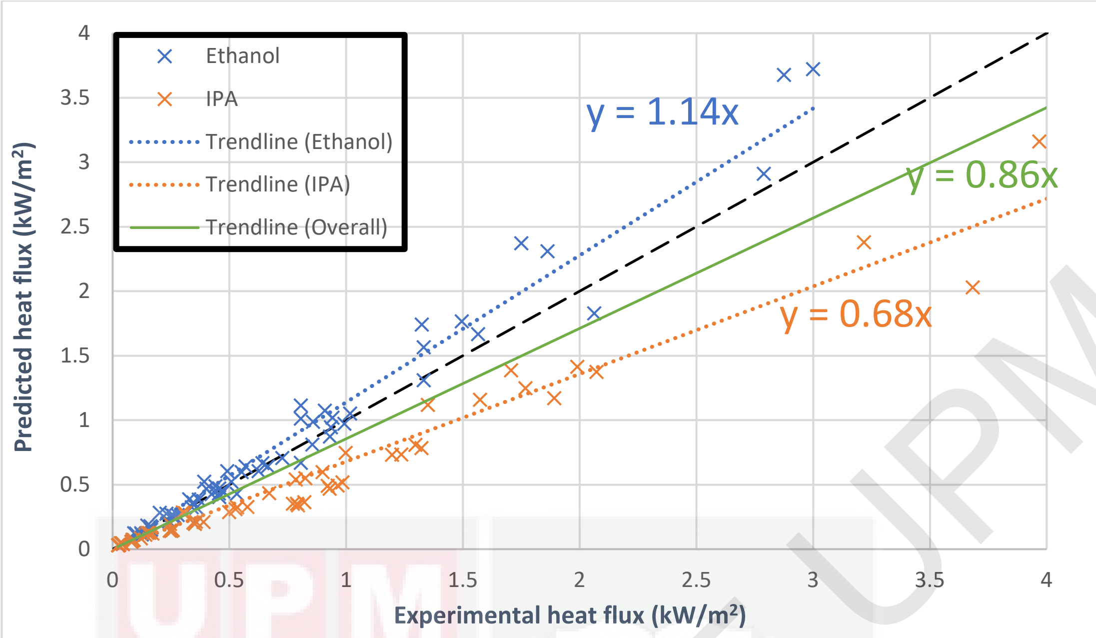

Figure 5.1: Comparison of Estimated Heat Flux and the Experimental Heat Flux Using the Single Point Source Model for Liquid Pool Fires

The equality graph for the best-performing model, the single point source model, provides valuable insights into its performance when compared to the liquid pool fire experiment dataset. Upon analysing the graph, it can be observed that a majority of the points are clustered near the diagonal line, particularly for heat flux values below 1 kW/m^2. This indicates a close agreement between the model predictions and the actual measurements in this lower heat flux range. However, a more noticeable deviation from the diagonal line is observed as the heat flux values increase. This suggests that the model's accuracy decreases for higher heat flux levels.

The overall trendline for the single point source model is represented by the equation y = 0.86x, which indicates a tendency for the model to slightly underestimate heat flux values as the slope is less than one. When separated by fuel type, the ethanol-specific trendline y = 1.14x demonstrates a slight overestimation tendency, with a slope greater than one. This suggests that for ethanol, the model is more accurate overall, with values clustering closely around the equality line, particularly for lower heat flux values. Conversely, the trendline for IPA, y = 0.68x, shows a stronger underestimation tendency, especially at higher heat flux values, where it deviates more noticeably from the equality line.

This difference between ethanol (non-sooting) and IPA (sooting) flames can be attributed to their distinct radiative properties. In ethanol flames, the radiation is primarily in the form of non-luminous infrared emissions, which result from molecular transitions in gaseous combustion products. In contrast, IPA flames emit both non-luminous radiation and luminous radiation due to soot particles. The soot particulates in sooty flames emit continuum radiation across the visible and infrared spectrum, significantly enhancing the flame's radiative intensity and contributing to the observed underestimation at higher heat flux levels in the model's predictions (Tien & Lee, 1984).

Despite the slight differences in performance between the two fuel variants, the general trendlines produced by the single point source model remain consistent, exhibiting minimal deviation from the diagonal line. This indicates that the model is capable of capturing the overall behaviour and characteristics of both ethanol and isopropyl alcohol pool fires. These findings highlight the strengths of the single point source model in accurately estimating heat flux values, particularly for lower heat flux levels. However, it also highlights the need for further improvements in the model's performance for higher heat flux scenarios.

Following closely, the weighted multi point source model emerges as the second best-performing model for the liquid pool fires dataset, exhibiting a marginal difference of only 0.8% compared to the single point source model. This finding indicates a high level of consistency and similarity in performance between these two models, differing from the previous assessment conducted on propane gas fire, where notable differences are observed between the two models. The graphical representation of the agreement between the predictions of the weighted multi point source model and the corresponding actual measurements is presented in Figure 5.2.

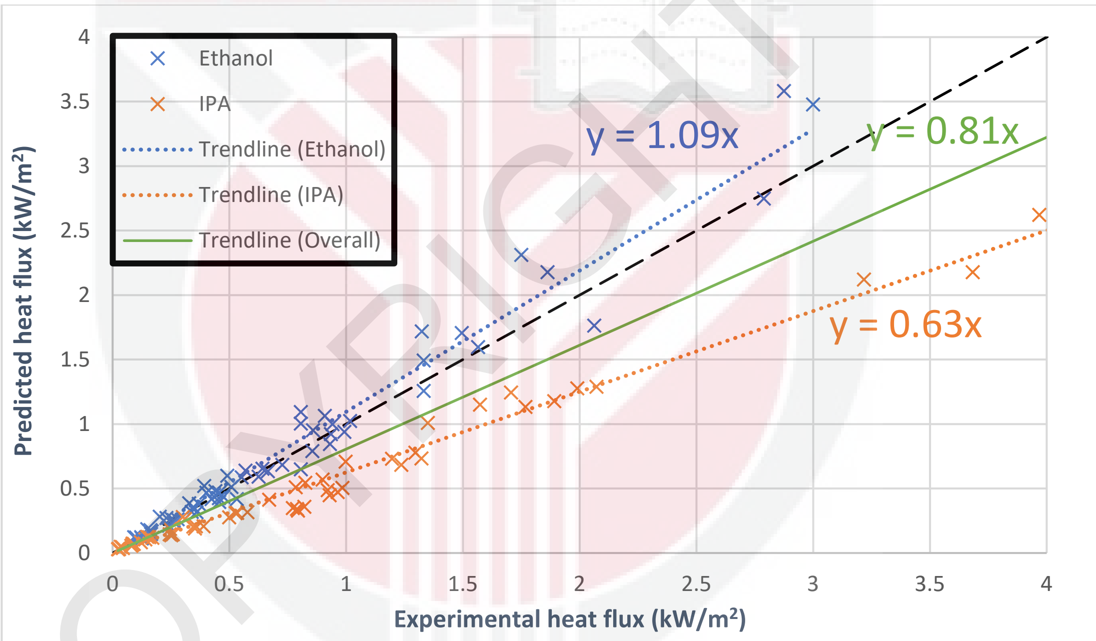

Figure 5.2: Comparison of Estimated Heat Flux and the Experimental Heat Flux Using the Weighted Multi Point Source Model for Liquid Pool Fires

Upon analysing the equality graph for the weighted multi point source model, it is evident that the distribution of data points closely resembles that of the single point source model. This consistency reinforces the findings presented in Table 5.4. However, a notable difference between the equality graphs of the weighted multi point source model and its predecessor model can be observed in the slope of the best-fit line, represented by y =0.81x. This slope, being less than unity, reflects a tendency for the model to underestimate the heat flux values across the dataset, showing a slightly larger deviation from the unity value than the single point source model's trendline, with a difference of approximately 0.05.

When examining fuel-specific trendlines, further insights into model performance emerge. For ethanol, the trendline y = 1.09x suggests an almost perfect estimation of heat flux values, with a slope close to unity. This slight overestimation, represented by a slope slightly above one, implies a highly accurate prediction for ethanol, in fact, surpassing the performance of the single point source model. Such accuracy indicates the model's ability to capture the radiative characteristics of ethanol fires, particularly at lower to moderate heat flux levels, where the alignment with actual values is exceptionally close. Conversely, the trendline for IPA, y = 0.63x, highlights a stronger underestimation across the dataset, especially at higher heat flux values where deviations from the equality line become more pronounced. This result suggests that, as discussed in the single point source model analysis, the weighted multi point source model faces additional challenges in accurately predicting heat flux for IPA due to the increased soot production and distinct radiative properties of this fuel type.

Despite the slight discrepancies in slope values and the model's increased tendency to underestimate heat flux for IPA, the weighted multi point source model performs reliably across both fuel types, particularly at lower heat flux levels. The high precision observed with ethanol makes this model a strong candidate if the focus is primarily on predicting heat flux for ethanol fires, where it slightly outperforms the single point source model.

Following the weighted multi point source model are the cuboid flame model and the multi cuboid flame model, which rank among the top-performing models, as illustrated in Table 5.4. These two models are unique among those investigated, as they are the only models based on cuboidal flame geometry. Notably, both cuboid-based models surpass the performance of not only the newly developed cylindrical flame model (multi cylinder flame model) but also the conventional cylindrical flame models (Shokri and Beyler detailed method, Mudan method, Dayan and Tien method). Within the cuboid-based category, the cuboid flame model demonstrates superior performance compared to the multi cuboid flame model, as depicted in Figure 5.3 and Figure 5.4.

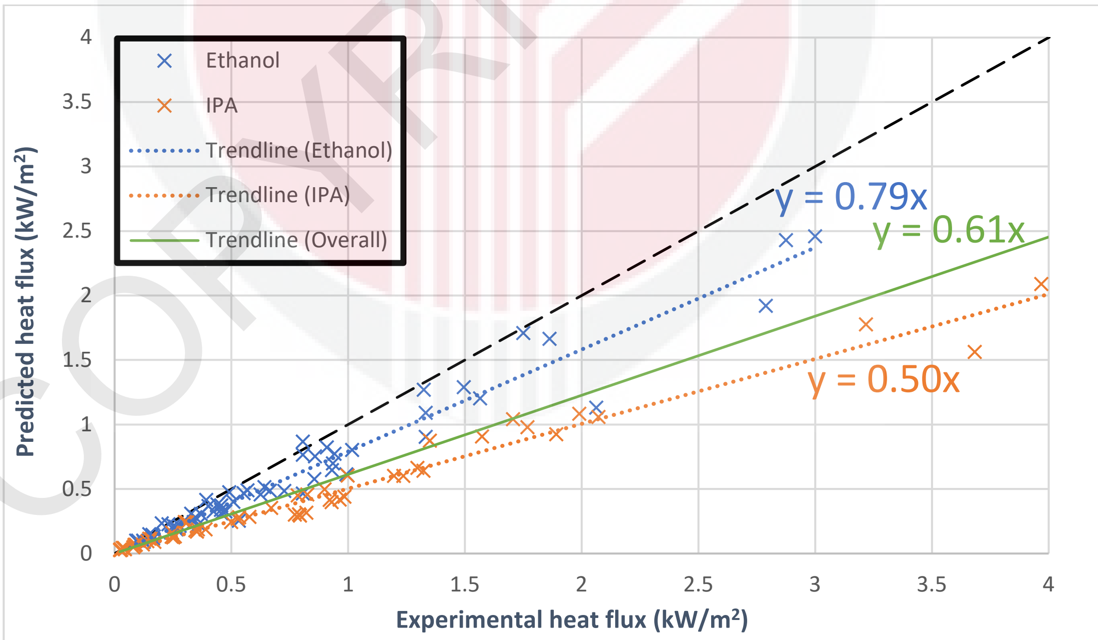

Figure 5.3: Comparison of Estimated Heat Flux and the Experimental Heat Flux Using the Cuboid Flame Model for Liquid Pool Fires

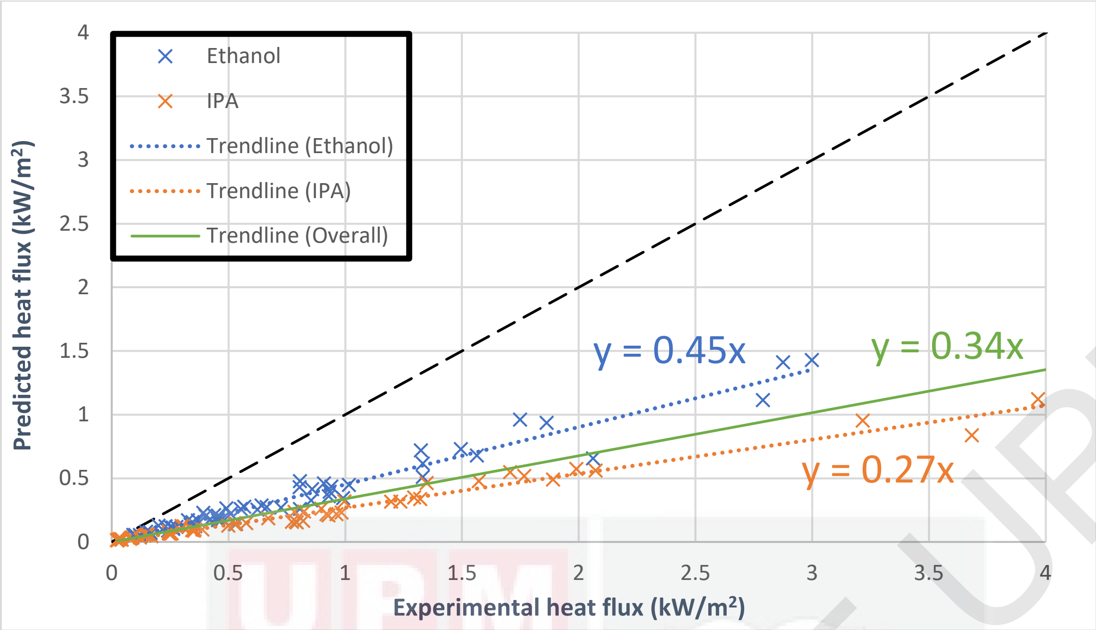

Figure 5.4: Comparison of Estimated Heat Flux and the Experimental Heat Flux Using the Multi Cuboid Flame Model for Liquid Pool Fires

Examining the equality graphs for the cuboid flame model in Figure 5.3 and the multi cuboid flame model in Figure 5.4, the cuboid flame model achieves a notably closer alignment with the experimental data, evidenced by its trendline slope of y = 0.61x. This slope, although less than one, suggests a moderate underestimation of heat flux values, but with a better fit than the multi cuboid flame model, which has a considerably lower trendline slope of y = 0.34x. The greater underestimation tendency in the multi cuboid flame model, reflected by the lower slope, contributes to its higher MAPE of 61%, nearly double that of the cuboid flame model at 30.7%. This contrast in slope values and MAPE emphasises the cuboid flame model's relative accuracy in predicting heat flux across the dataset.

The cuboid flame model shows trendlines of y = 0.79x for ethanol and y = 0.50x for IPA, indicating that while it achieves predictions slightly closer to the actual heat flux, the model's accuracy varies more noticeably between fuels. In contrast, the multi cuboid flame model displays trendlines of y = 0.45x for ethanol and y = 0.27x for IPA, with the trendlines for ethanol, IPA, and the overall data clustering more closely together. This tighter grouping across fuel types suggests that, although the multi cuboid flame model consistently underestimates heat flux values, it achieves a higher level of precision across different fuel types, albeit without the improved accuracy observed in the cuboid flame model for ethanol.

The fifth best-performing model and the best-performing cylindrical flame model examined in this research is the multi cylinder flame model. In contrast to the cuboid flame model, assuming that the division of a larger flame into smaller identical flames enables the multi cylinder flame model to achieve a lower MAPE of 88.1%, compared to the performance of conventional cylindrical models such as the Shokri and Beyler detailed method (400.3%), Mudan method (1083.3%), and Dayan and Tien Method (720.6%). The performance of the multi cylinder flame model is further elucidated in the equality graph depicted in Figure 5.5.

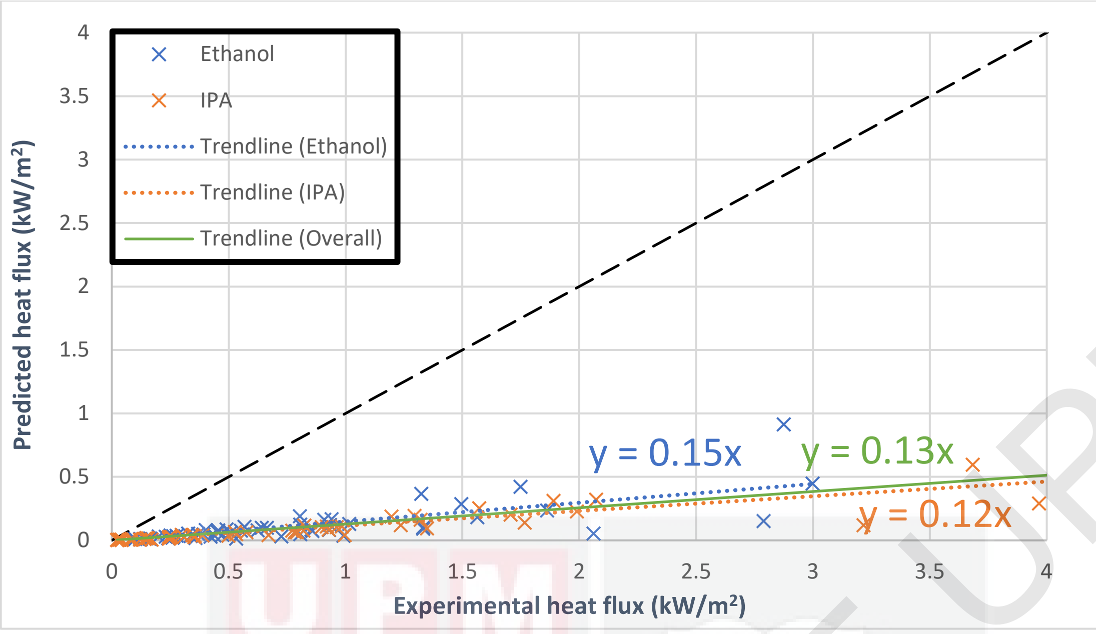

Figure 5.5: Comparison of Estimated Heat Flux and the Experimental Heat Flux Using the Multi Cylinder Flame Model for Liquid Pool Fires

Upon analysing the equality graph for the multi cylinder flame model, it becomes evident that the model exhibits a clear bias towards underestimating heat flux values, as indicated by a trendline with a slope significantly below unity (y = 0.13x for the overall trendline). However, the trendline slopes for ethanol (y = 0.15x) and IPA (y = 0.12x) are closely aligned with each other and the overall trendline, demonstrating minimal variation across different fuels. This indicates that while the multi cylinder flame model may lack accuracy, it consistently produces similar underestimations across fuel types, making it a highly precise model.

The data points are tightly clustered along the trendline, particularly for heat flux values lower than 2 kW/m^2. Despite its underestimation bias, this precision suggests that the multi cylinder flame model could still be valuable in fields like fire safety engineering, where consistent trends are essential, even if adjustments are needed to correct the bias. Appropriate correction factors or parameter adjustments could mitigate the underestimation, making this model adaptable for use when high precision is prioritised over direct accuracy.

Reviewing Table 5.4, it is evident that the rectangular planar model emerges as the best-performing model within the conventional model category. While not among the top five models overall, the rectangular planar model stands out among the conventional models with a MAPE comparable to that of the advanced model. In fact, the MAPE of the rectangular planar model (89.3%) is only 1.2% higher than the worst-performing advanced model, which is the multi cylinder flame model at 88.1%. The performance of the rectangular planar model is illustrated in Figure 5.6.

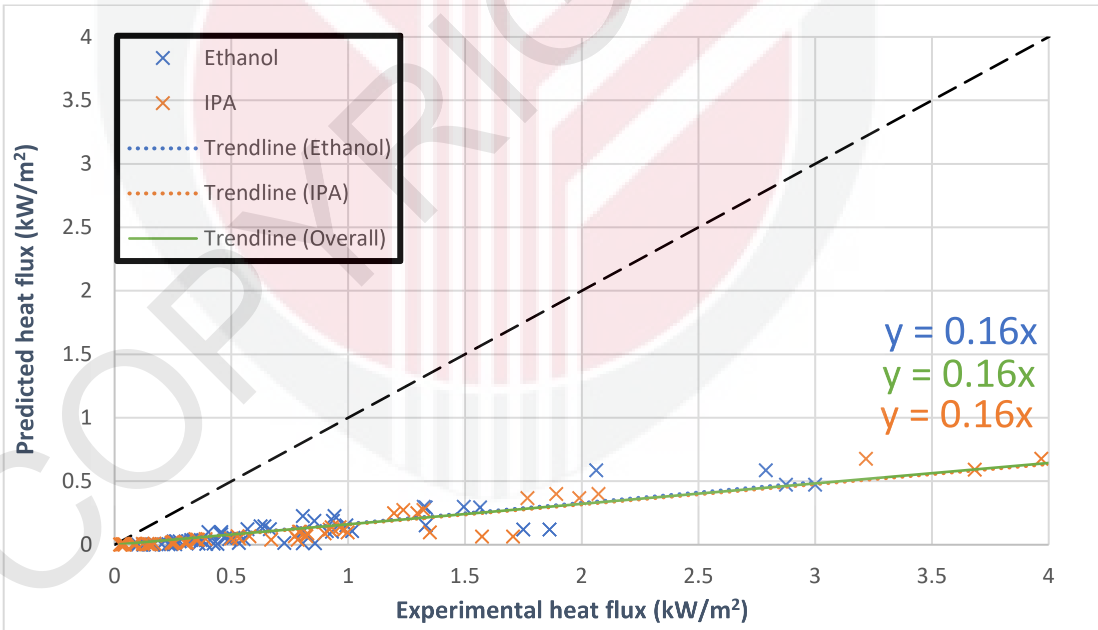

Figure 5.6: Comparison of Estimated Heat Flux and the Experimental Heat Flux Using the Rectangular Planar Model for Liquid Pool Fires

The equality graph for the rectangular planar model shows a trend that closely mirrors the performance of the multi cylinder flame model, with a similar pattern of underestimating heat flux values. However, the rectangular planar model demonstrates a higher level of precision, with its data points more tightly clustered around the trendline, particularly across ethanol and IPA where the slopes (y = 0.16x) remain consistent. This uniformity across different fuels reflects the model's strong consistency, marking it as even more precise than the multi cylinder flame model.

The limitations of the rectangular planar model can be attributed to the view factor introduced by Ivanova and Muneer (2017), which assumes parallel planes for both the flame source and the receiving target. While this assumption reduces computational complexity, it also introduces constraints by disregarding variations in the target's height when calculating heat flux, resulting in accumulated percentage errors. Nevertheless, the rectangular planar model's precision and consistency make it a robust choice within the conventional category, especially in scenarios where computational simplicity is a priority.

Continuing with the conventional models, the Shokri and Beyler correlation emerges as the quickest and simplest approach for predicting radiant heat flux. This correlation disregards the shape of the fire and relies on only a few parameters. However, the trade-off for its simplicity is a lower level of accuracy and precision in estimating heat flux values. Both the Shokri and Beyler correlation and the Shokri and Beyler detailed method consistently perform poorly, yet they consistently overestimate heat flux values for all fuel types. This overestimation could be advantageous in fire engineering applications, as fire engineers often design for worst-case scenarios. In cases where higher readings are beneficial for safety margins, these models might offer a preliminary, conservative estimate. Applying a correction factor could further improve their usability.

Despite its limitations, the performance of the Shokri and Beyler correlation surpasses that of the upgraded model, namely the Shokri and Beyler detailed method, when tested against ethanol and isopropyl alcohol pool fires experiment. The Shokri and Beyler detailed method, which incorporates additional parameters such as the emissive power and height of the flame, is initially expected to outperform its predecessor. However, the experimental data from the liquid pool fires reveal otherwise. The MAPE for the Shokri and Beyler detailed method (400.3%) is 17.7% higher than that of the Shokri and Beyler correlation (382.6%). The performance discrepancy between these two thermal radiation models is depicted in Figure 5.7 and Figure 5.8.

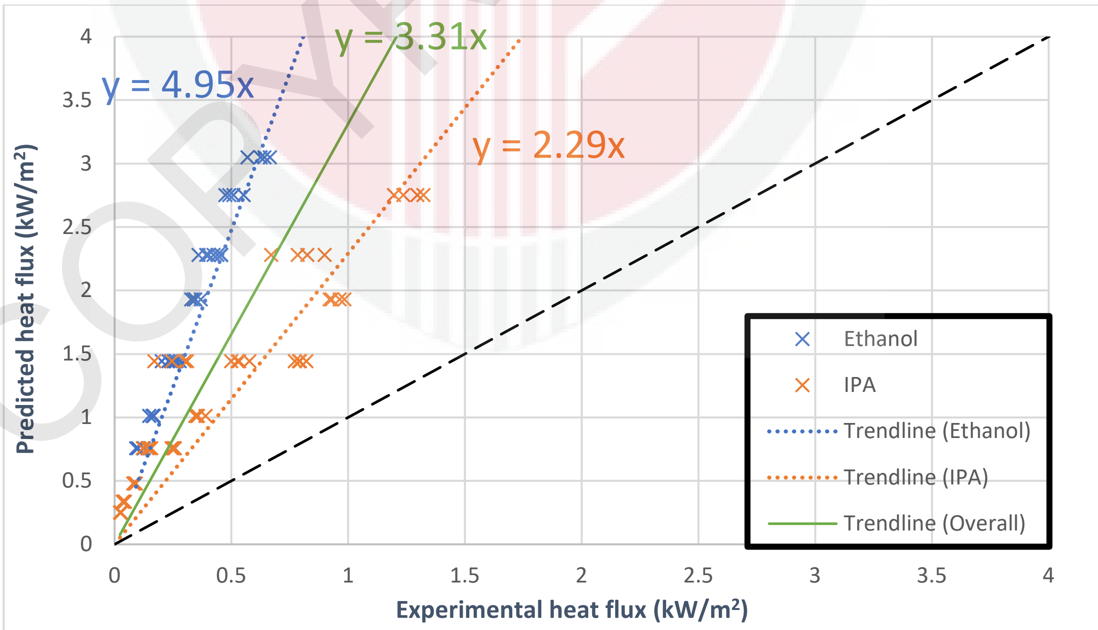

Figure 5.7: Comparison of Estimated Heat Flux and the Experimental Heat Flux Using Shokri and Beyler Correlation for Liquid Pool Fires

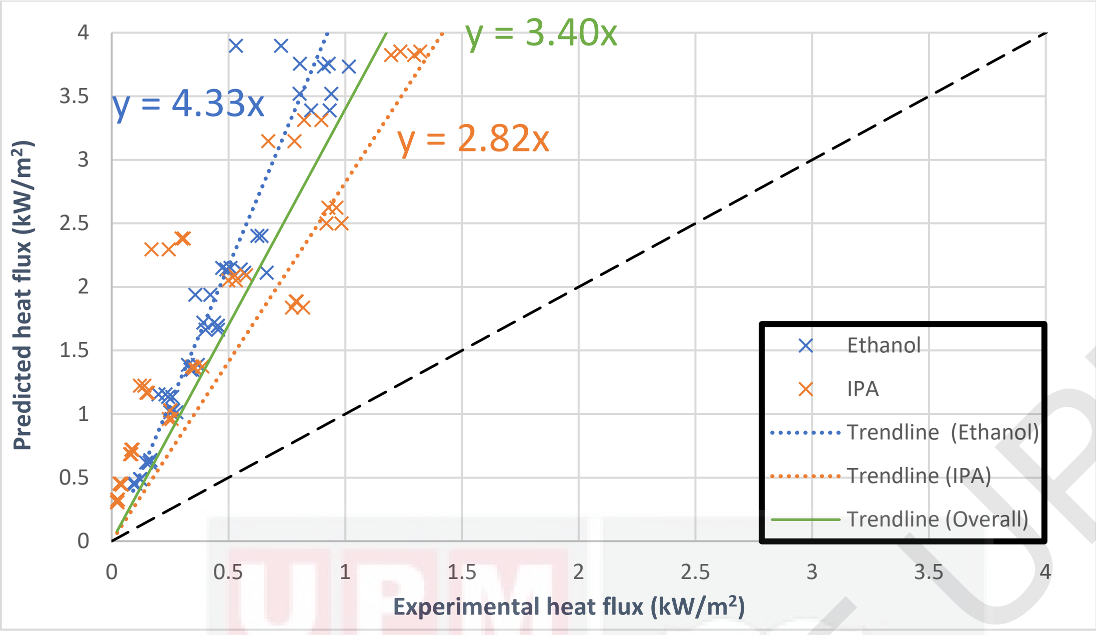

Figure 5.8: Comparison of Estimated Heat Flux and the Experimental Heat Flux Using Shokri and Beyler Detailed Method for Liquid Pool Fires

The equality graph for the Shokri and Beyler correlation and the Shokri and Beyler detailed method shows that both models exhibit a trendline with values greater than 1. This indicates a tendency to overestimate the heat flux values for ethanol and isopropyl alcohol pool fires. Notably, the Shokri and Beyler detailed method shows a trendline with a higher slope than the Shokri and Beyler correlation, indicating a higher degree of overestimation and larger deviation from the experimental values. Despite this difference, the data points for both models are widely scattered and deviate significantly from the equality line, further underscoring their lack of precision and accuracy.

The analysis of the figures reveals significant discrepancies between both of the proposed models by Shokri and Beyler (1989) and the actual heat flux values of liquid pool fires. The data points in the figures are noticeably scattered and deviate significantly from the diagonal line, indicating the models' inability to predict the heat flux accurately. These findings suggest that the models proposed by Shokri and Beyler (1989) are unsuitable for effectively estimating heat flux in the context of ethanol and isopropyl alcohol liquid pool fires. The poor performance of these models can be attributed to their inherent limitations. The Shokri and Beyler correlation, originally developed for targets at ground level, does not account for changes in target height in its mathematical equation. Consequently, the correlation struggles to provide satisfactory results, as depicted in Figure 5.7. On the other hand, despite being developed based on various pool fire experiments involving kerosene, fuel oil, gasoline, JP-4, JP-5, and LNG, the Shokri and Beyler detailed method fails to capture the specific characteristics of ethanol and isopropyl alcohol pool fires, as shown in Figure 5.8. This highlights the limited generalisability of this data-driven modelling approach, which is constrained by the data available during model development.

Lastly, the worst-performing thermal radiation models assessed in this research, as indicated in Table 5.4, are the Mudan method, followed by the Dayan and Tien method. These models, both assuming cylindrical flame geometry, demonstrated notably high MAPE values for the liquid pool fire experiments. The Dayan and Tien method recorded a MAPE of 720.6%, while the Mudan method exhibited a MAPE of 1083.3%. Despite sharing a common theoretical foundation regarding flame shape, these models are independent of each other in terms of view factor computation. Consequently, they yield different heat flux estimations, as illustrated in Figure 5.9 and Figure 5.10.

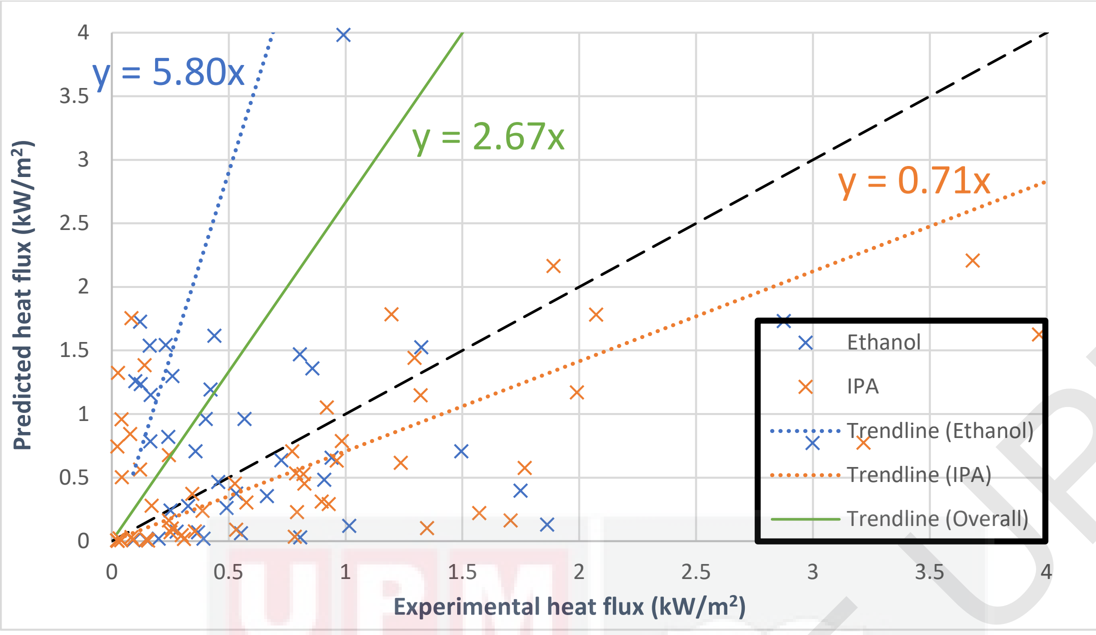

Figure 5.9: Comparison of Estimated Heat Flux and the Experimental Heat Flux Using the Dayan and Tien Method for Liquid Pool Fires

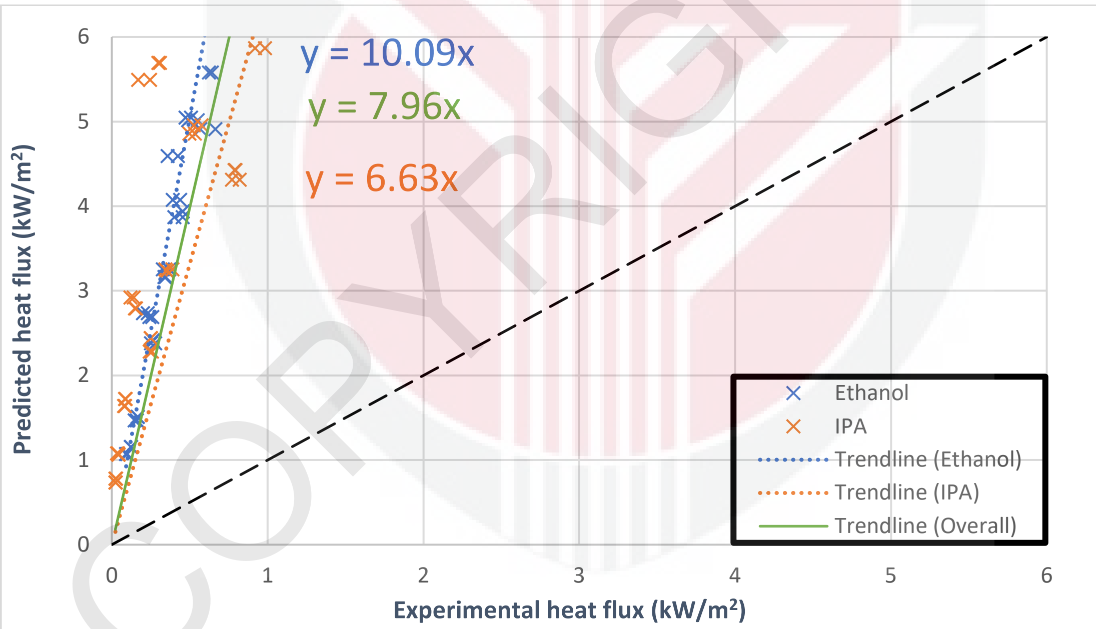

Figure 5.10: Comparison of Estimated Heat Flux and the Experimental Heat Flux Using the Mudan Method for Liquid Pool Fires

Both the Mudan method and the Dayan and Tien method are characterised by a pronounced overestimation of radiant heat flux, as highlighted by the slopes of their respective trendlines. The Mudan method, in particular, performs notably poorly, with a trendline that diverges substantially from the diagonal line, indicating consistent overestimation. Although this overestimation could be advantageous in conservative fire engineering applications, alternative models, such as the Shokri and Beyler detailed method, provide similarly conservative estimates with improved accuracy.

The Dayan and Tien method, however, displays a highly scattered data distribution, reflecting substantial variability in its predictions, which undermines its reliability and renders it less suitable for precise fire engineering applications. Overall, the significant inconsistencies and extreme deviations in predictions from both the Mudan and the Dayan and Tien methods suggest that these models are less practical for accurately representing actual fire scenarios in the context of liquid pool fires.

5.3.2 Median Absolute Percentage Error (MdAPE) Analysis

The MdAPE is an important metric that complements the MAPE in assessing the performance of models. While MAPE measures the average percentage deviation between predicted and actual values, MdAPE focuses on the median percentage error. The importance of MdAPE lies in its ability to mitigate the influence of outliers on the overall assessment of model accuracy. Unlike MAPE, which can be heavily affected by extreme values, MdAPE considers the central tendency of the percentage errors by using the median value. In addition, MdAPE provides a more robust evaluation of model accuracy, especially when dealing with datasets that contain outliers or skewed error distributions. It helps identify any discrepancies or irregularities in the error distribution and provides insights into the model's ability to predict values consistently across different scenarios. The results of the MdAPE analysis are shown in Table 5.5.

Table 5.5: MdAPE analysis for liquid pool fire experiments

Performance ranking	Thermal radiation model		MdAPE (%)
1st	Models assessed in Chapter 4 (Advanced models)	Single point source model	20.5
2nd		Weighted multi point source model	21.6
3rd		Cuboid flame model	30.4
4th		Multi cuboid flame model	61.2
5th		Multi Cylinder flame model	88.6
6th	Models assessed by Fleury et al. (2011) (Conventional models)	Dayan and Tien method	88.8
7th		Rectangular planar model	89.7
8th		Shokri and Beyler detailed method	302.0
9th		Shokri and Beyler correlation	400.7
10th		Mudan method	847.6

In the case of the advanced model, the MdAPE results align with the MAPE findings, both in terms of error percentages and ranking. This consistency indicates that the advanced model exhibits stable and consistent performance across the evaluated scenarios. The agreement between the MdAPE and MAPE results reinforces the reliability of the advanced model in accurately estimating radiant heat flux for liquid pool fires. It suggests that the model's predictions have a balanced distribution of errors and are not heavily influenced by outliers or extreme values.

On the other hand, discrepancies in performance rankings are observed among the conventional models when comparing MAPE (refer to Table 5.4) and MdAPE (refer to Table 5.5). Notably, the Dayan and Tien method exhibits significant percentage error changes, with a MAPE of 720.6% and a MdAPE value of 88.8%. This shift in ranking moves the Dayan and Tien method from the 9th best-performing model according to MAPE to the 6th best-performing model based on MdAPE analysis. This disagreement highlights the sensitivity of MAPE to outliers or extreme errors, which can impact the overall ranking of the models.

From these observations, it can be concluded that the assessment of the advanced model is more reliable and consistent, as reflected by the alignment between MdAPE and MAPE results. On the other hand, the assessment of the conventional models is more susceptible to outliers, indicating that their performance rankings may be influenced by a few extreme errors. Nonetheless, the results for the top five performing models remain valid, indicating their superior performance compared to the other models evaluated.

5.3.3 Sensitivity Analysis

This section will focus on conducting a sensitivity analysis specifically for the top five best-performing models identified in the previous sections. The reliability and validity of the advanced model, as highlighted by the MAPE and MdAPE analyses, provide a strong basis for selecting these models for further investigation. The sensitivity analysis examines how key parameter variations impact the models' predictions. Specifically, the analysis will explore the sensitivity of the models to changes in the distance from the centre of fire, the height of the target from the flame base, and the area of the flame base. By studying the models' response to these influential parameters, a deeper understanding of their performance characteristics can be gained, thereby enhancing insights into their practical applicability.

5.3.3.1 Distance from the Centre of Fire

The sensitivity analysis in this subsection focuses on the horizontal distance of the measurement location, ranging from 0.5 m to 1.5 m from the centre of the fire. The performance evaluation of the top-performing thermal radiation models is conducted at five specific horizontal distances, with increments of 0.25 m, covering the entire range. The findings of the sensitivity analysis are presented in Table 5.6, providing valuable insights into the models' performance under varying distances from the fire source.

Table 5.6: Mean absolute percentage error at different distance parameters from the centre of pool fire

	Mean Absolute Percentage Error (%)				
Distance (m)	Single Point Source Model	Weighted Multi Point Source Model	Cuboid Flame Model	Multi Cuboid Flame Model	Multi Cylinder Flame Model
0.50	20.5	22.0	31.8	62.2	89.6
0.75	20.9	22.2	31.0	62.2	88.5
1.00	23.0	23.9	30.5	61.6	87.7
1.25	22.6	22.9	29.3	59.9	87.7
1.50	26.4	26.7	30.7	59.0	87.1

As indicated by Table 5.6, the variations in the horizontal distance have minimal impact on the performance of the thermal radiation models. This is evident from the maximum mean percentage point deviation between the furthest and nearest tested distances, which does not exceed 6% according to the data presented in Table 5.6. Notably, both the single point source model and the weighted multi point source model exhibit remarkable performance with comparable results. This suggests that these models are robust and reliable, as they consistently provide accurate estimations regardless of the distance from the flame centre.

5.3.3.2 Height of Target from Flame Base

In the ethanol and isopropyl alcohol pool fire experiments, the measurement locations are selected at varying heights, ranging from 0.1 m to 0.61 m. To examine the sensitivity to flame height, the MAPE is categorised into four distinct target height parameters, each with a step increment of 0.17 m. The findings of this sensitivity analysis are presented in Table 5.7.

Table 5.7: Mean absolute percentage error at different target height parameters from the base of pool fire

Mean Absolute Percentage Error (%)					
Height (m)	Single Point Source Model	Weighted Multi Point Source Model	Cuboid Flame Model	Multi Cuboid Flame Model	Multi Cylinder Flame Model
0.10	30.4	29.8	25.0	55.5	83.3
0.27	22.1	22.2	27.4	59.6	87.0
0.44	17.1	18.4	31.1	62.3	90.0
0.61	21.2	23.7	39.1	66.6	92.2

Upon examining Table 5.7, it is evident that the performance of the models is influenced by the variation in the target's height. The heat flux values exhibit variations across different height parameters, as shown in Table 5.7, with a mean percentage point deviation ranging from 6.1% to 14.1%. Analysing Table 5.7, a clear trend emerges: the MAPE increases as the height of the target increases for the cuboid flame model, the multi cuboid flame model, and the multi cylinder flame model. Conversely, the MAPE decreases for the single point source model and the weighted multi point source model as the target height increases from 0.1 m. Notably, the single point source model and the weighted multi point source model consistently perform comparably across different target height parameters.

5.3.3.3 Area of Flame Base

Four different sizes of square pans are used to collect experimental data from liquid pool fire experiments. To assess the sensitivity of thermal radiation models, the MAPE is analysed from the perspective of pan geometry (area of flame base). The performance of the models is evaluated separately for pan sizes of 0.1 m x 0.1 m, 0.2 m x 0.2 m, 0.3 m x 0.3 m, and 0.4 m x 0.4 m, as presented in Table 5.8.

Table 5.8: Mean absolute percentage error at different area parameters of flame base for liquid pool fire

	Mean Absolute Percentage Error (%)				
Area (m^2)	Single Point Source Model	Weighted Multi Point Source Model	Cuboid Flame Model	Multi Cuboid Flame Model	Multi Cylinder Flame Model
0.01	20.8	21.9	24.6	55.0	88.1
0.04	26.0	27.1	32.4	62.3	90.3
0.09	26.0	27.3	36.5	65.3	88.0
0.16	11.3	10.5	21.6	55.7	84.2

The results presented in Table 5.8 demonstrate that the effect of varying flame size differs among different thermal radiation models. The cuboid flame model, multi cuboid flame model, and multi cylinder flame model show minimal sensitivity to changes in pool fire geometry, with a mean percentage point deviation of less than 4% between the smallest and largest pool fire sizes tested. On the other hand, the single point source model and the weighted multi point source model exhibit a significant increment in performance as the pool fire area increases from 0.01 m^2. This is evident from the mean percentage point deviation of 9.5% and 11.4% between the smallest and largest pool fire sizes for the single point source model and the weighted multi point source model, respectively.

Table 5.8 highlights a distinct trend in heat flux predictions as flame base area varies, particularly in the multi cuboid and multi cylinder models. As expected, given that heat flux is measured per unit area, an increase in flame base area correlates with a reduction in per-unit heat flux values. This effect is most pronounced in the multi cuboid and multi cylinder models, where the assumption of segmented or distributed flame geometries results in a dispersed radiation profile across a larger surface. Consequently, as the effective radiating area expands, the intensity of per-unit heat flux readings declines. While these models effectively capture distributed radiation effects across varied flame sizes, this trend suggests that they may be less suited to applications needing precise, high-intensity flux measurements in scenarios involving larger flame bases.

In contrast, the single point source and weighted multi point source models demonstrate a positive response to high heat flux scenarios associated with reduced measurement distances and increased flame size. As measurement points move closer to the flame, the intensified radiative exposure more accurately aligns with these models' predictions, resulting in decreased error margins in high heat flux regions. Similarly, as the effective radiative surface area grows with larger flame sizes, these models show enhanced performance in capturing expected heat flux intensities. Therefore, the single point source model and weighted multi point source model may be particularly effective for predicting heat flux in larger ethanol and isopropyl alcohol pool fires. This trend underscores the models' suitability for high-intensity zones, especially when larger flame areas or closer measurement points are prioritised for accurate high flux measurements.

5.4 Summary

In summary, the findings from both the MAPE and MdAPE analyses in Chapters 5 consistently reinforce the superior performance of the single point source model, corroborating the results obtained in Chapter 4. This research demonstrates that the single point source model excels not only in gas fire experiments but also in accurately predicting heat transfer in liquid pool fires. The comprehensive assessment conducted in this study, encompassing various fire scenarios and fuel types, highlights the versatility and applicability of the single point source model. Its ability to estimate heat flux accurately across different fire scenarios underscores its reliability and effectiveness. Additionally, the sensitivity analysis conducted further confirms the robustness of the single point source model, as it consistently performs well across variations in flame sizes, target heights, and distances from the fire centre.

These results solidify the single point source model's position as a valuable tool in the field of fire safety engineering.

This research's significance lies in its implications for advancing fire safety engineering practices. The validated performance of the single point source model provides engineers and researchers with a reliable and versatile tool for predicting heat flux. This is crucial for designing effective fire protection systems, evaluating the performance of building materials, and ensuring the safety of occupants. Moreover, the consistent agreement between the findings of Chapter 4 and Chapters 5 establishes the single point source model as an ideal benchmark for simulation environments and future research endeavours. It serves as a reference point for developing and validating new semi-empirical thermal radiation models.

CHAPTER 6

DEVELOPMENT OF NEW RADIATION MODEL

6.1 Overview

Building upon on the comprehensive assessment of thermal radiation models' performance carried out in the previous chapters (Chapter 4 and Chapter 5), this chapter focuses on refining and enhancing the single point source model, identified as the best-performing model for both gas burner and pool fire scenarios in Chapters 4 and Chapter 5 respectively. Given its simplicity and accuracy in estimating radiant heat flux, the single point source model provides a solid foundation for developing a new thermal radiation model capable of capturing more complex fire dynamics across varied conditions.

This development phase aims to address limitations inherent in the single point source model by incorporating additional factors influencing thermal radiation, thus broadening its applicability to diverse fire scenarios. The chapter builds upon the model's established framework by introducing assumptions and modifications aligned with the findings from the propane gas, ethanol, and isopropyl alcohol experiments. These considerations allow the model to adapt to variations in heat flux resulting from different fuel types and experimental conditions, offering a more robust predictive tool.

The improved model utilises a semi-a priori modelling approach, blending empirical data with the model's framework to enhance predictive accuracy. The data from the propane gas fire, ethanol pool fire, and isopropyl alcohol pool fire experiments serve as valuable fitting datasets, enabling the model to adjust to fuel variations. These experiments, conducted in Chapter 4 and Chapter 5, revealed that the single point source model outperforms both conventional and advanced models in estimating thermal radiation, further validating its use as the base model in this study.

The refined model’s performance is rigorously evaluated by comparing its predictions with validation data obtained from additional experiments involving acetone and methanol pool fires, as well as simulation data for heptane and methane pool fires generated using the Fire Dynamics Simulator (FDS). By bridging empirical findings and computational approaches, this chapter contributes to the advancement of thermal radiation modelling by leveraging the single point source model’s foundational accuracy while incorporating new insights from experimental and simulated data. This research not only strengthens the model's utility in fire safety but also aligns with the goal of providing more reliable tools for fire safety assessments and design practices.

6.2 Model Development Through Semi-A Priori Modelling

This research explores a novel approach to developing a thermal radiation model by adopting an unconventional method known as semi-a priori modelling. This approach combines elements of both a priori modelling and data-driven modelling. A priori modelling, also known as blind modelling, involves conducting the modelling phase before conducting corresponding experiments (Rein et al., 2009; Spearpoint et al., 2014), while data-driven modelling utilises empirical data to construct models (Bhanja et al., 2023; Choi et al., 2022). By leveraging the strengths of both approaches, the semi-a priori modelling approach employed in this study proves particularly useful in engineering and other fields, where well-established physical laws and principles guide the initial model development, followed by refinement and validation based on real-world data. In this study, the model structure and parameters are derived from prior knowledge and assumptions about an existing thermal radiation model, i.e., single point source model, and model adjustment is performed by incorporating the wide range of empirical data used in the previous parts of the research for assessing the performance of thermal radiation models.

The data required for semi-a priori modelling is divided into fitting data, experimental validation data, and simulation validation data. Fitting data is utilised to optimise the model fit by adjusting parameters and modifying the model structure, while experimental data and simulation validation data are employed to evaluate the model's performance and assess its generalisability beyond the fitting dataset. The flow chart, shown in Figure 6.1, illustrates the step-by-step process of semi-a priori modelling.

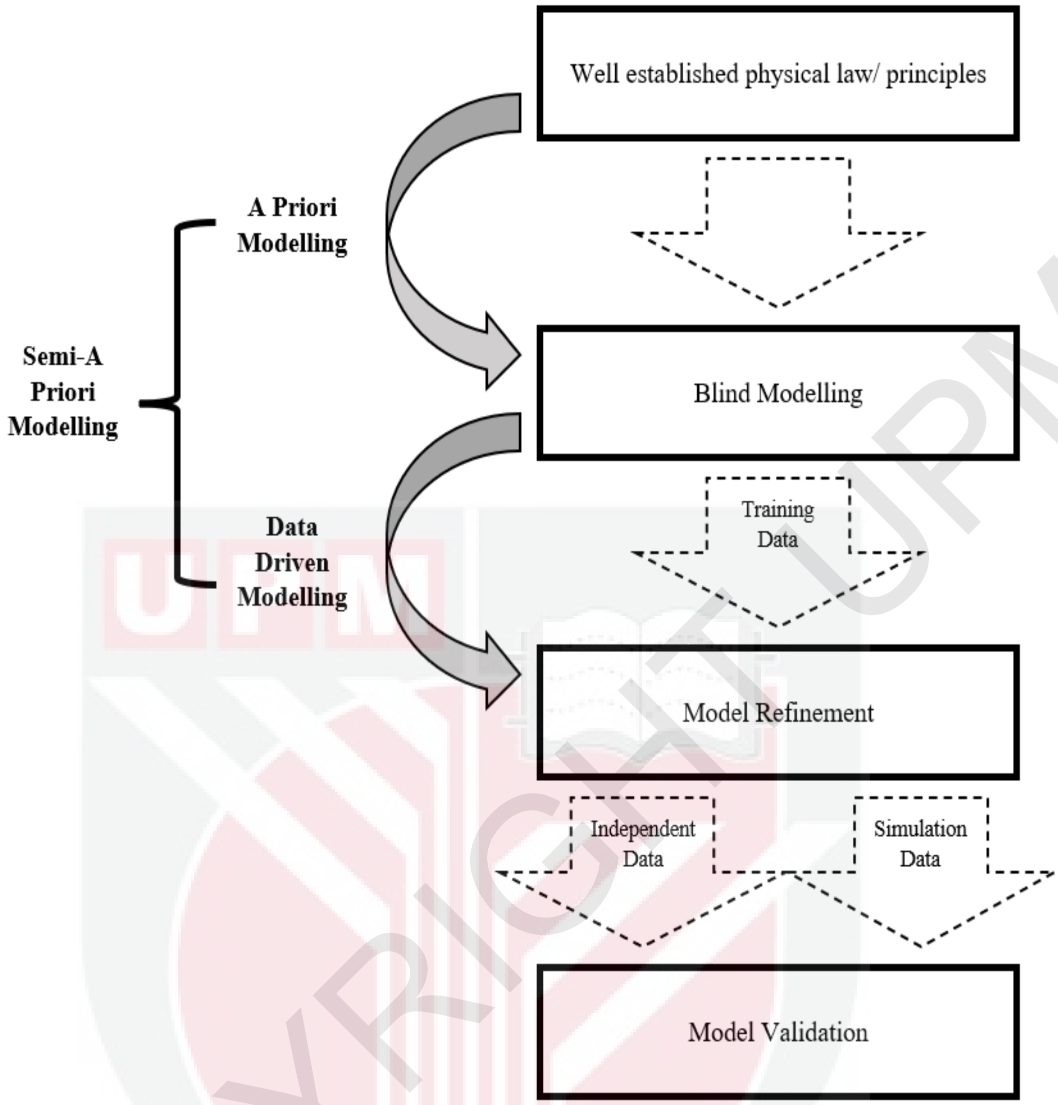

Figure 6.1: Flow Chart for Semi-A Priori Modelling Process

6.2.1 Fitting Data and Model Refinement

The fitting data plays a crucial role in fitting the model to the system being modelled. It enables adjustments to the model parameters, modifications to the model structure, and the incorporation of additional data to optimise its fit. This iterative process refines the model, enhancing its accuracy and generalisability. The refinement procedure will continue until a designated mean absolute percentage error (MAPE) between fitting data and estimated data has been achieved. By incorporating empirical information, the model calibration is guided, allowing it to systematically adjust to real-world measurements, which mitigates the risk of overfitting, a common pitfall in data-driven modelling that occurs when models are excessively tailored to specific data and struggle to generalise to new situations.

After the initial model (a priori model) has been developed through blind modelling, the calibration process aligns the model's predictions closely with the observed empirical data, ensuring its reliability across varied conditions. This involves fine-tuning various coefficients and input variables, ensuring that the model can consistently reproduce observed results across a range of test conditions. The effectiveness of the calibration is determined by how well the model can reduce discrepancies between predicted and actual values, without overfitting to specific datasets.

The model refinement process begins by comparing the heat flux estimation of the a priori model with the heat flux data obtained from propane gas, ethanol pool fire, and isopropyl alcohol pool fire experiment (fitting data). The difference between the model’s predictions and the actual data is quantified in terms of MAPE. During the process of achieving a better fit or model fitting, several coefficients are introduced into the a priori model; these coefficients are adjusted iteratively using Excel’s Goal Seek function to minimise the MAPE between the model’s estimations and the fitting data. In short, effective calibration here means finding an optimal combination of coefficients through iterative adjustments, such that the model can achieve the smallest possible MAPE for each fuel type used in the fitting data. This ensures the model’s predictions align closely with actual data, creating a strong foundation for reliable heat flux estimations across different fuel scenarios.

The MAPE serves as an error measurement that quantifies the accuracy of the model's predictions. A lower MAPE indicates a better fit between the model and the fitting data. Nevertheless, it is important to note that while the ultimate aim is to achieve zero MAPE, it is practically impossible to create a model that perfectly replicates the complexities of real fires. Hence, by refining the model and minimising the MAPE, the new model can enhance its predictive capability and ensure that its estimations align closely with the actual heat flux data.

The implementation of more than one fuel type as fitting data allows the new model to capture the characteristics and variations of different fuel types, enhancing its versatility and applicability. This multi-fuel fitting approach enables the model to generalise well and not be restricted to single-fuel data during its development, making it more robust and capable of accurately estimating heat flux in various fire scenarios involving different fuel compositions.

In the case of semi-a priori modelling, the fitting data exclusively consists of experimental data collected from Chapter 4 and Chapters 5 of this research. These experimental datasets form a critical component of semi-a priori modelling because they provide a means to incorporate empirical information into the model and ensure that it accurately reflects the modelled system. Specifically, two sources of experimental data are employed for the modelling process: primary data from ethanol and isopropyl pool fire experiments and secondary data from propane gas fire experiments. By utilising these diverse datasets, the model can be calibrated effectively and capture the essential characteristics of different fuel scenarios, ensuring robust and accurate predictions of radiative heat flux under varied fire conditions.

6.2.2 Experimental Validation Data

The subsequent steps for semi-a priori modelling involve testing the performance of the developed model using experimental data that is not used during model development. This validation process serves as a critical check on the model's generalisability. Using untested experimental data for validation helps guard against overfitting by testing the model's ability to generalise for other fuel variants. On the other hand, if the model performs poorly on the validation data, it suggests that the model may be too narrowly tailored to the characteristics of the fitting data and may not be suitable for making predictions in new situations.

For this chapter, additional experiments are conducted to obtain the untested data for model validation. Following a methodology similar to that used in Chapters 5 (refer to section 3.3), acetone and methanol pool fire experiments are conducted, and the collected data are used to test the performance of the newly formulated thermal radiation model. The specifications for both set of experiments, each conducted with repetition, are shown in Table 6.1.

Table 6.1: Parameter combinations for acetone and methanol pool fire experiment

Fuel	Area of pool fires (m^2)		Distance of measurement location from the centre of the flame (m)	Height of measurement location from the base of the flame (m)
Acetone	**Area 1:**	**0.01**	0.5	0.27 0.61
	Area 2:	**0.04**	1.0	0.27 0.61
	Area 3:	**0.09**	1.5	0.27 0.61
Methanol	**Area 1:**	**0.01**	0.5	0.27 0.61
	Area 2:	**0.04**	1.0	0.27 0.61
	Area 3:	**0.09**	1.5	0.27 0.61

Model validation serves multiple purposes. Firstly, it assesses the accuracy of the model's predictions, helping to identify any discrepancies or uncertainties in the model's output. Secondly, it builds confidence in the model's reliability, ensuring it can be trusted to make informed decisions or draw reliable conclusions. Ultimately, model validation is essential to ensure that the model fits its intended purpose and can provide valuable insights into various real-world scenarios.

6.2.3 Simulation Validation Data

To further validate the effectiveness of the new thermal radiation model, simulation data for methane and heptane pool fires are generated using the Fire Dynamics Simulator (FDS). FDS is a widely recognised computational fluid dynamics (CFD) software specially designed by National Institute of Standards and Technology (NIST) for simulating fire-driven flows and heat transfer phenomena with additional modelling for chemistry effect (Guibaud et al., 2023; McGrattan & Hostikka, 2012; Zhu et al., 2022). It solves the low Mach number Navier-Stokes equations and the Smagorinsky model, enabling fire behaviour prediction throughout the entire computational domain (Pope & Bailey, 2006). By leveraging the capabilities of FDS, this study aimed to rigorously evaluate and compare the performance of the newly developed model by assessing its predictions against the results obtained from FDS simulations. This approach allowed for a comprehensive analysis of the model's accuracy, reliability, and applicability in simulating fire dynamics and related phenomena.

6.3 Development of New Correlation

Semi-a priori modelling combines elements of both a priori modelling, which relies on fundamental principles and theoretical frameworks, and data-driven modelling, which leverages empirical data for model calibration. In the initial phase of model development, a preliminary blind correlation is constructed based on existing theoretical knowledge. Notably, the assessment of the thermal radiation model's performance for gas burner fire experiments (Chapter 4) and liquid pool fire experiments (Chapter 5) has demonstrated the superiority of the single point source model. In addition, the simple configurational of the single point source model eliminates the need for complex configuration factors, which are often present for a realistic solid flame model (Beyler, 2016). The single point source model's simplicity, along with its overall effectiveness, make it the optimal foundation for the blind modelling approach in this research. Taking into account the limitations of the single point source model highlighted by Huang et al. (2019) and Ji et al. (2020), particularly in predicting radiation in the near field of a fire source due to its disregard for flame geometry as well as recognising the potential for improvement if flame geometry is properly considered, this study aims to enhance and refine the single point source model to capture the complexities of thermal radiation more comprehensively.

Building upon the original single point source equation (refer to Equation 2.6) and foundational principles of radiative transfer, an a priori correlation is proposed to incorporate the morphography of flame. The new correlation is rooted in established theoretical concepts from thermal radiation modelling and heat transfer principles, including key physical behaviours inherent to combustion scenarios, such as the inverse-square law governing radiation intensity with distance and the impact of flame geometry on radiative distribution. Several terms were tested during the model development phase, ranging from simple to more complex formulations, with the presented correlation demonstrating the best predictive performance. The new correlation takes into account several parameters, including the sizes of the flame base (area and diameter) and the height of the flame for the estimation of radiant heat flux.

In the new correlation, a dimensionless variable is introduced (refer to variable (d)), involving the rearrangement of several parameters with the same primary dimension (m). This dimensionless approach facilitates the comparison of radiant heat flux across different configurations. The parameters included are the height of the flame, the diameter of the flame base, and the displacement from the flame to the receiving target, reflecting core factors that influence radiative intensity and distribution as described by the inverse-square law and related radiative heat transfer concepts. In addition, another variable that combines the function of the flame area and the displacement from the flame to the receiving target is also introduced (refer to term (c)), contributing to the inverse square meter term in the kW/m^2 for the radiant heat flux. The a priori correlation is shown in Equation 6.1.

$$\dot{q}'' = \underset{(a)}{\dot{Q}_r} \quad \underset{(b)}{\frac{\cos\theta}{\pi}} \quad \underset{(c)}{\left[\frac{A^{\alpha}}{R^{2+2\alpha}}\right]} \quad \underset{(d)}{\left[\frac{H_t + D}{L + D + R}\right]} \qquad 6.1$$

The radiative heat output, denoted by term (a), plays a crucial role as it is the only term that accounts for the impact of changes in fuel type. Different types of fuel possess varying heat of combustion, which influences the total heat release rate. This term allows the correlation to differentiate between different fuels and consider their specific characteristics in the estimation of radiant heat flux. Subsequently, term (b) represents the directionality factor. It takes into account the angle of incidence between the radiating surface and the receiving surface. This factor considers the spreading of radiant energy in different directions, as not all of the radiation emitted by a surface will be directed towards the hemisphere of interest.

Term (c) offers a concise depiction of the interplay between separation distance and flame size. It acknowledges that larger flames generally yield higher intensities, while greater distances lead to lower intensities, following the principles of the inverse square law. By combining these relationships, the exponential function of 2+2α ensures dimensional homogeneity, ensuring the radiant heat flux is correctly represented. Specifically, the area is measured in square meters (m^2) and radius (length) in meters (m). Consequently, the expression Area$^{2(\alpha)}$ /(Length)$^{1(2+2\alpha)}$ yields units of m^{-2}, ensuring dimensional consistency. This homogeneity is critical for accurate physical modelling because it aligns the equation's units and ensures the variables interact correctly without discrepancies.

Furthermore, term (d) also relates flame size and separation distance. However, it involves only parameters with a primary dimension of length. It represents the ratio of the summation of parameters defining the flame size to the summation of parameters used to define the separation between the point source and receiving target. This normalised variable identifies essential relationships between several length parameters and applies them to understanding the behaviour of the system.

By considering not only the spatial distribution between the flame source and the receiving target, but also the geometry of flame, the correlation captures the intricate interplay between various flame characteristics, providing a more comprehensive representation of radiant heat flux than the pioneer model. Furthermore, the inclusion of the dimensionless variable enables standardisation across different configurations, making the model more adaptable and consistent for a range of scenarios. This normalisation facilitates comparisons and analyses, making the correlation adaptable to diverse practical applications.

Despite including additional parameters, the a priori correlation model alone is not readily made to accurately estimate radiative heat flux without the calibration using actual data. Hence, the new correlation necessitates the involvement of fitting data (propane gas, ethanol pool fire, and isopropyl alcohol pool fire experimental data) to guide the correlation in producing precise heat flux predictions. In the subsequent phase of semi-a priori modelling, the elements of data-driven modelling are incorporated, where several coefficients are introduced to the a priori correlation as depicted in Equation 6.2. During this stage, the coefficients are adjusted and refined using a combination of least-squares regression (Excel's Goal Seek function) to minimize the deviation between the model's predictions and the observed data. The error tolerance was set to ensure that the model predictions fell within an acceptable range of the experimental results (fitting data). The iterative procedure continues until the optimal combination of coefficients, yielding the smallest deviation between estimated and experimental data, has been identified. In this study, a total of six coefficients are included in the initial a priori correlation, and the best combination of coefficients is presented in Table 6.2.

$$\dot{q}'' = a\dot{Q}_r \frac{\cos\theta^b A^c}{\pi R^{2+2c}} \left[\frac{H_t + D}{L + D + R} + d \right]^e \qquad 6.2$$

Table 6.2: Best combination of coefficients for the proposed thermal radiation model

Coefficient	Optimum Value
a	0.3418
b	0.4373
c	0.0223
d	0.0000
e	0.1114

In order to bridge the gap between the initial a priori correlation and the final refined model, the involvement of fitting data becomes crucial. The utilisation of experimental data from propane gas fire, ethanol pool fire, and isopropyl alcohol pool fire experiments provides valuable insights into the behaviour of thermal radiation. These insights serve as key elements for refining the model and improving its accuracy and reliability in predicting radiative heat flux. By incorporating these datasets, the fitting process ensures that the constants are adjusted to minimize discrepancies and accurately reflect different combustion scenarios.

In relation to the refined model, the original concept of a single point of origin for heat transfer, as illustrated in Figure 6.2, is preserved. Retaining similar assumptions as the pioneer model, the new thermal radiation model developed in this research builds upon the foundation of the single point source model while incorporating additional refinements and enhancements through semi-a priori modelling. This approach allows for refinement and adjustment of coefficients to reduce the mean absolute percentage error (MAPE) to a level that balances model accuracy without overfitting.

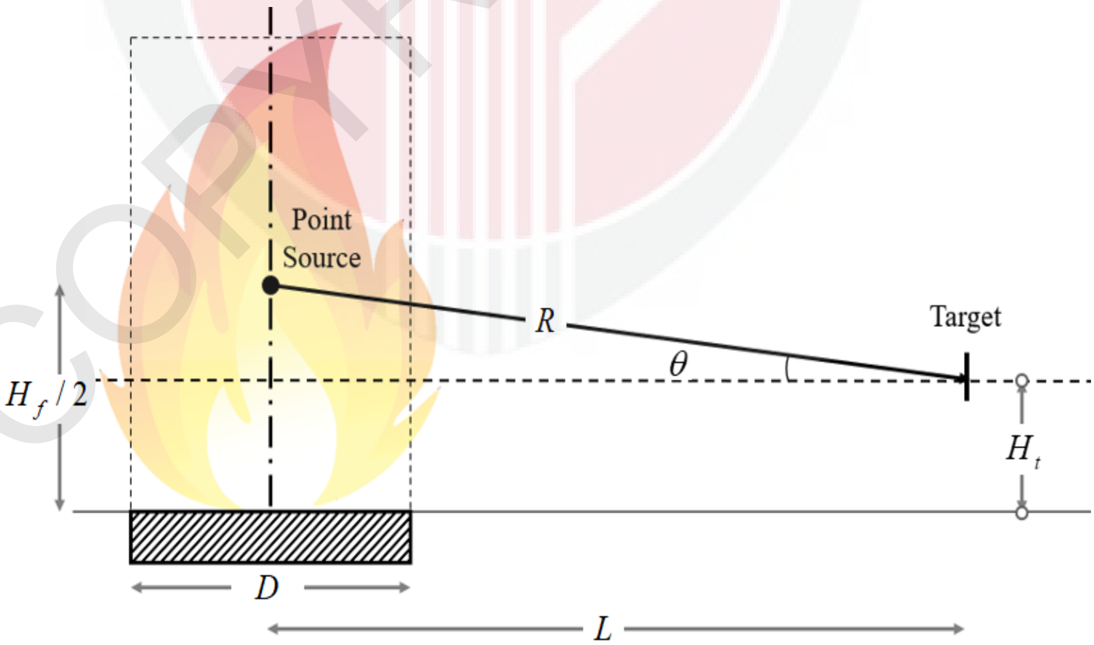

Figure 6.2: Schematic Representation of the New Thermal Radiation Model

The equation formulated for this model, as proposed by this research, is presented as Equation 6.3. This equation captures the improved representation of thermal radiation behaviour, incorporating empirical insights and data-driven advancements.

$$\dot{q}'' = 0.3418\dot{Q}_r \frac{\cos\theta^{0.4373} A^{0.0223}}{\pi R^{2.0446}} \left[\frac{H_t + D}{L + D + R}\right]^{0.1114} \qquad 6.3$$

where

$\dot{q}''$ is the radiant heat flux (kW/m^2)

$\dot{Q}_r$ is the radiative heat output (kW)

θ is the angle between normal and line of sight from target to point source

A is the area of the flame base (m^2)

R is the displacement from the point source to target (m)

H_t is the height of measurement location from the flame base (m)

D is the diameter of the flame base (m)

L is the horizontal distance from the centre of the fire to the target (m)

6.4 Results and Discussion

6.4.1 Performance Evaluation (Fitting Data)

The new model is developed to surpass the present-day established top-performing models by upgrading the existing functionality of the single point source model in estimating the radiative heat flux from the flame source. Table 6.3 indicates the difference in MAPE between the newly developed model and the single point source model in comparison to the fitting data.

Table 6.3: Comparison of MAPE for the fitting dataset

Fire Experiment	MAPE (%)	
	Single Point Source Model	New Model
Propane	30.9	23.6
Ethanol	12.7	24.9
Isopropyl Alcohol	32.7	24.8
Overall	26.2	24.3

Table 6.3 indicates that the performance of the single point source model is highly dependent on the type of fuels tested. It is evident by the lower percentage error for the prediction of the ethanol fire experiment (12.7%) in comparison to the MAPE for the isopropyl alcohol and propane fire experiment (32.7% and 30.9%, respectively). On the other hand, the newly developed model shows a more consistent performance regardless of the variation in the type of fuel tested. From Table 6.3, the MAPE for each variant of the fire experiment is within 1% mean percentage point deviation from one another, where none of the MAPEs exceeded the 25% mark. Overall, despite improving the overall performance of the single point source model by only a small margin (1.9%), significant improvement can be detected in the robustness of the model's performance, where the performance of the proposed model is no longer sensitive to changes of fuel variants.

Despite the notable improvement achieved by the extended correlation for propane and isopropyl alcohol fire experiments, the proposed model did not consistently exhibit lower MAPE values for all sets of fitting data, particularly in the case of ethanol fire experiments. This disparity suggests that while the new model enhances performance across various fuels, its applicability to certain fuel types, particularly ethanol, may be constrained by fuel-specific radiative characteristics that are not fully captured in the model's formulation. This could be due to the unique combustion dynamics and radiative properties of ethanol compared to propane and isopropyl alcohol, which may require additional model adjustments to accurately reflect ethanol's lower sooting tendency and gas-phase radiation contributions.

It is worth highlighting that the primary objective of this study is to develop a thermal radiation model that offers superior performance across a diverse range of fuel variants and fire scenarios. The focus of the model's formulation is on achieving a high level of generalisation and consistency in predicting heat flux, enabling it to maintain reliable estimations across different fuel types. While the underperformance in the specific case of ethanol pool fires is acknowledged, it can be considered a necessary trade-off to ensure that the proposed model achieves its broader objective of robust and consistent heat flux estimation. The improvement in heat flux estimation is further highlighted by the equality graph shown in Figure 6.3 and Figure 6.4.

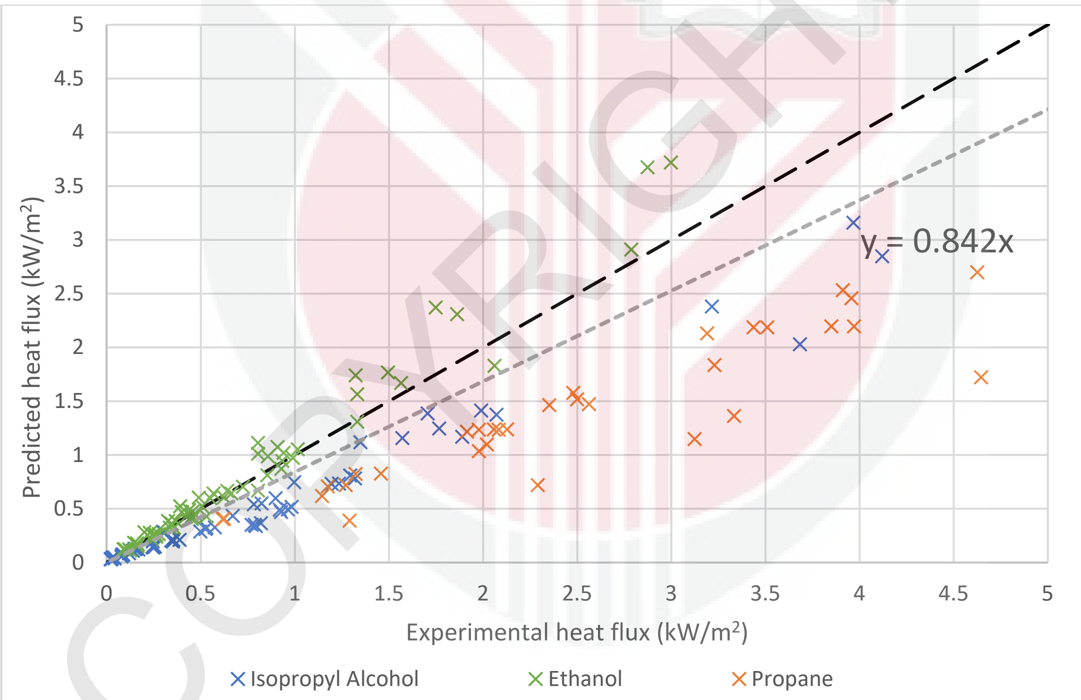

Figure 6.3: Comparison of Heat Flux Values: Single Point Source Model vs. Fitting Data

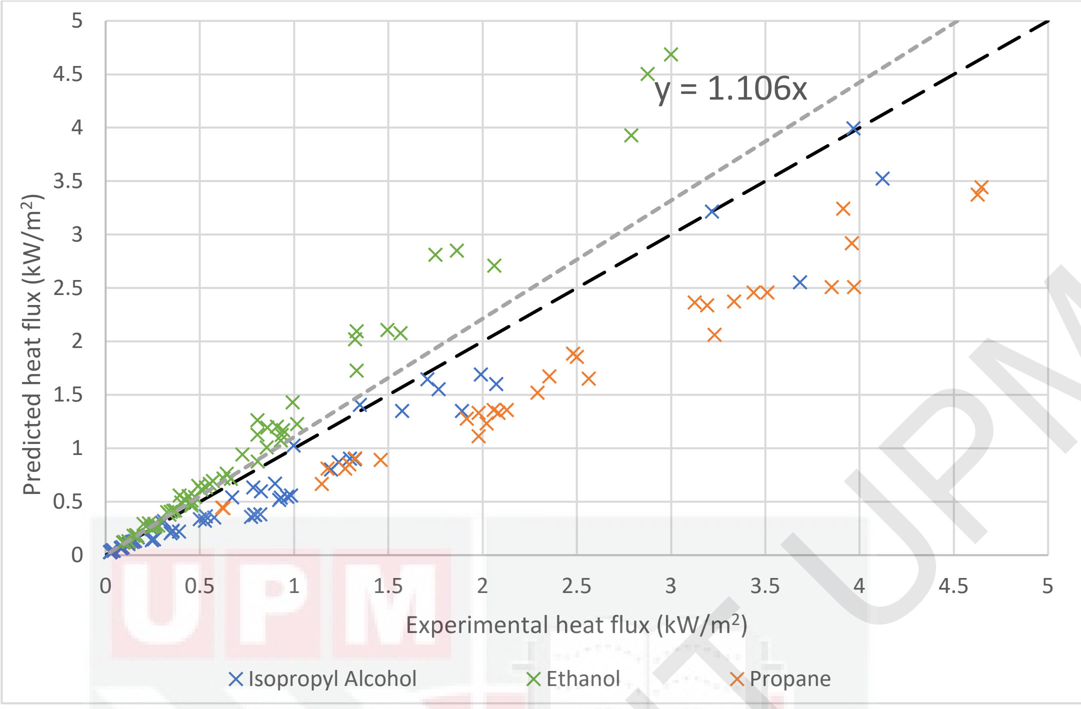

Figure 6.4: Comparison of Heat Flux Values: Newly Developed Model vs. Fitting Data

The comparison between both figures reveals significant insights into the newly developed and single point source models' performance. The equality graph, which represents the relationship between the predicted heat flux values and its experimental heat flux values, showcases distinct differences between the two models. Notably, the trendline generated by the new model aligns better with the equality line, indicating a better agreement between the predicted and real heat flux values. In contrast, the trendline of the single point source model deviates more from the equality line than the newly developed model.

Another noteworthy observation is that the gradient produced by the newly developed model's trendline is higher than one, indicating that the model has a higher tendency to overestimate the heat flux values. On the other hand, the trendline of the single point source model generally exhibits a gradient of less than one, suggesting an underestimation of the heat flux values. Nevertheless, it is essential to highlight that the degree of overestimation demonstrated by the newly developed model is noticeably lower than the degree of underestimation displayed by the single point source model, making the newly developed model better in terms of heat flux estimation.

Based on these observations, it can be confidently concluded that the newly developed model demonstrates superior performance compared to the single point source model. The trendline's closer alignment with the equality line, as well as its lower deviation from a gradient of one, clearly indicate that the newly developed model offers more accurate predictions of the heat flux values. These findings provide some evidence for the improved effectiveness and reliability of the newly developed model in estimating heat flux.

6.4.2 Model Validation (Experimental Validation Data)

Model development is often accompanied by model validation to ensure the model's accuracy, reliability, and generalisability. During a priori modelling, the equations, parameters, and coefficient for parameters are adjusted to fit the heat flux data for propane, ethanol, and isopropyl alcohol fire experiments. Hence, model validation is essential to assess the generalisability of the model beyond the data used for model development. It helps determine if the model can accurately predict the outcomes for a new dataset and is not overly tailored to the fitting dataset.

For this research, the validation data are obtained from conducting acetone and methanol pool fire experiments, and the overall MAPE for the new model and the single point source model against the validation dataset are shown in Table 6.4.

Table 6.4: Comparison of MAPE for the experimental validation dataset

Pool Fire Specification		MAPE (%)	
Fuel	Pan Size (m^2)	Single Point Source Model	New Model
Acetone	0.1 x 0.1	8.2	11.3
	0.2 x 0.2	15.0	11.3
	0.3 x 0.3	19.6	13.9
Overall		**14.2**	**12.2**
Methanol	0.1 x 0.1	4.0	17.6
	0.2 x 0.2	10.0	11.8
	0.3 x 0.3	12.1	11.0
Overall		**8.7**	**13.5**

Table 6.4 illustrates that both the single point source model and the newly developed model can accurately predict the thermal interaction for acetone and methanol pool fire. The single point source model outperforms the new model in terms of accuracy for the methanol pool fire experiment with an average MAPE of 8.7%, in comparison to the 13.5% MAPE for the new model. In contrast, the new model performs better for the acetone pool fire experiment with an average MAPE of 12.2%, compared with the MAPE of the single point source model at 14.2%. Nevertheless, the single point source model exhibited a lack of robustness, as evidenced by a distinct 5.5% mean percentage point deviation between the experimental data of acetone and methanol pool fire experiments.

While the proposed model may not consistently exhibit a lower MAPE for the entire experimental validation dataset, it consistently demonstrates a high level of accuracy and robustness, effectively estimating the radiative heat flux with a MAPE lower than 14% for both fuels and less than 2% mean percentage point deviation between the two fuels tested. The observed underperformance for the methanol fire experiment indicates a necessary trade-off to ensure the model's generalisability while maintaining a high level of reliability and accuracy in estimating heat flux. Despite being refined based on propane, ethanol, and isopropyl alcohol fitting dataset, the new model's results consistently align with the data obtained from validation experiments (acetone and methanol pool fire experiment). Figure 6.5 and Figure 6.6 highlighted the robustness of the new model and its ability to generalise across different fuel sources.

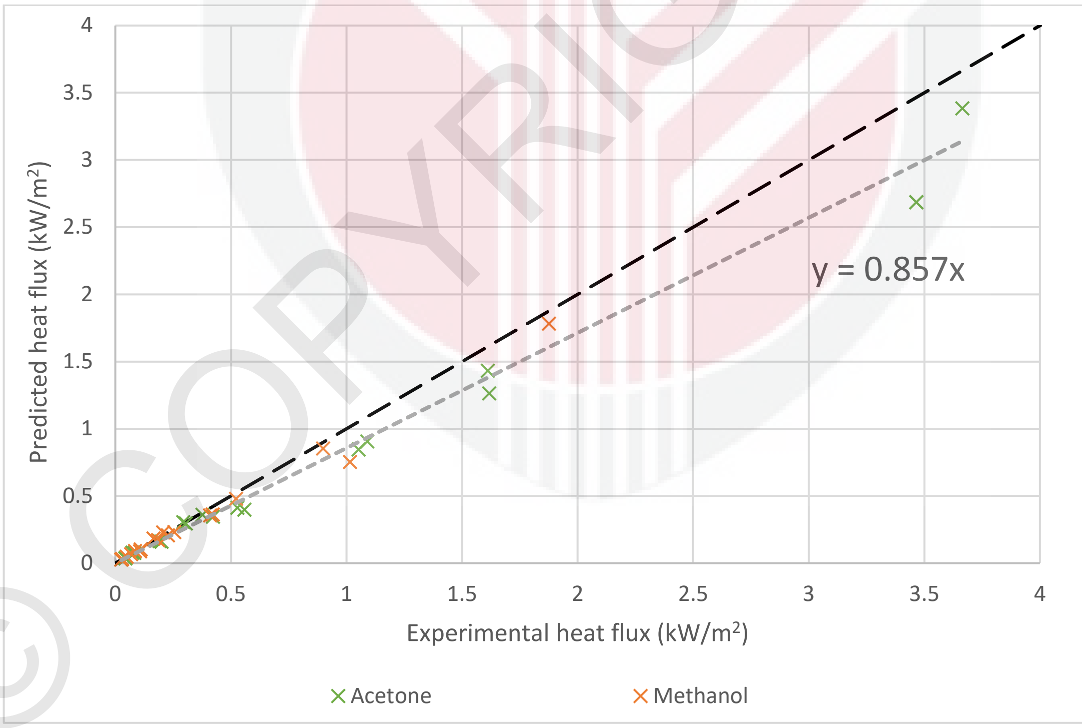

Figure 6.5: Comparison of Heat Flux Values: Single Point Source Model vs. Experimental Validation Data

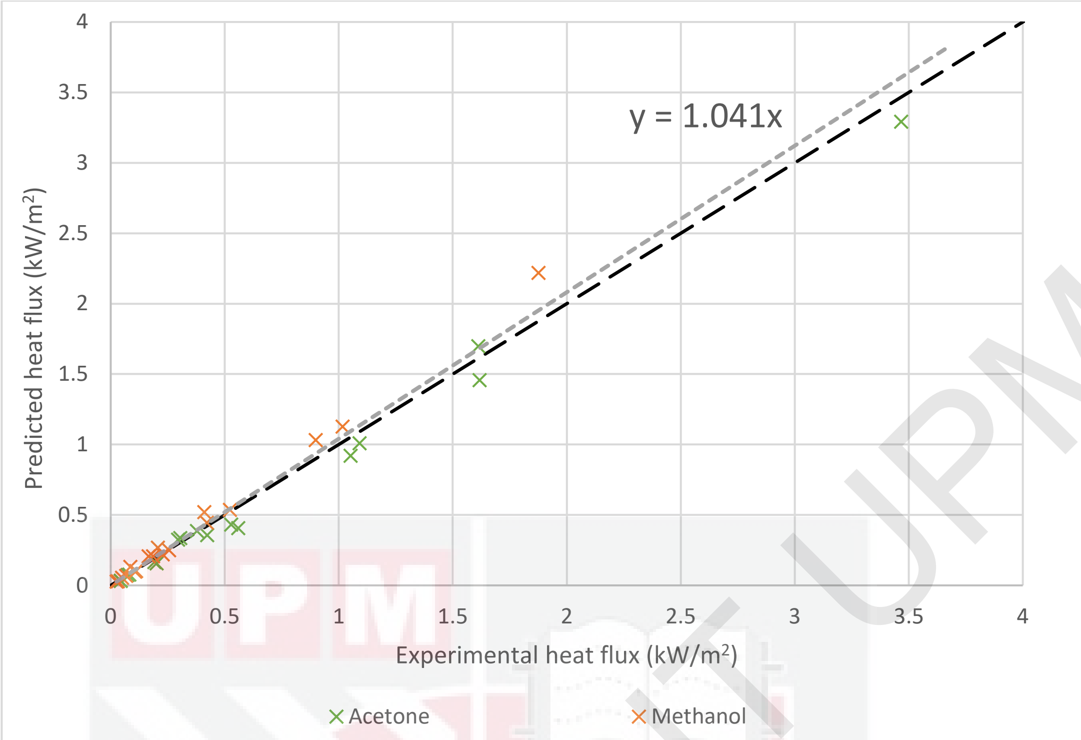

Figure 6.6: Comparison of Heat Flux Values: Newly Developed Model vs. Experimental Validation Data

The findings from the equality graphs comparing the predictions of the single point source model and the new model with experimental validation data provide valuable insights into the improvement achieved by the new model in accurately predicting heat flux values. Generally, both models exhibit good alignment with the observed values at lower heat flux values (< 1 kW/m^2), indicating their effectiveness in capturing the behaviour of the system in this range. However, as the heat flux values increase, the single point source model tends to deviate more from the observed values, while the new model maintains a closer prediction to the equality line. The trendlines of the two models further highlight their differences. The trendline of the single point source model lies beneath the equality line, suggesting a tendency to underestimate the heat flux values. On the other hand, the trendline of the new model is slightly above the equality line, indicating that the new model has the tendency to slightly overestimate heat flux values.

The observed patterns of overestimation and underestimation across different fuel types, rather than fuel phase alone, can be further analysed by comparing the trends of the new model in Figure 6.4 and Figure 6.6. The new model's performance appears to be more sensitive to variations in fuel type (i.e., specifically in sooting tendency and radiative characteristics) than to changes in fuel phase (i.e., gas versus liquid). While phase does influence combustion dynamics, the dominant factor impacting radiative heat flux predictions is the fuel's sooting propensity and associated radiative intensity. This finding underscores the model's dependence on the fuel-specific characteristics rather than simply whether the fuel is in a gaseous or liquid state. The new model tends to overestimate for fuels such as propane (gas burner), acetone, and isopropyl alcohol (all of which show higher heat flux values), while it underestimates for ethanol and methanol fires.

For instance, fuels that produce higher soot levels, such as isopropyl alcohol and acetone, exhibit an increased radiative output due to the presence of solid soot particles in the flame. These particles contribute significantly to the radiation profile by emitting continuum radiation across both the visible and infrared spectra, which augments the radiative intensity captured by the model. This additional radiative component, often concentrated in the visible and near-infrared ranges, is challenging to predict accurately without specific adjustments in the model for high-soot fuels. As a result, the model tends to overestimate heat flux values for these fuels, reflecting its current calibration, which appears to account for moderate to high soot levels by default.

On the other hand, fuels with minimal sooting, such as ethanol and methanol, primarily emit radiation through gas-phase molecular transitions rather than particulate-based emissions. In these low-soot flames, radiation is typically concentrated within the infrared bands due to vibrational and rotational transitions in the gas-phase combustion products (primarily carbon dioxide and water vapour). These transitions emit less radiant energy per unit volume than soot particles, leading to lower overall radiative intensity. Consequently, the model tends to underestimate heat flux for such fuels, as its formulation does not fully account for the lower emissivity and the predominantly gas-phase radiation mechanisms in low-soot flames. This finding is consistent with observed discrepancies in radiative heat flux values, particularly at higher flux levels, where the model's assumptions on radiative output from soot are not applicable to low-soot fuels.

Despite the model's improvements, its applicability to longer-chain hydrocarbons or aromatic hydrocarbons remains untested. Fuels with larger molecular structures and higher sooting tendencies, such as benzene or hexane, often exhibit more complex radiative profiles. These fuels typically produce greater levels of soot and particulate emissions, which intensify radiant heat flux in combustion scenarios. The current model, while generalisable within the scope of C_3 and lower fuels, may face limitations in accurately capturing the radiative effects of such fuels. Future studies could incorporate these larger hydrocarbons to evaluate the model's robustness in representing a broader range of fire scenarios.

Overall, the findings indicate that the new model outperforms the single point source model in predicting heat flux values, particularly at higher heat flux values, demonstrating improved accuracy and reliability through its close alignment with observed values. However, the performance differences for the new model appear to be influenced more by fuel type and sooting characteristics than by fuel phase, with a tendency to overestimate for high-soot fuels and underestimate for low-soot fuels, highlighting current limitations in capturing the full range of radiative behaviours. These results highlight the significance of incorporating additional refinements and enhancements through semi-a priori modelling, potentially including a more nuanced treatment of soot emissions, to enhance the model's applicability across diverse fuel types. Together, these advancements contribute to the development of a more robust and accurate thermal radiation model, offering valuable insights for fire safety assessment and mitigation strategies in the field of thermal radiation modelling.

6.4.3 Model Validation (Simulation Data)

Comparison between the model's estimations and simulation data provides an opportunity to evaluate its performance and validate its accuracy. This comparison determines whether the model aligns with other modelling approaches or established simulation techniques. In the context of this research, the simulation of heptane and methane pool fires is carried out using FDS. The heat flux outputs from the FDS simulations are then compared to the estimated values obtained from both the single point source model and the proposed model, allowing for a comprehensive assessment of their performance in capturing the thermal behaviour of the pool fires. The results are shown in Table 6.5.

Table 6.5: Comparison of MAPE for the simulation dataset

Simulation Specification		MAPE (%)	
Fuel	Pan Size (m^2)	Single Point Source Model	New Model
Heptane	0.2 x 0.2	35.6	27.6
	0.3 x 0.3	31.5	21.2
	0.4 x 0.4	29.4	18.4
Overall		**32.2**	**22.4**
Methane	0.2 x 0.2	37.8	30.0
	0.3 x 0.3	25.4	15.9
	0.4 x 0.4	29.5	18.2
Overall		**30.9**	**21.4**

Based on the findings presented in the table above, both the single point source model and the proposed model exhibited a consistent performance in comparison to the simulation data for heptane and methane pool fire experiments. However, it is noteworthy that the new model outperformed the single point source model in terms of accuracy, showcasing a significant advantage. The new model achieved an approximately 10% lower MAPE for both heptane and methane pool fire experiments, indicating its superior ability to provide more precise estimations. The improvement in accuracy is crucial as it enhances the reliability and usefulness of the proposed model as an advanced approach that can yield more accurate results in predicting thermal interactions, thereby supporting the decision-making process, system design, and risk assessment in fields such as fire safety engineering and energy systems.

Furthermore, the alignment between the estimated heat flux values of the new model and the simulation results for different fuel types significantly enhances the model's generalisability. By providing a low MAPE for both methane and heptane simulations, the model demonstrates a degree of versatility, adapting to different radiative behaviours inherent to both high-sooting (heptane) and low-sooting (methane) fuels. This aligns with the objective of developing a model that offers a more generalised application across diverse fire scenarios, bridging the gap between hand-calculated predictions and the more detailed, computationally intensive CFD simulations. The low average MAPE displayed by the proposed model in both heptane and methane pool fire simulations (22.4% and 21.4%, respectively) underscores its capacity to be confidently applied to new scenarios beyond the specific conditions employed during the model's development process. A visual representation of the models' performance is provided through the equality graphs, as shown in Figure 6.7 and Figure 6.8, which compare the predicted heat flux values of the single point source model and the new model with the simulation data.

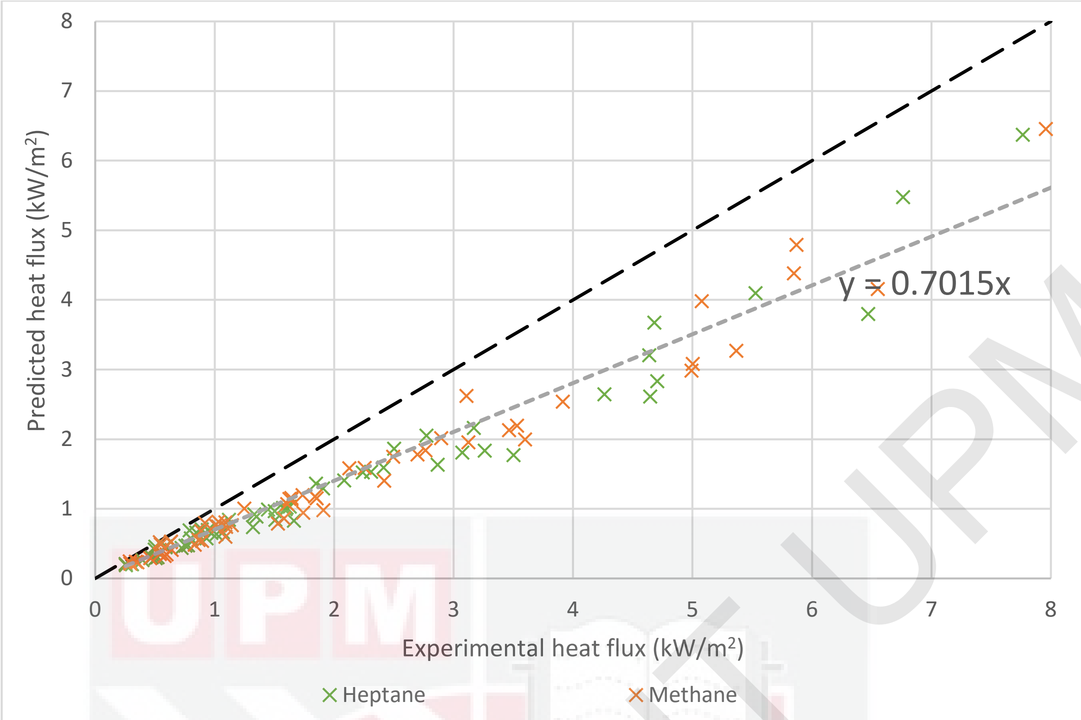

Figure 6.7: Comparison of Heat Flux Values: Single Point Source Model vs. Simulation Data

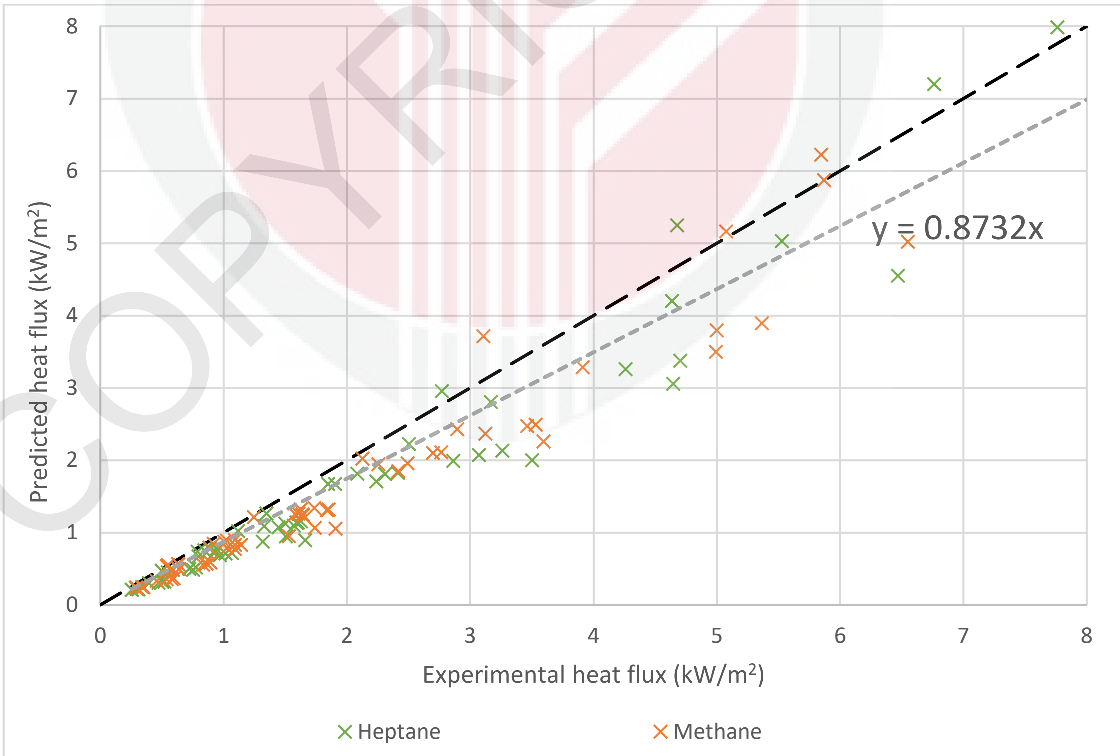

Figure 6.8: Comparison of Heat Flux Values: Newly Developed Model vs. Simulation Data

Comparing both Figure 6.7 and Figure 6.8, a distinct behaviour can be observed between the single point source model and the new model in predicting heat flux values. Figure 6.7, representing the predictions of the single point source model, shows all the data points located below the diagonal line, indicating consistent underestimation of the heat flux. In contrast, Figure 6.8 displays the predictions of the new model, where the data points are distributed both above and below the diagonal line.

The trendline in Figure 6.7 for the single point source model consistently falls below the equality line, suggesting a systematic bias towards lower heat flux values. This indicates limitations in accurately capturing the true heat flux behaviour, particularly at higher values. On the other hand, the trendline in Figure 6.8 for the new model also lies below the equality line but exhibits a closer alignment with the equality line, indicating reduced bias and a better overall fit to the simulated data.

While data points above the diagonal line in Figure 6.8 suggest, instances where the new model slightly overestimates the heat flux, the majority of data points and the overall trendline remain below the equality line, making the general trendline of the new model tend to slightly underestimate the heat flux. However, the distribution of data points both above and below the diagonal line suggests a more balanced and accurate performance than the single point source model. In essence, the model's underlying assumptions, equations, and parameters adeptly capture the essential elements of the system, enabling reliable prediction and analysis in diverse real-world situations.

6.4.4 Model Limitations

Despite the improvements provided by the proposed model, it is essential to acknowledge its limitations, particularly regarding the lack of parameters explaining the fuel-sooting propensity. Sooting tendencies of different fuels can vary significantly based on factors such as fuel properties (carbon content, hydrogen-to-carbon ratio, oxygen content) and combustion conditions (temperature, pressure, and oxygen availability). For instance, in estimating radiative heat output, the current model considers differences in fuel properties only during the calculation of total heat release rate (as indicated in Equation 3.2), while the radiative fraction utilised a single expression (as shown in Equation 2.4) for all fuel variants. The radiative fraction is inherently sensitive to the quantity of soot generated by the flame, thus reliant on the distinct characteristics of the fuel used. The use of a generic equation, rather than specific values for each fuel type, may lead to challenges in generalising its performance.

In the context of this study, where the model showed promising results and robustness for the tested fuels and distances, the effect of sooting might not be readily apparent. However, caution must be exercised when applying the model to scenarios involving heavy sooting fuels and extended distances. Soot produced in the combustion process may significantly affect radiative heat flux readings, especially for extended distances where the cumulative effect of soot becomes more pronounced. The lack of consideration for fuel-specific characteristics could limit the model's applicability in such cases. Although untested data sets have been introduced to explore the generalisability of the new model, the behavior and fit of fuels outside the scope of this research may exhibit different combustion dynamics, potentially leading to varying results. Therefore, further research is required to fully assess the model's limitations.

Additionally, the model's application has been focused on lower-chain hydrocarbons (C3 or smaller), which limits its ability to generalise across a broader range of fuels, particularly longer-chain hydrocarbons or aromatic compounds such as benzene, toluene, or hexane. These larger hydrocarbons introduce increased levels of soot and particulate emissions due to their structural complexity and higher carbon content. This difference alters radiative heat transfer dynamics, as larger molecules emit more intense radiative output, especially in the visible and infrared spectra. Consequently, the simplified emissive behaviour assumed in the new model may not adequately capture these effects, resulting in potentially inaccurate heat flux estimations for high-soot fuels. Incorporating fuel-specific parameters for emissivity and adjustments to radiative fraction could allow the model to account for the heightened soot production and higher radiant intensities typical of these fuels, enhancing its robustness for diverse fire scenarios.

Moreover, it is important to note that the experimental heat flux data in this research are exclusively recorded using sensors positioned at an angle perpendicular to the pool flame. As a result, the variation of heat flux parallel to the pool flame is not accounted for in this research. Future investigations exploring the results obtained from heat flux gauges positioned parallel to the pool fire could provide valuable insights into the performance of the new model in that specific orientation. This additional analysis could further enhance the understanding and applicability of the proposed model for predicting radiative heat flux distribution in real-world scenarios.

6.5 Summary

In short, this study demonstrates the significance of model formulation and its role in advancing fire safety assessment. This study has provided alternative to the existing correlation for heat flux prediction. By integrating the strengths of both a priori and data-driven modelling approaches, the new model, represented by the equation formulated in Section 6.3:

$$\dot{q}'' = 0.3418\dot{Q}_r \frac{\cos\theta^{0.4373} A^{0.0223}}{\pi R^{2.0446}} \left[\frac{H_t + D}{L + D + R} \right]^{0.1114} \quad 6.3$$

has demonstrated improved performance in predicting thermal radiation compared to the single point source model, particularly in terms of generalisability. Notably, the incorporation of crucial parameters, such as the sizes of the flame base and the height of the flame, has enhanced the accuracy and comprehensiveness of the proposed model. A comparison of the model's performance against various datasets, including fitting data, experimental validation data, and simulation validation data, has proven the capability of the new model in consistently producing robust heat flux estimations with a MAPE lower than 25%. Furthermore, the proposed model outperforms the single point source model in most cases, with the exception of the methanol and ethanol pool fire experiments.

This research contributes to the field of fire safety by providing a new model for assessing thermal radiation and its impact on fire scenarios. The findings emphasise the importance of continuous improvement and development of thermal radiation models to enhance the understanding of fire dynamics and enable the design of effective fire prevention and mitigation strategies. Future research can further explore the application of the new model in different fire scenarios, i.e., solid combustible fires, and investigate additional factors that influence thermal radiation.

CHAPTER 7

CONCLUSION AND RECOMMENDATION

7.1 Conclusions

This thesis addresses the research gap identified by Fleury et al. (2011) by evaluating a broader range of thermal radiation models across different fuel sources. Comprehensive experiments and analyses identified the single point source model as the most accurate and robust model for predicting heat flux across various fire scenarios, demonstrating consistent performance in sensitivity analyses across flame sizes, target heights, and distances.

Beyond existing models, this research developed a novel thermal radiation model using a semi-a priori approach, combining theoretical and data-driven insights to significantly enhance accuracy and comprehensiveness. The new model achieved a mean absolute percentage error (MAPE) below 25%, outperforming the single point source model in most scenarios. The findings support fire safety engineering by validating reliable models for thermal radiation prediction, contributing to effective fire protection system design, material evaluation, and occupant safety.

7.2 Fulfilment of Research Objectives

The research objectives aimed to assess radiation models for gas and liquid fire scenarios and develop a new model with improved generalisability. This was achieved through three key stages:

- **Gas Fire Experiments (Chapter 4)**: This chapter identified the single point source model as the best-performing model for gas fires, using a dataset consistent with Fleury et al. (2011).
- **Liquid Fire Experiments (Chapter 5)**: The single point source model also outperformed other models for ethanol and isopropyl alcohol pool fires, providing a robust benchmark for both gas and liquid fire scenarios.
- **Model Development (Chapter 6)**: A new model was formulated using propane, ethanol, and isopropyl alcohol fire data, performing well in untested experimental and simulation datasets. This model offers practitioners a reliable alternative for both gas and liquid fire applications.

7.3 Recommendations for Future Research

Based on the findings and limitations of this research, the following recommendations are made for further studies in the field:

7.3.1 Conducting Larger-Scale Pool Fire Experiments

Since the maximum pool fire tested for this research is limited to 0.16 m^2, conducting a larger-scale pool fire would surely benefit the findings of this research. Listed below are the recommendations for conducting a larger-scale pool fire experiment:

- Expanding pool fire size: Conducting larger-scale pool fire experiments beyond the current limit of 0.16 m^2 is useful for capturing a broader range of fire behaviour and assessing thermal radiation models' performance under more realistic and challenging conditions.
- Optimize video capture: Utilise a high-quality video capture device to ensure accurate and detailed image capture during the larger-scale pool fire

experiments. This will enable a more precise analysis of flame characteristics and behaviour, particularly for capturing blue flames.

- Address flame height limitation: Implement a higher exhaust hood or modify the experimental setup to avoid limitations in measuring flame height caused by the obstruction of the hood. This will provide clearer visibility and enable more accurate measurements.
- Address weighing scale capacity limitation: Instead of opting for a precision weighing scale, consider incorporating a gas calorimeter or similar equipment to collect data on oxygen consumption rates, enabling the determination of the heat release rate. This additional information will contribute to a comprehensive understanding of fire dynamics and enhance the accuracy of thermal radiation modelling.

7.3.2 Validation of Proposed Models with Different Gas Burners

In order to enhance the validity and generalisability of the research findings, it is recommended to extend the validation of thermal radiation models beyond the confines of pool fire experimental data. By including various gas burners, not limited to propane alone, the research can evaluate how well the thermal radiation models capture the behaviour of different fuel sources. This expanded validation approach will contribute to a more robust understanding of the models' effectiveness across a broader spectrum of fire scenarios, enabling better decision-making in fire safety engineering.

7.3.3 Expansion of Research Scope

To improve and validate the research findings, the following recommendations are suggested:

- Larger-Scale Pool Fires: Conducting larger-scale experiments beyond 0.16 m^2 to capture a wider range of fire behaviour. Improving video capture, adjusting flame height limitations, and expanding weighing capabilities could offer more comprehensive data.
- Validation with Diverse Fuel Sources: Validating thermal radiation models with fuels beyond propane, including other gas burners, could enhance model generalisability and improve decision-making in fire safety.
- Expanded Scope and Complexity: Incorporating sooty fuels, diverse pool fire geometries, and multiple flame sources would improve model robustness. Evaluating different simulation tools may also identify the most reliable approaches for varied fire scenarios.

Additionally, benchmarking against external datasets and broader validation is essential for future studies to further substantiate model accuracy. Expanding validation with additional fuel types and combustion conditions, as proposed in this chapter, will enhance confidence in the model's applicability and robustness across diverse fire scenarios. These recommendations aim to enhance the research by broadening the scope of experiments, improving experimental techniques, and exploring additional factors and fuels to further validate and refine the thermal radiation models used.

REFERENCES

Abbott, H. C. (1942). Common Fire Hazards. In *Fire Protection Engineering: A Symposium of Papers Presented at a Summer Conference at the Massachusetts Institute of Technology* (pp. 56–72). Quincy, MA: National Fire Protection Association.

Ahrens, M., & Evarts, B. (2021, September). Fire Loss in the United States During 2020. *National Fire Protection Association.*

Airgas. (2005). *Safety data sheet: Propane* (Carbon, 1173(i), 1–8). Airgas, Inc.

Audouin, L., Kolb, G., Torero, J. L., & Most, J. M. (1995). Average centreline temperatures of a buoyant pool fire obtained by image processing of video recordings. *Fire Safety Journal*, *24*(2), 167–187. https://doi.org/10.1016/0379-7112(95)00021-K

Babrauskas, V. (1983). Estimating large pool fire burning rates. *Fire Technology*, *19*(4), 251–261. https://doi.org/10.1007/BF02380810

Bahrami, M. (2005, Spring). *Chapter 12: Radiation Heat Transfer*. E&CE 309 course notes, 1–20. University of Waterloo. Retrieved from http://www.mhtl.uwaterloo.ca/courses/ece309_mechatronics/lectures/pdffiles/summary_ch12.pdf

Bal, N. (2018). Forty years of material flammability: An appraisal of its role, its experimental determination and its modelling. *Fire Safety Journal*, *96*(April 2015), 46–58. https://doi.org/10.1016/j.firesaf.2017.11.012

Begley, J. P. (2004). *Performance-Based Fire Safety Design - Facilities Management Insights*. FIRE SAFETY/PROTECTION. https://www.facilitiesnet.com/firesafety/article/Performance-Based-Fire-Safety-Design--2017

Beyler. (2016). Fire hazard calculations for large, open hydrocarbon fires. In *SFPE Handbook of Fire Protection Engineering, Fifth Edition* (pp. 2591–2663). https://doi.org/10.1007/978-1-4939-2565-0

Bhanja, S. N., Coon, E. T., Lu, D., & Painter, S. L. (2023). Evaluation of distributed process-based hydrologic model performance using only a priori information to define model inputs. *Journal of Hydrology*, *618*(June 2022), 129176. https://doi.org/10.1016/j.jhydrol.2023.129176

Carmignana, L. (2021). *Flame Tracker: An image analysis program to measure flame characteristics*. SoftwareX, 15(July 2021), 100791. https://doi.org/10.1016/j.softx.2021.100791

Castillo Soto, M. E., Molina Martínez, J. R., Bonilla B, S., & Moreno García, R. A. (2022). Calculating minimum safety distance against wildfires at the wildland-urban interface in Chile and Spain. *Heliyon*, *8*(11), e11238. https://doi.org/10.1016/j.heliyon.2022.e11238

Choi, Y., An, N., Hong, S., Cho, H., Lim, J., Han, I. S., Moon, I., & Kim, J. (2022). Time-series clustering approach for training data selection of a data-driven predictive model: Application to an industrial bio 2,3-

butanediol distillation process. *Computers and Chemical Engineering*, *161*, 107758. https://doi.org/10.1016/j.compchemeng.2022.107758

Chow, W. K., Li, Y. Z., Han, S. S., & Yi, L. (2006). Importance of including thermal radiation in designing discharge concentration of gas protection systems. *International Journal on Engineering Performance-Based Fire Codes*, *8*(1), 21–27.

Comitis, S. C., Glasser, D., & Young, B. D. (1996). An experimental and modeling study of fires in ventilated ducts. Part II: PMMA and stratification. *Combustion and Flame*, *104*(1–2), 138–156. https://doi.org/10.1016/0010-2180(95)00114-X

Dayan, A., & Tien, C. L. (1974). Radiant Heating from a Cylindrical Fire Column. *Combustion Science and Technology*, *9*(I), 41–47. https://doi.org/10.1080/00102207408960335

Ezekoye, O. A., Hurley, M. J., Torero, J. L., & McGrattan, K. B. (2013). Applications of heat transfer fundamentals to fire modeling. *Journal of Thermal Science and Engineering Applications*, *5*(2), 1–11. https://doi.org/10.1115/1.4024015

Filkov, A. I., Tihay-Felicelli, V., Masoudvaziri, N., Rush, D., Valencia, A., Wang, Y., Blunck, D. L., Valero, M. M., Kempna, K., Smolka, J., De Beer, J., Campbell-Lochrie, Z., Centeno, F. R., Ibrahim, M. A., Lemmertz, C. K., & Tam, W. C. (2023). A review of thermal exposure and fire spread mechanisms in large outdoor fires and the built environment. *Fire Safety Journal*, *140*(September 2022), 103871. https://doi.org/10.1016/j.firesaf.2023.103871

Fleury, R., Spearpoint, M., & Fleischmann, C. (2011). Evaluation of Thermal Radiation Models for Fire Spread Between Objects. *Fire and Evacuation Modelling Technical Conference 2011*.

Fu, F. (2021). Fire Safety Design for Tall Buildings. In *Fire Safety Design for Tall Buildings*. https://doi.org/10.1201/9781003009818

Fukumoto, K., Wen, J. X., Li, M., Ding, Y., & Wang, C. (2020). Numerical simulation of small pool fires incorporating liquid fuel motion. *Combustion and Flame*, *213*, 441–454. https://doi.org/10.1016/j.combustflame.2019.11.047

Ganji, D. D., Sabzehmeidani, Y., & Sedighiamiri, A. (2017). Nonlinear systems in heat transfer: Mathematical modeling and analytical methods. In *Nonlinear Systems in Heat Transfer: Mathematical Modeling and Analytical Methods*. https://doi.org/10.1016/C2016-0-00401-1

Gavelli, F. (2021). The effect of barriers on reducing thermal heat fluxes from a hydrocarbon pool fire. *Journal of Loss Prevention in the Process Industries*, *72*(May), 104554. https://doi.org/10.1016/j.jlp.2021.104554

Gibson, L., Engelbrecht, J., & Rush, D. (2019). Detecting historic informal settlement fires with sentinel 1 and 2 satellite data - Two case studies in Cape Town. *Fire Safety Journal*, *108*(May), 102828. https://doi.org/10.1016/j.firesaf.2019.102828

Gossiaux, A., Bachelet, P., Bellayer, S., Ortgies, S., König, A., & Duquesne, S. (2021). Small-scale single burning item test for the study of the fire behavior of building materials. *Fire Safety Journal*, *125*(August). https://doi.org/10.1016/j.firesaf.2021.103429

Guibaud, A., Mindeguia, J. C., Albuerne, A., Parent, T., & Torero, J. (2023). Notre-Dame de Paris as a validation case to improve fire safety modelling in historic buildings. *Journal of Cultural Heritage*, *xxxx*. https://doi.org/10.1016/j.culher.2023.05.008

He, Y. (2001). Evaluation of the maximum configuration factor for cylindrical flame hazard calculation. *Journal of Fire Sciences*, *19*(2), 121–136. https://doi.org/10.1106/J5TA-D9CU-6MF6-5VMJ

Heskestad, G. (1983). Luminous heights of turbulent diffusion flames. *Fire Safety Journal*, *5*(2), 103–108. https://doi.org/10.1016/0379-7112(83)90002-4

Huang, X., Wang, Y., Zhu, H., He, L., Tang, F., & Wen, J. (2020). Experimental study on the radiant heat flux of wall-attached fire plume generated by rectangular sources. *International Journal of Thermal Sciences*, *159*(May 2020), 2–8. https://doi.org/10.1016/j.ijthermalsci.2020.106605

Huang, X., Zhuo, X., Huang, T., Xing, C., Cheng, C., & Chow, W. (2019). Thermal radiation model for the buoyancy-controlled diffusion plumes from rectangular fire sources. *International Journal of Thermal Sciences*, *150*(December 2019), 106234. https://doi.org/10.1016/j.ijthermalsci.2019.106234

Hurley, M. J., Gottuk, D., Hall, J. R., Harada, K., Kuligowski, E., Puchovsky, M., Torero, J., Watts, Jj. M., & Wieczorek, C. (2016). SFPE handbook of fire protection engineering, fifth edition. In *SFPE Handbook of Fire Protection Engineering, Fifth Edition*. https://doi.org/10.1007/978-1-4939-2565-0

Hurley, M. J., & Rosenbaum, E. R. (2015). Performance-based fire safety design. In *Performance-Based Fire Safety Design*. https://doi.org/10.1201/b18375

Ibrahim, M. N., Ibrahim, M. S., Mohd-Din, A., Abdul-Hamid, K., Yunus, R. M., & Yahya, M. R. (2011). Fire risk assessment of heritage building - Perspectives of regulatory authority, restorer and building stakeholder. *Procedia Engineering*, *20*, 325–328. https://doi.org/10.1016/j.proeng.2011.11.173

IFEA. (2018). *Performance-based design*. Fire Safety Engineering. Retrieved from http://www.ifea.my/performance-based-design/

Ivanova, S. M., & Muneer, T. (2017). *Derivative view factors between parallel and non-parallel rectangular surfaces NON-PARALLEL RECTANGULAR SURFACES. February 2018*.

James M. (n.d.). *What are the advantages of performance-based fire design?* Performance-Based Design. Retrieved from https://reaxengineering.com/fire-protection-engineering/performance-based-design/

JBPM. (2018). *Jabatan Bomba dan Penyelamat Malaysia (Malaysian Fire and Rescue Department), Laporan Tahunan 2018 (Annual Report 2018)*. 1–224.

Ji, J., Ge, F., & Qiu, T. (2020). Experimental and theoretical research on flame emissivity and radiative heat flux from heptane pool fires. *Proceedings of the Combustion Institute*, *000*, 1–9. https://doi.org/10.1016/j.proci.2020.05.052

Ji, J., Gong, C., Wan, H., Gao, Z., & Ding, L. (2019). Prediction of thermal radiation received by vertical targets based on two-dimensional flame shape from rectangular n-heptane pool fires with different aspect ratios. *Energy*, *185*, 644–652. https://doi.org/10.1016/j.energy.2019.07.083

Kim, B., Lee, J., & Shin, W. G. (2022). Sensitivity analysis of input variables to establish fire damage thresholds for redundant electrical panels. *Nuclear Engineering and Technology*, *54*(1), 84–96. https://doi.org/10.1016/j.net.2021.07.044

Klassen, M., & Gore, J. P. (1993). Temperature and soot volume fraction statistics in toluene-fired pool fires. *Combustion and Flame*, *93*(3), 270–278. https://doi.org/10.1016/0010-2180(93)90108-F

Kodur, V., Kumar, P., & Rafi, M. M. (2019). Fire hazard in buildings: review, assessment and strategies for improving fire safety. *PSU Research Review*, *4*(1), 1–23. https://doi.org/10.1108/prr-12-2018-0033

Kulkarni, V. S., & Shaw, C. (2016). Aerosols and Nasal Sprays. *Essential Chemistry for Formulators of Semisolid and Liquid Dosages*, 71–97. https://doi.org/10.1016/b978-0-12-801024-2.00006-6

Lab-Chem. (2016). Isopropyl Alcohol (2-Propanol). *Material Safety Data Sheet*, *77*(58), 1–7.

Li, M., Zhang, C., Wang, C., Liu, Z., & Wang, B. (2021). Ignition behavior and critical distance of flammable liquids by radiant heat flux from adjacent pool fire. *International Journal of Thermal Sciences*, *168*(May), 107043. https://doi.org/10.1016/j.ijthermalsci.2021.107043

Li, X., Zhang, M., Zhong, Y., Li, X., Wang, H., & Ding, Y. (2023). Upwind thermal radiation prediction of multi-scale aviation kerosene pool fire on the flight deck for emergency rescue: Experiment, numerical simulation and machine learning. *International Journal of Thermal Sciences*, *190*(March), 108308. https://doi.org/10.1016/j.ijthermalsci.2023.108308

Li, Y., Huang, H., Wang, Z., Zhang, J., Jiang, C., & Dobashi, R. (2015). An experimental and modeling study of continuous liquid fuel spill fires on water. *Journal of Loss Prevention in the Process Industries*, *33*, 250–257. https://doi.org/10.1016/j.jlp.2015.01.006

Liu, J., Li, D., Wang, Z., & Chai, X. (2021). A state-of-the-art research progress and prospect of liquid fuel spill fires. *Case Studies in Thermal Engineering*, *28*(August), 101421. https://doi.org/10.1016/j.csite.2021.101421

Liu, J., & Zhou, Z. (2019). Examination of radiative fraction of small-scale pool fires at reduced pressure environments. *Fire Safety Journal*, *110*(August), 102894. https://doi.org/10.1016/j.firesaf.2019.102894

Loy, Y. Y., Rangaiah, G. P., & Lakshminarayanan, S. (2018). Surrogate modelling of net radiation flux from pool fires in a hydrocarbon storage facility. *Process Safety and Environmental Protection*, *114*, 296–309. https://doi.org/10.1016/j.psep.2017.12.024

Martínez, I. (2019). *Heat transfer and thermal radiation modelling.* In *Isidoro Martínez's lectures on Heat and Mass Transfer*. Retrieved from http://imartinez.etsiae.upm.es/~isidoro/tc3/Heat%20transfer%20and%20thermal%20radiation%20modelling.pdf

McGrattan, K., & Hostikka, S. (2012). Verification and validation process of a fire model. *11th International Probabilistic Safety Assessment and Management Conference and the Annual European Safety and Reliability Conference 2012, PSAM11 ESREL 2012*, *8*, 6823–6831.

Modak, A. T. (1977). Thermal radiation from pool fires. *Combustion and Flame*, *29*(C), 177–192. https://doi.org/10.1016/0010-2180(77)90106-7

Mudan, K. S. (1984). Thermal radiation hazards from hydrocarbon pool fires. *Progress in Energy and Combustion Science*, *10*(1), 59–80. https://doi.org/10.1016/0360-1285(84)90119-9

Nguyen, H. L., & Kohno, M. (2023). Numerical model of heat transfer for protected steel beam with cavity under ISO 834 standard fire. *Fire Safety Journal*, *140*(July), 103876. https://doi.org/10.1016/j.firesaf.2023.103876

Palazzi, E., Caviglione, C., Reverberi, A. P., & Fabiano, B. (2017). A short-cut analytical model of hydrocarbon pool fire of different geometries, with enhanced view factor evaluation. *Process Safety and Environmental Protection*, *110*(2004), 89–101. https://doi.org/10.1016/j.psep.2017.08.021

Paquet, F., Ng, H. D., Paquet, M., Cottin, F., & Groulx, D. (2019). Modeling propellant fires radiant heat flux. *Journal of Energetic Materials*, *37*(1), 110–124. https://doi.org/10.1080/07370652.2018.1542468

Parot, R., Rivera, J. I., Reszka, P., Torero, J. L., & Fuentes, A. (2022). A simplified analytical model for radiation dominated ignition of solid fuels exposed to multiple non-steady heat fluxes. *Combustion and Flame*, *237*, 111866. https://doi.org/10.1016/j.combustflame.2021.111866

Pinto, P., Littin, M., Rivera, J. I., Severino, G., Cruz, J. J., & Fuentes, A. (2023). A simpler tractable contour technique to model thermal radiation from buoyant diffusion flames. *Experimental Thermal and Fluid Science*, *149*(April), 111027. https://doi.org/10.1016/j.expthermflusci.2023.111027

Pope, N. D., & Bailey, C. G. (2006). Quantitative comparison of FDS and parametric fire curves with post-flashover compartment fire test data. *Fire Safety Journal*, *41*(2), 99–110. https://doi.org/10.1016/j.firesaf.2005.11.002

Prosen, E. J., & Rossini, F. D. (1944). Heats of combustion of eight normal paraffin hydrocarbons in the liquid state. *J. Res. NBS*, *33*, 255–272.

Pula, R., Khan, F. I., Veitch, B., & Amyotte, P. R. (2005). Revised fire consequence models for offshore quantitative risk assessment. *Journal of Loss Prevention in the Process Industries*, *18*(4–6), 443–454. https://doi.org/10.1016/j.jlp.2005.07.014

Raj, P. K. (2007). Large hydrocarbon fuel pool fires: Physical characteristics and thermal emission variations with height. *Journal of Hazardous Materials*, *140*(1–2), 280–292. https://doi.org/10.1016/j.jhazmat.2006.08.057

Rein, G., Torero, J. L., Jahn, W., Stern-Gottfried, J., Ryder, N. L., Desanghere, S., Lázaro, M., Mowrer, F., Coles, A., Joyeux, D., Alvear, D., Capote, J. A., Jowsey, A., Abecassis-Empis, C., & Reszka, P. (2009). Round-robin study of a priori modelling predictions of the Dalmarnock Fire Test One. *Fire Safety Journal*, *44*(4), 590–602. https://doi.org/10.1016/j.firesaf.2008.12.008

Rengel, B., Mata, C., Pastor, E., Casal, J., & Planas, E. (2018). A priori validation of CFD modelling of hydrocarbon pool fires. *Journal of Loss Prevention in the Process Industries*, *56*(May), 18–31. https://doi.org/10.1016/j.jlp.2018.08.002

Rew, P. J., Hulbert, W. G., & Deaves, D. M. (1997). Modelling of thermal radiation from external hydrocarbon pool fires. *Process Safety and Environmental Protection*, *75*(2), 81–89. https://doi.org/10.1205/095758297528841

Rossini, F. D. (1931). The heats of combustion of methane and carbon monoxide. *J. Res. NBS*, *6*, 37–49.

Rostamzadeh, H., Gholizadeh, T., Rostamzadeh, S., Vosoughi, S., & Farshad, A. A. (2021). Role of ejector expander in optimal inherently safety design of cascade NH3/Propane/CO2 vapor compression refrigeration systems. *Process Safety and Environmental Protection*, *146*, 745–762. https://doi.org/10.1016/j.psep.2020.12.009

Sayin, S. (2015). a Review on Performance Based Design of Multi Story Building. *International Journal of Advance Engineering and Research Development*, *2*(12), 28–30. https://doi.org/10.21090/ijaerd.021216

Seo, D., Kim, D., Kim, B., & Kwon, Y. (2013). An experimental study on the combustibles investigation and fire growth rate for predicting initial fire behavior in building. *Procedia Engineering*, *62*, 671–679. https://doi.org/10.1016/j.proeng.2013.08.113

Sharma, A., Vishwakarma, P. K., Mishra, S., & Mishra, K. B. (2020). Visible length and thermal radiation of WCO biodiesel and ethanol pool fires. *Fuel*, *280*(July), 118396. https://doi.org/10.1016/j.fuel.2020.118396

Shen, G., Zhou, K., Wu, F., Jiang, J., & Dou, Z. (2019). A Model Considering the Flame Volume for Prediction of Thermal Radiation from Pool Fire. *Fire Technology*, *55*(1), 129–148. https://doi.org/10.1007/s10694-018-0779-y

Shokri, & Beyler. (1989). Large pool fires. *Fire Protection Engineering*, *1*(4), 141–149.

Sikanen, T., & Hostikka, S. (2016). Modeling and simulation of liquid pool fires with in-depth radiation absorption and heat transfer. *Fire Safety Journal*, *80*, 95–109. https://doi.org/10.1016/j.firesaf.2016.01.002

Singleton, P. (2002). Performance modelling - What, why, when and how. *BT Technology Journal*, *20*(3), 133–143. https://doi.org/10.1023/A:1020860029447

Spearpoint, M., Baker, G. B., Limited, G., Wade, C., & Fleischmann, C. (2014). *a Comparison of a Priori Modelling Predictions With Experimental Results To*. *October 2017*.

Spearpoint, M., Hopkin, C., & Hopkin, D. (2020). Modelling the thermal radiation from kitchen hob fires. *Journal of Fire Sciences*, *38*(4), 377–394. https://doi.org/10.1177/0734904120923566

Stewart, J. R., Phylaktou, H. N., Andrews, G. E., & Burns, A. D. (2021). Evaluation of CFD simulations of transient pool fire burning rates. *Journal of Loss Prevention in the Process Industries*, *71*(April), 104495. https://doi.org/10.1016/j.jlp.2021.104495

Tang, F., Hu, L. H., Delichatsios, M. A., Lu, K. H., & Zhu, W. (2012). Experimental study on flame height and temperature profile of buoyant window spill plume from an under-ventilated compartment fire. *International Journal of Heat and Mass Transfer*, *55*(1–3), 93–101. https://doi.org/10.1016/j.ijheatmasstransfer.2011.08.045

Thermofisher. (2022). *ETHANOL AHYD HISTO 4L-SDS-Thermofisher*. *7*, 1–10.

Tien, C. L., & Lee, S. C. (1984). Flame Radiation. *Prog. Energy Combust. Sci.*, *8*, 41–59.

Tohir, M. Z. M., & Spearpoint, M. (2019). Probability of Fire Spread Between Vehicles in Car Parking Buildings. *GCEC 2017*, *9*(January), 1357–1366. https://doi.org/10.1007/978-981-10-8016-6_97

Tsui, S. C. (2004). Performance-Based Fire Safety Design in Hong Kong. *International Journal on Engineering Performance-Based Fire Codes*, *6*(4), 223–229.

Varlet, V., Smith, F., & Augsburger, M. (2014). New trends in the kitchen: Propellants assessment of edible food aerosol sprays used on food. *Food Chemistry*, *142*, 311–317. https://doi.org/10.1016/j.foodchem.2013.07.036

Viskanta, R., & Mengüç, M. P. (1987). Radiation heat transfer in combustion systems. *Progress in Energy and Combustion Science*, *13*(2), 97–160. https://doi.org/10.1016/0360-1285(87)90008-6

Walls, R., Olivier, G., & Eksteen, R. (2017). Informal settlement fires in South Africa: Fire engineering overview and full-scale tests on “shacks”. *Fire Safety Journal*, *91*(February), 997–1006. https://doi.org/10.1016/j.firesaf.2017.03.061

Wan, H., Gao, Z., Ji, J., Sun, J., Zhang, Y., & Li, K. (2018). Predicting heat fluxes received by horizontal targets from two buoyant turbulent diffusion flames of propane burning in still air. *Combustion and Flame*, *190*, 260–

269. https://doi.org/10.1016/j.combustflame.2017.12.003

Wan, H., Gao, Z., Ji, J., & Zhang, Y. (2019). Experimental study on flame radiant heat flux from two heptane storage pools and its application to estimating safety distance. *Energy*, *182*, 11–20. https://doi.org/10.1016/j.energy.2019.06.006

Wang, H. Y., & Joulain, P. (2007). Numerical simulation of wind-aided flame propagation over horizontal surface of liquid fuel in a model tunnel. *Journal of Loss Prevention in the Process Industries*, *20*(4–6), 541–550. https://doi.org/10.1016/j.jlp.2007.04.002

Wang, L., Li, W., Feng, W., & Yang, R. (2021). Fire risk assessment for building operation and maintenance based on BIM technology. *Building and Environment*, *205*(April), 108188. https://doi.org/10.1016/j.buildenv.2021.108188

Wang, Q., Hu, L., Tang, F., Zhang, X., & Delichatsios, M. (2013). Characterization and comparison of flame fluctuation range of a turbulent buoyant jet diffusion flame under reduced- and normal pressure atmosphere. *Procedia Engineering*, *62*, 211–218. https://doi.org/10.1016/j.proeng.2013.08.057

Wu, Y., Zhou, K., Zhou, M., Huang, M., Wang, C., & Jiang, J. (2022). Radiant heat feedback from a jet flame to the ruptured tank surface. *International Journal of Thermal Sciences*, *172*(PA), 107322. https://doi.org/10.1016/j.ijthermalsci.2021.107322

Xu, L., Lu, Y., Ding, C., Guo, H., Liu, J., & Zhao, Y. (2022). A generic flame shape model and analytical models for geometric view factor calculation on the fire exposure surface. *International Journal of Thermal Sciences*, *173*(December 2021). https://doi.org/10.1016/j.ijthermalsci.2021.107392

Yang, J., Zhang, B., Chen, L., Diao, X., Hu, Y., Suo, G., Li, R., Wang, Q., Li, J., Zhang, J., & Dou, Z. (2023). Improved solid radiation model for thermal response in large crude oil tanks. *Energy*, *284*(May). https://doi.org/10.1016/j.energy.2023.128572

Ye, X., Ma, J., Shen, Y. X., & Lin, L. Y. (2016). Suppression Effect of Sprinkler System on Fire Spread in Large Commercial Buildings. *Procedia Engineering*, *135*, 455–462. https://doi.org/10.1016/j.proeng.2016.01.155

Yuan, J., Zhao, J., Wang, W., Yang, R., Chen, C., & Fu, M. (2021). The study of burning behaviors and quantitative risk assessment for 0# diesel oil pool fires. *Journal of Loss Prevention in the Process Industries*, *72*(January), 104568. https://doi.org/10.1016/j.jlp.2021.104568

Zainudin, S. Z., Tapsir, S. H., Adam, N. M., & Kassim, Z. M. (2003). *Future of fire safety for Malaysian housing.* Paper presented at the International Conference on Industrialised Building Systems, Kuala Lumpur, Malaysia. Universiti Teknologi Malaysia. Retrieved from https://eprints.utm.my/2875/1/SHTapsir2003_future_of_fire_safety_for_Malaysian_housing.pdf

Zalosh, R. G. (2003). Appendix A: Flame. *Industrial Fire Protection Engineering* (pp. 337-346). Wiley

Zhou, K., & Jiang, J. (2016). Thermal radiation from vertical turbulent jet flame: Line source model. *Journal of Heat Transfer*, *138*(4), 1–8. https://doi.org/10.1115/1.4032151

Zhou, K., Liu, J., & Jiang, J. (2016). Prediction of radiant heat flux from horizontal propane jet fire. *Applied Thermal Engineering*, *106*, 634–639. https://doi.org/10.1016/j.applthermaleng.2016.06.063

Zhou, K., & Wang, X. (2019). Thermal radiation modelling of pool fire with consideration on the nonuniform temperature in flame volume. *International Journal of Thermal Sciences*, *138*(September 2018), 12–23. https://doi.org/10.1016/j.ijthermalsci.2018.12.033

Zhu, Z., Guo, Q., Quiel, S. E., & Naito, C. J. (2022). Rapid prediction of fire-induced heat flux on the liners of horseshoe and circular tunnels with longitudinal ventilation at critical velocity. *Fire Safety Journal*, *130*(October 2021), 103590. https://doi.org/10.1016/j.firesaf.2022.103590

APPENDICES

Appendix A: Lab Manual

This section outlines the general laboratory procedures for conducting pool fire experiments. The provided lab manual is applicable to all pool fire experiments conducted within this research. It encompasses experiments involving ethanol and isopropyl alcohol pool fires (Chapter 5), as well as acetone and methanol pool fires (Chapter 6), with the specific parameters outlined in their respective chapters. Table A.1 provides the equipment labelling used throughout the manual.

Table A.1: Equipment labelling for liquid pool fire experiment

Heat flux sensor 1	G1	Thermocouple 3	T5
Heat flux sensor 2	G2	Thermocouple 4	T6
Thermocouple 1	T3	Thermocouple 5	T7
Thermocouple 2	T4	Thermocouple 6	T8

Equipment Set Up:

<u>Heat flux sensors (heat flux gauges)</u>

1. Attach heat flux gauges to the trolley. (Starting from the lowest height level)
2. Connect the cooling pipe to the heat flux gauges and ensure that valve (V1) is in "open" mode.
3. Connect the data output cable to the data logger. (G1→ Port 1, G2 → Port 2)

<u>Thermocouple (not required for acetone and methanol pool fire experiments)</u>

1. Attach Thermocouple T3, T4, T5, and T6 to retort stand (R1) for the recording of flame temperature (T_f) and connect the data output cable to the data logger. (T3 → Port 3, T4 → Port 4, T5 → Port 5, T6 → Port 6)
2. Attach Thermocouple T5 and T6 to retort stand (R2) for the recording of ambient temperature (T_a) and connect the data output cable to the data logger. (T7 → Port 7, T8 → Port 8)

Trolley

1. Make sure the trolley is aligned at the same axis as the flame.
2. Heat flux gauges are attached from the bottom level up to the higher level.
3. Horizontal displacement of a trolley will start from the nearest distance up to the furthest location.

Weighing scale

1. Make sure the weighing scale is in a stable orientation.
2. Check the battery level for the weighing scale.
3. Turn on the weighing scale and connect it to the computational unit (PC).

Video recorder

1. Arrange the black screen to the correct position.
2. Make sure the black-painted face of the pan is facing the video recording device.
3. Ensure the video recording device is in the video recording phase and position the camera stand at an imaginary plane parallel to the pan.

Pan

1. Prepare a sufficient amount of tissue paper to contain fuel spillage during fuel transfer.
2. Transfer fuel from the fuel reservoir into the beaker using a pump.
3. Select a suitable size of pan to be used and fill the pan with fuel up until it reaches the 1 cm mark on the indicator.
4. Place the pan on top of the weighing scale and ensure the midpoint of the pan is aligned with the marking on the floor labelled as "CENTRE OF FIRE".
5. Ensure that the black-painted surface of the pan is facing the video recorder.

Starting Experiment:

1. Check battery level (Weighing scale, PC, Video recording device).
2. Switch on the exhaust fan (E1 & E2) and exhaust hood (S1).
3. Turn on the water supply (P1).
4. Switch off the standing fan if present.
5. Ensure the video recording device is in the video recording phase.
6. Ensure the weighing scale has been connected to the PC through a "serial port to USB" cable.
7. Ensure Simple Data Logger (SDL) is ready and a blank csv. file has been created. (Make sure the file selected is correct)
8. Ensure the data logger has been connected to the PC.

9. Ensure the Pico Log is in the correct format and ready for data collection. (Make sure to press “data reset” before starting to burn the fuel)

Data Recording:

1. Start video recording.
2. Click “start” on SDL.
3. Start data recording on Pico Log (Local capture > continuous capture) and change interface to table format.
4. Light up the fuel and wait until it burns out.
5. Show experimental code prior to ending video recording.
6. Click “end” on SDL and check the exported csv. file.
7. End data recording on Pico Log, save the log file and export data to csv. file.

Clean Up:

1. Switch off exhaust fan (E1 & E2) and exhaust hood (S1).
2. Turn off the water supply (P1).
3. Switch on the standing fan (if necessary).
4. Detach the weighing scale cable and data logger cable from the PC.
5. Store the cooling pipe in its designated container.
6. Store all equipment (data logger with extension cable, weighing scale, camera stand) in the designated box.
7. Switch off the standing fan.
8. Keep the thermocouple tree, heat flux gauge trolley, and equipment box within the designated compartment.

Appendix B: Experimental Equipment and Specifications

Figure B.1: TC-08 Data Logger with Eight Miniature Sockets

Figure B.2: TC-08 Data Logger Specification
(Source: Picotech manual)

Figure B.3: Heat Flux Gauges Mounted on a Mobile Trolley for Heat Flux Measurements

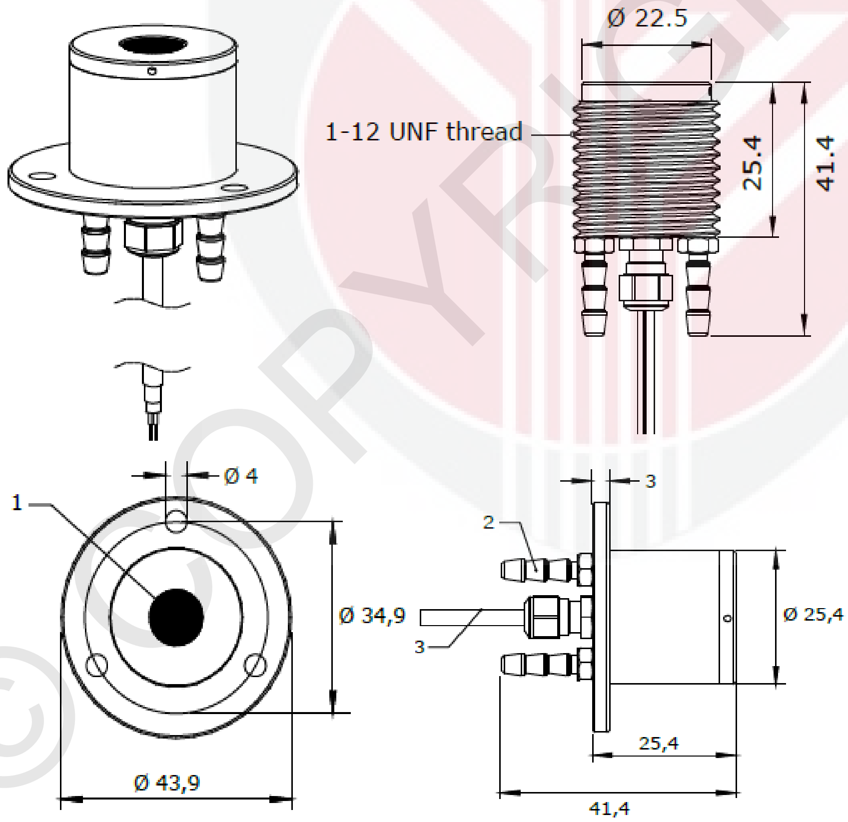

(1) thermopile sensor with black coating. diameter sensing area: 10 x 10^{-3} m
(2) water cooling tube. outer diameter tubes: 4.2 x 10^{-3} m
(3) PTFE cable. standard cable length is 2 m.

Figure B.4: SGB01 Heat Flux Sensor Specification
(Source: SBG01 manual v2023)

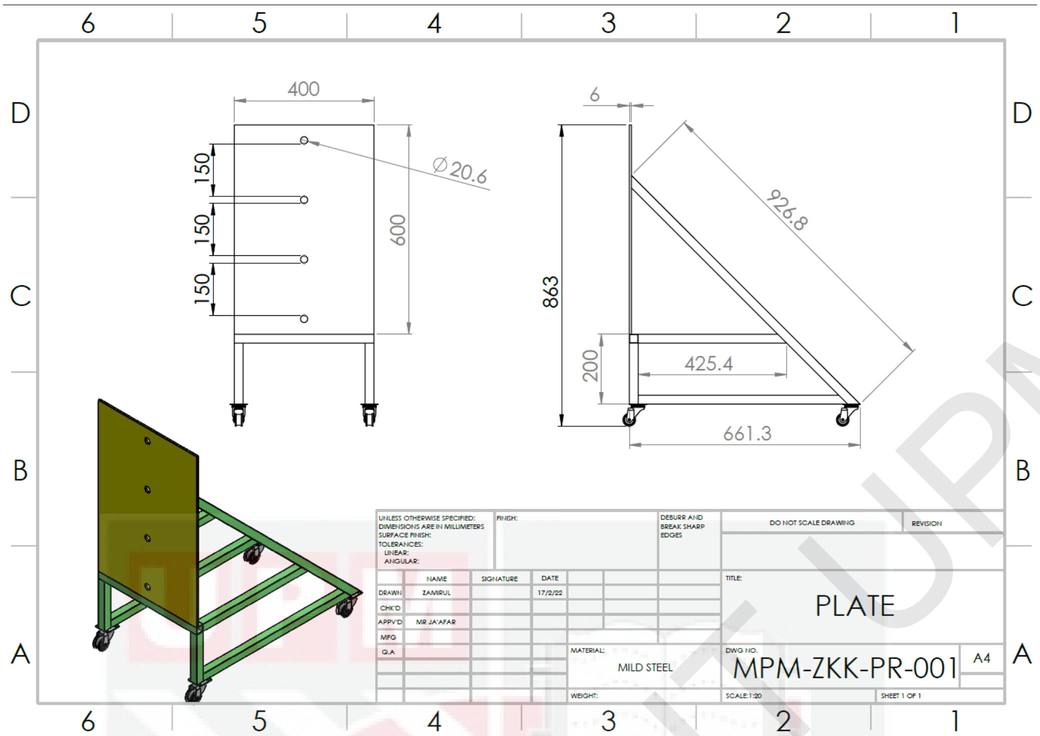

Figure B.5: Trolley Specification

Figure B.6: Type K Thermocouple Mounted on Retort Stand (Left) with Extension Cables (Right)

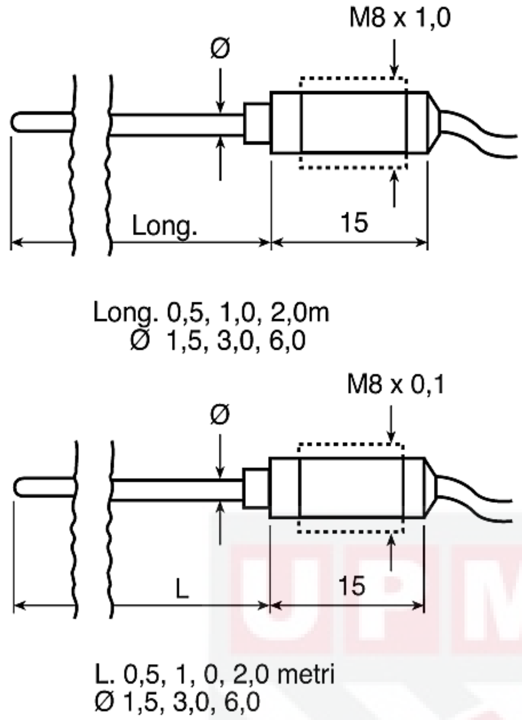

Figure B.7: RS PRO Type K Thermocouple Specification

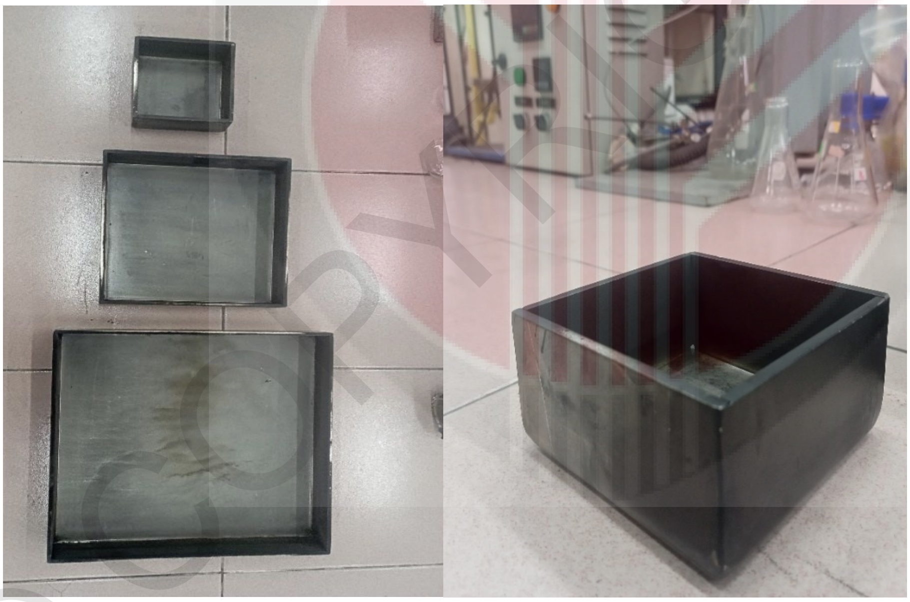

Figure B.8: SS304 Square Pans for Containing Liquid Fuel in Liquid Pool Fire Experiments

Figure B.9: OHAUS Ranger Count 4000 Weighing Scale for Precise Mass Loss Rate Measurement

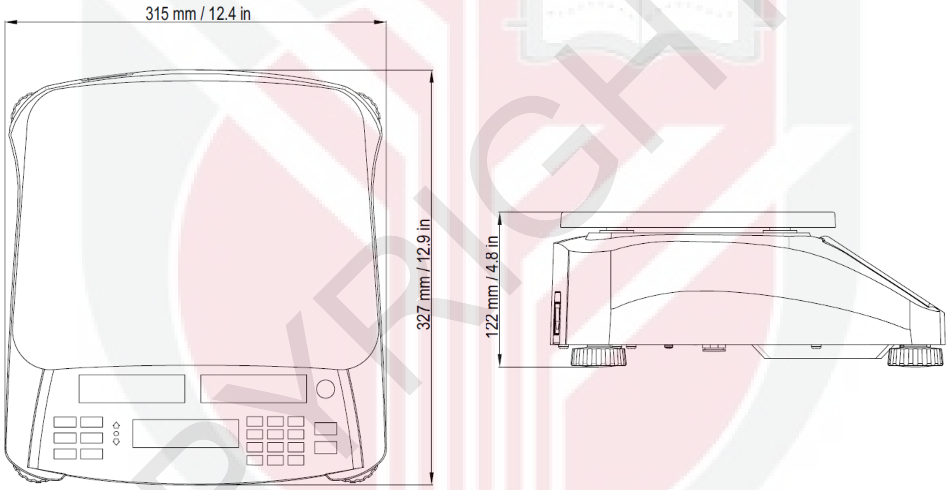

Figure B.10: Ranger Count 4000 Specification
(Source: OHAUS product manual)

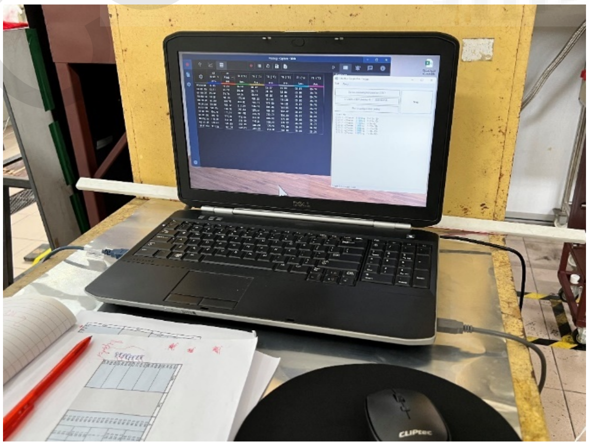

Figure B.11: Data Collection Process Using Computational System

BIODATA OF STUDENT

Michael Chong Vui San was born in October 1998 in Sabah, Malaysia. He successfully completed his Bachelor of Engineering (Chemical) with Honours from Universiti Putra Malaysia in 2021. Driven by his passion for the field of chemical engineering, he decided to continue his academic journey by pursuing a Doctor of Philosophy (Ph.D.) degree. His research focuses on the assessment of thermal radiation models' performance for gas and liquid fuels.

As a dedicated researcher in the field of fire safety engineering, Michael aims to utilise the comprehensive knowledge and skills acquired during his postgraduate studies to contribute to the advancement of fire safety practices. With a strong desire to make a positive impact, he has successfully embarked on a fulfilling career in the realm of fire safety upon the completion of his Ph.D. program.

LIST OF PUBLICATIONS

Michael Chong Vui San, Mohd Zahirasri Mohd Tohir, Michael Spearpoint, Syamimi Saadon, and Abd. Rahim Abu Talib. (2024). An Assessment of Recent Thermal Radiation Model Performance for Propane Gas Fire Experiments. Journal of Fire Sciences, 42(2), 89–116. https://doi.org/10.1177/07349041231222010

Michael Chong Vui San, Mohd Zahirasri Mohd Tohir, Syamimi Saadon, and Abd. Rahim Abu Talib. (2024). Developing an Enhanced Thermal Radiation Model through a Semi-A Priori Approach. International Journal of Thermal Sciences, 197(June 2023), 108784. https://doi.org/10.1016/j.ijthermalsci. 2023.108784.

UNIVERSITI PUTRA MALAYSIA

STATUS CONFIRMATION FOR THESIS / PROJECT REPORT AND COPYRIGHT

ACADEMIC SESSION : SECOND SEMESTER 2024/2025

TITLE OF THESIS / PROJECT REPORT :

DEVELOPMENT OF A REFINED THERMAL RADIATION MODEL FOR GAS AND LIQUID FUELS

NAME OF STUDENT : MICHAEL CHONG VUI SAN

I acknowledge that the copyright and other intellectual property in the thesis/project report belonged to Universiti Putra Malaysia and I agree to allow this thesis/project report to be placed at the library under the following terms:

1. This thesis/project report is the property of Universiti Putra Malaysia.
2. The library of Universiti Putra Malaysia has the right to make copies for educational purposes only.
3. The library of Universiti Putra Malaysia is allowed to make copies of this thesis for academic exchange.

I declare that this thesis is classified as :

*Please tick (√)

[ ]	**CONFIDENTIAL**	(Contain confidential information under Official Secret Act 1972).
[ ]	**RESTRICTED**	(Contains restricted information as specified by the organization/institution where research was done).
[√]	**OPEN ACCESS**	I agree that my thesis/project report to be published as hard copy or online open access.

This thesis is submitted for :

[ ]	**PATENT**	Embargo from ________ until ________ (date) (date)

Approved by:

(Signature of Student)
New IC No/ Passport No.: 981029125407

Date : 16/4/2025

DR. MOHD ZAHIRASRI BIN MOHD TOHIR
Pensyarah Kanan
Jabatan Kejuruteraan Kimia & Alam Sekitar
Fakulti Kejuruteraan
Universiti Putra Malaysia
43400 UPM Serdang
Selangor, Malaysia

(Signature of Chairman of Supervisory Committee)
Name: Associate Professor Dr. Mohd Zahirasri Bin Mohd Tohir

Date : 16/4/2025

[Note : If the thesis is CONFIDENTIAL or RESTRICTED, please attach with the letter from the organization/institution with period and reasons for confidentially or restricted.]